IEEE Access
Multidisciplinary | Rapid Review | Open Access Journal

Received October 13, 2016, accepted November 14, 2016, date of publication November 16, 2016, date of current version January 27, 2017.

Digital Object Identifier 10.1109/ACCESS.2016.2629671

Quantum-Assisted Joint Multi-Objective Routing and Load Balancing for Socially-Aware Networks

DIMITRIOS ALANIS[1], (Student Member, IEEE), JIE HU[2], (Member, IEEE), PANAGIOTIS BOTSINIS[1], (Member, IEEE), ZUNAIRA BABAR[1], SOON XIN NG[1], (Senior Member, IEEE), AND LAJOS HANZO[1], (Fellow, IEEE)

[1]School of Electronics and Computer Science, University of Southampton, Southampton, SO17 1BJ, U.K.
[2]School of Communication and Information Engineering, University of Electronic Science and Technology of China, Chengdu 61173, China

Corresponding author: L. Hanzo (lh@ecs.soton.ac.uk)

This work was supported in part by EPSRC under Grant EP/L018659/1, that of the European Research Council, Advanced Fellow Grant and in part by the Royal Society's Wolfson Research Merit Award. The work of J. Hu was supported in part by the University of Electronic Science and Technology of China under Grant A03013023601053 and in part by the National Natural Science Foundation of China under Grant 61601097.

ABSTRACT The widespread use of mobile networking devices, such as smart phones and tablets, has substantially increased the number of nodes in the operational networks. These devices often suffer from the lack of power and bandwidth. Hence, we have to optimize their message routing for the sake of maximizing their capabilities. However, the optimal routing typically relies on a delicate balance of diverse and often conflicting objectives, such as the route's delay and power consumption. The network design also has to consider the nodes' user-centric social behavior. Hence, the employment of socially aware load balancing becomes imperative for avoiding the potential formation of bottlenecks in the network's packet-flow. In this paper, we propose a novel algorithm, referred to as the *multi-objective decomposition quantum optimization* (MODQO) algorithm, which exploits the quantum parallelism to its full potential by reducing the database correlations for performing multi-objective routing optimization, while at the same time balancing the teletraffic load among the nodes without imposing a substantial degradation on the network's delay and power consumption. Furthermore, we introduce a novel socially aware load balancing metric, namely, the normalized entropy of the normalized composite betweenness of the associated socially aware network, for striking a better tradeoff between the network's delay and power consumption. We analytically prove that the MODQO algorithm achieves the full-search based accuracy at a significantly reduced complexity, which is several orders of magnitude lower than that of the full search. Finally, we compare the MODQO algorithm to the classic non-dominated sort genetic algorithm II evolutionary algorithm and demonstrate that the MODQO succeeds in halving the network's average delay, while simultaneously reducing the network's average power consumption by 6 dB without increasing the computational complexity.

INDEX TERMS DTNs, routing, load balancing, quantum computing, NDQIO, BBHT-QSA, DHA, Grover's QSA, NSGA-II.

LIST OF ACRONYMS

BBHT	Boyer, Brassard, Høyer and Tapp
BER	Bit Error Ratio
CD	Classical Domain
CF(E)	Cost Function (Evaluation)
CM	Classical Merging
CNOT	Controlled-NOT quantum gate
DHA	Durr-Høyer-Algorithm
HP	Hardware Parallelism
MC	Mesh Client
MODQO	Multi-Objective Decomposition Quantum Optimization
MR	Mesh Router
NDQIO	Non-Dominated Quantum Iterative Optimization
NSGA-II	Non-dominated Sort Genetic Algorithm II
(O)PF	(Optimal) Pareto Front
OSN	Online Social Network
OW	(Global/Local) Oracle Workspace
QCR	Quantum Control Register

QD	Quantum Domain
QIR	Quantum Index Register
QM	Quantum Merging
QP	Quantum Parallelism
QSA	Quantum Search Algorithm
UF	Utility Function
UV	Utility Vector
WMN	Wireless Mesh Network

LIST OF SYMBOLS

B_{sin}	Singular Betweenness
B_{com}	Composite Betweenness
$\bar{B}_{com}$	Normalized Composite Betweenness
$D(x)$	x-th Route Delay
$\bar{D}(S)$	Route-Combination S Average Network Delay
$\mathbf{f}(x)$	Utility Vector of the x-th route
$f_k^{\bullet}(x, i)$	Comparison Function Between the x-th and the i-th Routes based on the $\bullet$ operator
$\mathcal{F}_{\text{MC}}$	MC Friendship Matrix
$\mathcal{F}_{\text{MR}}$	MR Friendship Matrix
$\mathcal{G}$	Grover's QSA Operator
$g(x, i)$	Dominance Operator Function Between the x-th and the i-th Routes
H	Quantum Hadamard Gate
$\bar{H}$	Normalized Entropy
L_{ES}	Complexity of the Exhaustive Search
L_{BBHT}	Complexity BBHT-QSA
$L_{\text{CM}}^{\text{outer}}$	Complexity of the CM method for the MODQO outer step
$L_{\text{CM}}^{\text{ref}}$	Reference Complexity of the CM Method for the MODQO Outer Step
L_{DHA}	Complexity of DHA
L_{NDQIO}	Complexity of the NDQIO Algorithm
$L_{\text{MODQO}}^{\text{inner}}$	MODQO Algorithm Inner Step Complexity
$L_{\text{MODQO}}^{\text{outer}}$	MODQO Algorithm Outer Step Complexity
$L_{\text{MODQO}}^{\text{tot}}$	MODQO Algorithm Total Complexity
$L_{\text{QM}}^{\text{outer}}$	Complexity of a Single Iteration of the QM Method for the MODQO Outer Step
$L_{\text{QM}}^{\text{ref}}$	Reference Complexity of a Single Iteration of the QM Method for the MODQO Outer Step
N	Total Number of Legitimate Routes
N_{MC}	Number of Mesh Clients
N_{MR}	Number of Mesh Routers
N_{OPF}	Number of Pareto-optimal Routes
N_r	Total Number of Active Routes
O	Grover's QSA Quantum Oracle Gate
P_e	Bit Error Ratio
$P^{t,act}$	Transmission Power Matrix of all the Network Links
ρ	Surviving Route-Combinations' Growth Factor
S	Set of Legitimate Routes
S^{OPF}	Set of Pareto-optimal Route-Combinations
$S_{(n)}^{\text{OPF}}$	Set of Pareto-optimal Route-Combinations after n Trellis Stages
$S_{\text{MC}}^{\text{OPF}}$	Set of Pareto-optimal MC Routes
$S_{\text{MR}}^{\text{OPF}}$	Set of Pareto-optimal MR Routes
U_f	Generic Quantum Unitary Operator implementing the function $f(x)$
U_{f_k}	Quantum Unitary Operator implementing the Comparison Operator $f_k(x, i)$
U_g	Parallel Quantum Unitary Operator implementing the Dominance Operator $g(x, i)$
U_G	Quantum Unitary Operator for Parallel Activation of Multiple U_g Operators
x	Index of the Legitimate Route in the Route List
$\|\psi\rangle$	Quantum State ψ

I. INTRODUCTION

Back in 1991, Weiser [1] unveiled his vision for ubiquitous computing, where most aspects of human life would be supported by portable computing units, which he termed as ''pads''. Twenty five years later, this vision has come to fruition, since indeed our daily lives rely on ''pads'', which are commonly known as *tablets* and *smart phones*. More specifically, for the latter, there is a prediction by *eMarketer*[1] that their market penetration will surpass 2 billion mark in 2016, accounting for about 30% of the world's population. Additionally, based on a recent report conducted by *Shareholic*,[2] 31.24% of the overall network traffic in 2014 has been generated by *Online Social Networks* (OSN), such as Facebook and Pinterest, while having an increase of about 10% compared to the previous year. Additionally, from a slightly different perspective, namely from that of the *Internet of Things* (IoT) [2], networked devices perpetually proliferate [3], [4] and they also tend to exhibit social behavior [5], [6].

Explicitly, the nodes' social behavior combined with their increased number results in a paradigm shift as to how the networks are designed and maintained [7], leading to encapsulating *Social Network Analysis* (SNA) [8] tools into the network's design. From this perspective, networks, which are often comprised by remote nodes having limited power, ought to configure their end-to-end links for satisfying diverse and often coflicting *Quality-of-Service* (QoS) criteria, such as the *Bit-Error-Ratio* (BER), the *Packet-Loss-Ratio* (PLR), total power dissipation or the overall delay. This requires the joint optimization of the aforementioned QoS criteria. As a further aspiration, Boldrini *et al.* pointed out in [9] that optimal multihop routing is more beneficial for socially aware networks than for the socially oblivious ones.

The authors of [10]–[16] advocated routing schemes, where both the specific QoS criteria and SNA-aided design are considered. To elaborate further, Bulut and Szymanski [13] proposed a routing scheme in the context of *Delay-Tolerant Networks* (DTN) for maximizing the associated routing efficiency by grouping the *Mobile Users* (MU) into clusters based on their contact history. Furthermore, Hui *et al.* [15] conceived a novel algorithm, namely

[1] http://www.emarketer.com/Article/2-Billion-Consumers-Worldwide-Smartphones-by-2016/1011694

[2] https://blog.shareaholic.com/social-media-traffic-trends-01-2015/

the so-called BUBBLE algorithm, which exploits the social networking metrics of the centrality [17] routinely used in the community detection [18] for the sake of performing socially aware multi-cast routing in the context of DTNs. In a similar context, namely that of *Vehicular Social Networks* (VSN), Xia *et al.* [16] employed *Bee Colony Optimization* (BCO) in the form of the so-called BEEINFO packet forwarding scheme for the sake of the sake of maximizing the associated packet delivery ratio.

Apart from the above-mentioned routing schemes considering SNA-related metrics, some contributions utilize the structure of a twin-layer composite network [19], where the top layer characterizes the users' social relationships, hence it is often referred to as an *Online Social Network* (OSN). By contrast, the bottom one is constituted by the technological network. To elaborate further, in [20], each MU is assumed to communicate with its contacts with a probability that is inversely proportional to their respective geographic distance [21], while the technological network is relies on a grid-based network. The same OSN layer has been deployed in [22] in conjunction with a mobile multi-cast network and a hybrid routing scheme has been proposed for the sake of improving the content dissemination among members of the same community. Additionally, epidemic routing [23] has been deployed [24], [25] in this specific cross-layer design, where the nodes allow their messages to ''flood'' their newly discovered contacts by mimicking the spread of a disease in a community. This scheme has a low complexity and a low delay, but it tends to use an excessive amount of resources, because multiple copies of the packets are allowed to flood the network.

Apart from optimal routing, the new socially aware design paradigm has to account for the nodes' *social selfishness* [26]. Explicitly, the nodes' social selfishness stems from their tendency to select specific routes for the sake of optimizing a specific utility, while being oblivious to the potential degradation of the overall network's performance inflicted by their particular choice [27], [28]. Naturally, the nodes' selfish route selection leads to the creation of bottlenecks in the network flow, especially for the case of nodes having a high centrality. This brings the requires socially-aware load balancing [29]–[31].

For the sake of mitigating the effect of social selfishness as well as the potential degradation [32] of the routing efficiency metrics, a multi-objective optimization approach can be employed by relying on the concept of Pareto-optimality [33] borrowed from socially-oblivious treatises.[3] Under this perspective, each pair of source and destination nodes would have a set of optimal routes, in which none of the parameters can be further improved without degrading the rest of the optimization objectives. Explicitly, this set provides a compelling trade-off among the optimization objectives. Nevertheless, identifying this set of Pareto-optimal solutions imposes an increased complexity, when compared to single component optimization, owing the fact that the Pareto-optimality problems are classified as NP-hard. To mitigate the increased complexity, evolutionary heuristic methods have been employed in [32] and [34]–[36] by relying on near-optimal accuracy for improving the performance of the associated socially-oblivious networking.

The recent advances in quantum computation [37]–[43] and in quantum information processing [44]–[46] provides us with an attractive framework, offering a significant complexity reduction by exploiting the concept of *Quantum Parallelism* (QP) [47]. In particular, Grover [37] proposed a *Quantum Search Algorithm* (QSA), which is capable of identifying the value sought in a database having uncorrelated entries by imposing a complexity on the order of $O(\sqrt{N})$, provided that the number of solutions[4] is known *a priori*. Based on Grover's QSA, comprehensive studies have been carried out in the context of quantum-assisted socially-oblivious multi-objective routing [42], [43]. In particular, the so-called *Non-Dominated Quantum Optimization* (NDQO) algorithm was proposed in [42] for the routing process in Self-Organizing Networks (SONs) for jointly optimizing the route's overall delay, its power dissipation and its BER at a significant complexity reduction with the advent of QP. An improved version of the NDQO algorithm, applied in the context of *Wireless Multihop Networks* (WMHNs), has been advocated in [43], where the so-called *Non-Dominated Quantum Iterative Optimization* (NDQIO) algorithm has been shown to achieve optimal accuracy at the expense of an even further complexity reduction compared to the NDQIO algorithm by exploiting the hybrid synergies between QP and *Hardware Parallelism*[5] (HP).

The NDQIO algorithm provides us with some clear design guidelines for the sake of addressing the joint multi-objective routing and load balancing problem of socially-aware networks. Explicitly, the hybrid framework exploiting the synergy between the QP and the HP provides substantial complexity reduction by a factor of $O(K\sqrt{N})$ [43], where the factor K corresponds to the number of parallel independent quantum processes stemming from the HP, while N is the database size. Nevertheless, as Zalka [48] pointed out, Grover's QSA and inherently all the Grover-based QSAs, such as the BBHT-QSA, the DHA and the NDQIO algorithm, are optimal in terms of their complexity reduction, as long as the database entries are uncorrelated. Naturally, Zalka's proof of Grover's QSA optimality provides us with a further design consideration, namely the *database correlation exploitation*, as portrayed in Fig. 1. We note that the actual complexity reduction offered by the database correlation exploitation

[3]To the authors' knowledge, there does not exist any treatise advocating the employment of Pareto-optimal routing.

[4]We define as a solution the database entries having the value sought by the search process.

[5]We define as *Hardware Parallelism* the parallel activation of K independent resource blocks supported by a specific hardware architecture. This type of parallelism should not be confounded with the QP, where the ''carrier'' of parallelism is the capability of quantum systems to be in the superposition of their basis states.

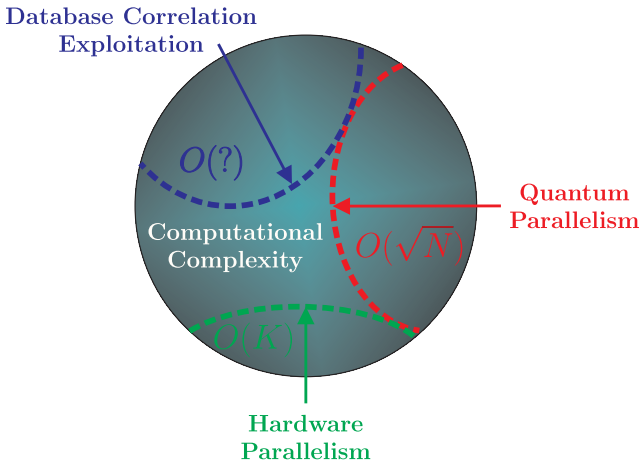

FIGURE 1. Eligible techniques of reducing the computational complexity. Explicitly, QP is capable of reducing the number of database calls from N on the order of $O(\sqrt{N})$, where N is the database length, while HP exhibits a complexity reduction on the order of $O(K)$, where K denotes the number of independent parallel processes. Finally, although the database correlation exploitation is problem-dependent and its complexity reduction cannot be readily quantified, it tends to rearrange the database into an uncorrelated one, substantially reducing the complexity imposed by both QP and HP, based on Zalka's [48] proof of Grover's QSA optimality.

strictly depends on the optimization problem and, thus, its achievable complexity reduction order is denoted by $O(?)$ in Fig. 1. Nevertheless, we can view this method as a means of transforming the database into a series of shorter uncorrelated ones, thus, effectively reducing the database length N for pushing the complexity reduction offered by the hybrid HP and QP framework to its full potential.

Based on these design considerations, our contributions are summarized as follows:

1) *We propose a quantum-assisted multi-objective optimization algorithm, namely the Mutli-Objective Decomposition-based Quantum Optimization (MODQO) algorithm, which relies on a novel optimal decomposition framework for jointly optimizing the routing and performing load balancing in socially-aware twin-layered networks.*
2) *We develop a novel framework for decomposing the joint multi-objective routing and load balancing problem into a series of low-complexity sub-problems and we prove that the Optimal Pareto Front of the decomposed problem is identical to the Optimal Pareto Front of its composite counterpart.*
3) *We propose a new metric for characterizing the distribution of the tele-traffic load, namely the normalized entropy $\bar{H}$ of the respective distribution, which circumvents the biasing towards the minimum delay solution imposed by relying on the use of the standard deviation of the respective distribution.*
4) *We analytically characterize the complexity imposed by the MODQO algorithm, which is on the order of $O(\sqrt{N})$ and $O(N_{MR}^{2N_{MC}^2})$ for networks having N_{MR} routers and N_{MC} users in the best-case and the worst-case scenarios, respectively, down from $O(N^{2N_{MC}^2})$ imposed by the exhaustive search, with $N \gg N_{MR}$ being the total number of Hamiltonian routes between two specific users. Additionally, we demonstrate that the average complexity of the MODQO algorithm is multiple orders of magnitude lower than that of the exhaustive search, when considering realistic network sizes.*
5) *Finally, we compare the MODQO accuracy to that of the* Non-dominated Sort Genetic Algorithm II *(NSGA-II) [49] operating at an identical computational complexity and demonstrate that the MODQO algorithm is capable of improving both the delay and power consumption by at least that of two-hop durations and at least 4 dB, respectively, for networks having 10 mesh routers.*

The rest of this paper is organized as follows. In Sec. II we will present the twin-layer network model considered and then we will define the joint multi-objective routing and load balancing problem. In Sec. III, we will provide a brief introduction to the quantum search algorithms used. Subsequently, our quantum-assisted approach to solving the joint routing and load balancing problem is presented in Sec. IV. Finally, in Sec. V we will provide the respective simulation results, followed by our conclusions in Sec. VI. The paper's structure is portrayed in Fig. 2.

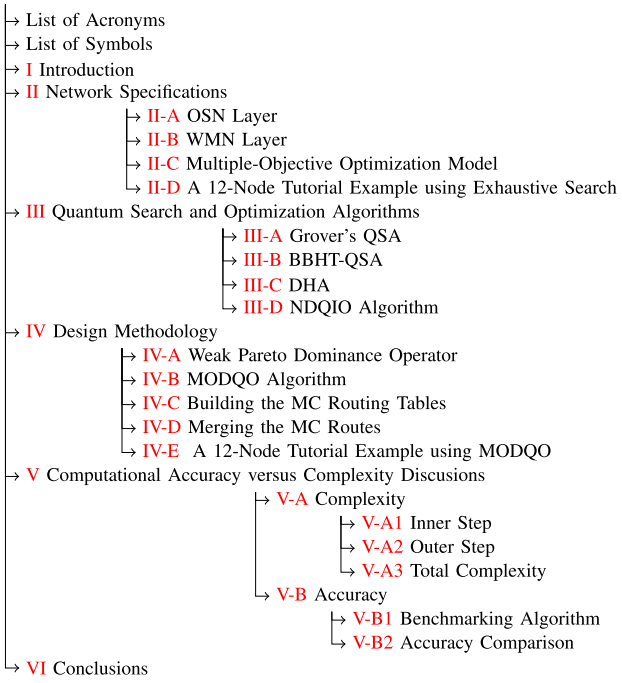

FIGURE 2. The structure of this paper.

Notation: Throughout this paper, the lower (upper) boldface letters represent vectors (matrices), while the superscripts $()^{\dagger}$ and $()^{T}$ denote the complex conjugate and simple matrix or vector transposition, respectively.

Moreover, the upper case italic letters denote the transfer matrices of quantum unitary operators. A single subscript in the quantum register state is used for the global quantum registers of the quantum circuit, whereas two subscripts, separated by comma, are used for the local quantum registers. Additionally, in the discussion of the algorithms the notation "Step $X.Y$" is used, in order to refer to the Y-th step of the X-th algorithm.

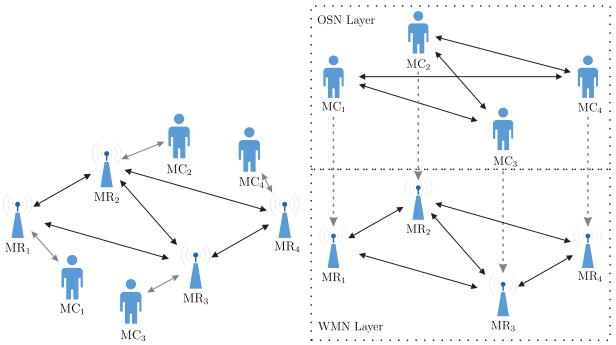

FIGURE 3. (a) Exemplified topology with $N_{MC} = 4$ MCs and $N_{MR} = 4$ MRs for the twin-layer network considered and (b) presentation of the two layers of (a). In the OSN layer the arrows among the MCs manifest their friendship status, whereas in the WMN layer the resective arrows correspond to links satisfying the QoS criteria. The gray-colored arrows denote the association of each MC with a specific MR.

II. NETWORK SPECIFICATIONS

We have considered a twin-layer network, which is shown in Fig. 3. To elaborate further, the network is comprised by a set of N_{MC} users, which from now on will be referred to aS *Mesh Clients* (MCs) and by a set of N_{MR} wireless *Mesh Routers* (MRs). The latter form the backbone of a *Wireless Mesh Network* (WMN), which supports the communications among the MCs. The WMN constitutes the bottom layer of our network. On the other hand, the MCs are assumed to exhibit a specific social behavior and, hence, they form an OSN, which incorporates the upper layer of our network.

The locations of both the MCs and of the MRs are assumed to be random, obeying a uniform distribution within a (100×100) m^2 square block, which is the network's coverage area we considered for this scenario, for the sake of approaching a the fully-connected scenario for in the WMN layer. Additionally, each of the MCs is exclusively served by its closest MR, as denoted by the gray arrows in Fig 3.

As far as the packet dissemination process is concerned, we have assumed that the source and destination nodes belong exclusively to the set of MCs. Therefore, the MRs of the WMN layer can only act as intermediate relays forwarding the packets of the source MC to the destination MC. Furthermore, the communication between MCs is only feasible via MRs. For instance, let us consider the case, where MC_1 has to send a packet to MC_3. Despite the fact that in Fig. 3a MC_1 and MC_3 are pretty close to each other, their communication can only be realized through MR_1 and MR_3. Hence, the shortest route in terms of the number of hops that the packet can follow is the route $MC_1 \rightarrow MR_1 \rightarrow MR_3 \rightarrow MC_3$. We note that our twin-layer network parameters are summarized in Table 1.

TABLE 1. Twin layer network parameters.

Description	Parameter
Coverage Area	(100×100) m^2 Square Block
Number of MRs	$N_{MR} = \{5, 6, 7, 8, 9, 10\}$ MRs
Number of MCs	$N_{MC} = \{2, 4, 8, 16\}$ MCs
Social Relationship	Karate Club Members [50]
Max. Trans. Power	$P_{\max}^{t,act} = 20$ dBm
Carrier Frequency	$f_c = 2.4$ GHz
Trans. Bandwidth	$W = 10$ MHz
AWGN PSD	$N_0 = -174$ dBm/Hz
Reference Distance	$d_0 = 1$ m
Path-loss Exponent	$\alpha = 3$
Modulation	QPSK
BER Threshold	$P_e^{th} = 0.01$, uncoded
Max. Tol. Interfernce	$I_{\max} = \{-83.96, -83.06, -82.25, -81.61, -81.01, -80.25\}$ dBm
Avg. MR Degree	$\{3.28,\ 3.81,\ 4.26, 4.72, 5.08, 5.32\}$ MRs

Having defined the basic topology of the twin-layer network considered in our case study, let us now proceed with a brief description of the two layers comprising the network.

A. OSN LAYER

As we have mentioned in the previous subsection, the MCs exhibit social behavior increasing the probability of their communication with a specific set of other MCs. This set of MCs is often referred to in WSN terminology as *friends*. Hence, the MCs' friendship status can be modeled by the binary friendship matrix $\mathcal{F}_{MC}$ that defines the set of MCs being friends to a specific MC. Naturally, the friendship matrix $\mathcal{F}_{MC}$ is symmetric, with all the elements of its diagonal being equal to zero. Equivalently, since each MC is associated with a specific MR, a binary friendship matrix $\mathcal{F}_{MR}$ may be defined in the context of MR as a cross-layer metric. The elements $\mathcal{F}_{MR,ij}$ of the latter matrix indicate whether MR_i and MR_j are associated with a pair of MCs having a friendship relationship. We note that the $\mathcal{F}_{MR}$ matrix is also symmetric; however, its diagonal elements may not be strictly equal to zero, corresponding the scenario where two friendly MCs are associated with the same MR.

As for generating the $\mathcal{F}_{MC}$ matrix, we have utilized the well-studied social relationship of the *Karate Club* for the sake of practicality, which was proposed by Zachary [50] and is portrayed in Fig 4. To elaborate further, the MCs are randomly generated similarly to the members of the *Karate Club*, while the sole constraint imposed is that of having a connected social graph for the sake of avoiding the potential isolation of certain MCs. In this way, packet dissemination emerging from a specific MC to the rest of the MCs is enabled, regardless of whether they have a friendship relationship by forwarding a packet in a friend-by-friend basis.

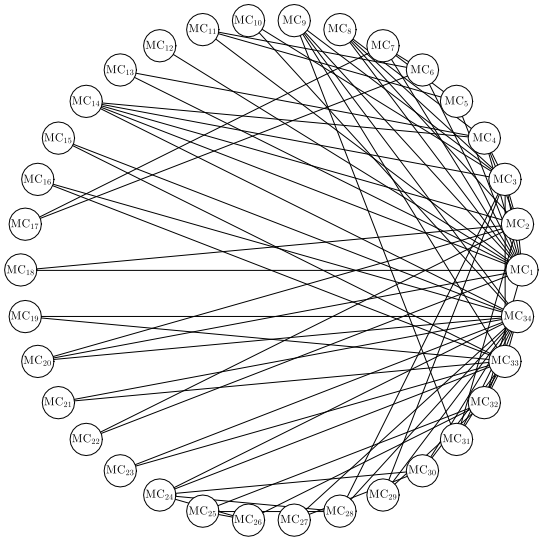

FIGURE 4. Complete karate club social relationship [50] used for determining the social relationship of the MCs in the OSN layer.

As mentioned in the introduction, the social behavior of the MCs provides us with the capability of employing SNA tools for analyzing the performance of socially-aware networks. In fact, the *betweenness centrality* B_{sin} metric has been proposed by Freeman in [51] for quantifying the information flow of each node MR_k of the WMNs. In this context, each node has been considered to have a social friendship with the specific nodes it can reliably communicate with using a single hop. The betweenness centrality metric actually quantifies the usage of each node MR_k as an intermediate relay. Explicitly, the *betweenness centrality* B_{sin} is defined as [51]:

$$B_{sin}(MR_k) = \sum_{\substack{i=1 \\ i \neq k}}^{M} \sum_{\substack{j=1 \\ j \neq i,k}}^{M} \frac{g_{MR_i,MR_j}(MR_k)}{g_{MR_i,MR_j}}, \tag{1}$$

where $g_{MR_i,MR_j}(MR_k)$ represents the number of times the node MR_k is involved in the shortest routes - in terms of the number of hops - spanning from the node MR_i to the node MR_j, while g_{MR_i,MR_j} denotes the number of the optimal routes and M corresponds to the total number of MRs. We note that the *normalized betweenness centrality* $\bar{B}_{sin}(MR_k)$, defined in Eq. (2), corresponds to the probability of MR_k being used as a relay and it is formulated as:

$$\bar{B}_{sin}(MR_k) = B_{sin}(MR_k) / \sum_{i=1}^{M} B_{sin}(MR_i). \tag{2}$$

We can adapt the *betweenness centrality* to the context of twin-layer networks by defining the so-called *composite betweenness centrality*. For the later, the friendship relationship is defined in a rather generic manner. To elaborate further, since the links between MCs that share a friendship are established on a exclusive basis, the *composite betweenness centrality* calculation is restricted to these specific routes. Therefore, the *composite betweenness centrality* $B_{com}(MR_k)$ is defined as [52]

$$B_{com}(MR_k) = \sum_{i=1}^{N_{MC}} \sum_{\substack{j=1 \\ j \neq i}}^{N_{MC}} \frac{g_{MC_i,MC_j}(MR_k)}{g_{MC_i,MC_j}} \mathcal{F}_{MC_i,MC_j}, \tag{3}$$

where $\mathcal{F}_{MC_i,MC_j}$ denotes the friendship relationship between MC_i as well as MC_j and it is equal to the element of the i-th row and the j-th column of the $\mathcal{F}_{MC}$ matrix. Additionally, the term $g_{MC_i,MC_j}(MR_k)$ corresponds to the number of optimal routes between MC_i and MC_j involving MR_k, while g_{MC_i,MC_j} is the total number of optimal routes for the same source and destination pair. Equivalently to the *normalized betweenness centrality*, the *normalized composite betweenness centrality* $\bar{B}_{com}(MR_k)$ quantifies the probability of a specific MR_k being used as an intermediate relay, in the context of the socially-aware network considered. The latter metric is defined as:

$$\bar{B}_{com}(MR_k) = B_{com}(MR_k) / \sum_{i=1}^{M} B_{com}(MR_i). \tag{4}$$

The vector $\bar{B}_{com}$ contains the probability distribution of the specific MRs being used as intermediate relays. Therefore, instead of optimizing a specific parameter, such as the sum-rate considered in [53], we can readily manipulate this distribution by selecting the appropriate routes. To guarantee fairness in terms of the forwarded tele-traffic load amongst the MRs, we will consider to be the desired set of route-solutions those that result in the normalized composite betweenness $\bar{B}_{com}$ approaching the uniform distribution.

A direct approach of equally distributing the relayed load amongst the MRs would be to minimize the standard deviation $\sigma_{\bar{B}_{com}}$ of the normalized composite betweenness. Nevertheless, there exist cases, where none of the active routes utilizes intermediate MRs, which results in an all-zero normalized composite betweenness distribution, i.e. we have $\bar{B}_{com}(MR_k) = 0, \forall k \in \{1, \ldots, N_{MR}\}$. This kind of distribution yields a standard deviation equal to $\sigma_{\bar{B}_{com}} = 0$, which is optimal; however, these route-solutions often exhibit poor performance in terms of their power consumption or BER.

Therefore we will propose a novel metric, namely the *normalized entropy* $\bar{H}(\bar{B}_{com})$ of the normalized composite betweenness, which is defined as follows:

$$\bar{H}(\bar{B}_{com}) = \frac{H(\bar{B}_{com})}{\log_2(N_{MR})}, \tag{5}$$

where $H(\bar{B}_{com})$ corresponds to the Shannonian entropy, which is defined as follows [54]:

$$H(\bar{B}_{com}) = \sum_{k=1}^{N_{MR}} \bar{B}_{com}(MR_k) \log_2[\bar{B}_{com}(MR_k)]. \tag{6}$$

We note that the normalization factor of Eq. (5) is used to make the normalized entropy value independent of the number of MRs, N_{MR} and bounds its value to the range [0, 1]. Explicitly, the entropy of a distribution can be viewed

as a metric of proximity of a specific distribution to the uniform one. This could be justified by the fact that the entropy of a specific distribution is inversely proportional to the *Kullback-Leibler divergence* $D_{KL}(\bar{B}_{com}||U)$ [55], where U denotes the uniform distribution of N_{MR} events. This is formally expressed as follows [56]:

$$H(\bar{B}_{com}) = \log_2(N_{MR}) - D_{KL}(\bar{B}_{com}||U), \tag{7}$$

where the Kullback-Leibler divergence $D_{KL}(\bar{B}_{com}||U)$ is defined as [56]:

$$D_{KL}(\bar{B}_{com}||U) = \sum_{k=1}^{N_{MR}} \bar{B}_{com}(MR_k) \log_2 \left[\frac{\bar{B}_{com}(MR_k)}{U(MR_k)} \right]. \tag{8}$$

Explicitly, it has been proven by Hobson [57] that the Kullback-Leibler divergence constitutes an appropriate metric of the difference between two different distributions. Hence, based on Eq. (8) the value of the divergence for the distributions $\bar{B}_com$ and U is bound to the range $[0, \log_2(N_{MR})]$. The upper bound of this region denotes complete divergence of the examined distributions, while its lower bound yields a perfect convergence of the two distributions. This can equivalently be translated into normalized entropy $\bar{H}(\bar{B}_{com})$ terms, where the perfect matching of the normalized composite betweenness distribution and the uniform one is achieved, when we have $\bar{H}(\bar{B}_{com}) = 1$, whereas they are uncorrelated when $\bar{H}(\bar{B}_{com}) = 0$. This metric circumvents the problem of the all-zero normalized composite betweenness distribution, since in this case its normalized entropy is equal to $\bar{H}(\bar{B}_{com}) = 0$. Therefore, efficient load balancing relies upon the maximization of the normalized entropy, leading to the optimization problem in terms of the active routes S formulated as:

$$\underset{\forall S}{\text{argmax}} \ \bar{H}\left[\bar{B}_{com}(S)\right]. \tag{9}$$

Observe that the optimization problem of Eq. (9) is unconstrained, and hence it does not take into account any other QoS criteria, such as the network delay or power consumption. This results in the route-solutions defined by Eq. (9) that either exhibit excessive delay or excessive power consumption or cannot be established at all owning to a maximum transmit power violation. In fact, the aforementioned QoS criteria, which stem from the WMN layer, are presented in the next subsection. From a cross-layer optimization perspective, they will be encapsulated in Eq. (9) in the form of a set of constraints, for the sake of guaranteeing an optimal performance in terms of the QoS criteria considered.

B. WMN LAYER

As mentioned at the beginning of this Section, the WMN layer is constituted by that specific set of the MRs, which facilitate communications among the MCs by forwarding the respective packets, as portrayed in the bottom layer of Fig. 3. Their locations are random, which is typical for an ad hoc deployment, but then are considered to be stationary. By contrast the MCs are mobile. Additionally, a rather strong *Line-of-Sight* (LoS) component [58] is assumed to be encountered by each MR to MR link and, thus, only the link's path-loss is taken into account. The path-loss $L_{i,j}$ for a link between MR_i and MR_j is calculated using the classic *Path-Loss Model*, which is formally formulated as [59]:

$$L_{i,j} \equiv \frac{P^t_{i,j}}{P^r_{i,j}} = L_0 \left(\frac{d_{i,j}}{d_0} \right)^{\alpha}, \tag{10}$$

where α corresponds to the *path-loss exponent*. Explicitly we set $\alpha = 3$, where $d_{i,j}$ is the Euclidean distance between MR_i and MR_j, while L_0 denotes the reference path-loss at the reference distance $d_0 = 1$ m and $P^r_{i,j}$ and $P^t_{i,j}$ denote the transmitted and received power, respectively. The reference path-loss L_0 is quantified using the free-space path-loss formula [58] of:

$$L_0 = \left(\frac{4\pi d_0 f_c}{c} \right)^2, \tag{11}$$

where f_c is the carrier frequency, which is set to $f_c = 2.4$ GHz and c corresponds to the speed of light.

As far as the forwarding scheme is concerned, we have utilized the *Decode-and-Forward* (DF) scheme [42], [60] due to the scheme's capability of encapsulating the routing information into the packet header. In this context, the modulation scheme adopted was QPSK [59]. As for the transmission environment, the links among the MRs are subjected to only *Additive White Gaussian Noise* (AWGN), while the links between the MCs and their associated MRs are established for transmission over *Rayleigh Fading* channels [58]. Additionally, we have adopted an adaptive power control scheme, where each link, either between two MRs or between MCs and their associated MRs, can be successfully established as long as the link's *Bit Error Ratio* (BER) is lower than a certain threshold P^{th}_e. This constraint is imposed for the sake of guaranteeing that the packets are successfully recovered from the intermediate MRs, hence mitigating the need for retransmission. In our scenario, we have set this BER threshold to $P^{th}_e = 10^{-2}$, which corresponds to the uncoded BER of each link, because powerful state-of-the-art channel coding schemes a capable of further reducing the BER to infinitesimally low values [59]. Therefore, at each link we will attempt to match the link BER value to that of its threshold, hence minimizing the potential interference experienced by the rest of the nodes owing to excessive interferences. This yields an equivalent *Signal to Noise plus Interference Ratio* (SINR) threshold $\gamma^{th}_{i,j}$, which is equal to:

$$\gamma^{th}_{i,j} = \frac{P^r_{i,j}}{N_0 + I_{\max}} = \begin{cases} \dfrac{2(1-2P^{th}_e)^2}{1-(1-2P^{th}_e)^2} & i \text{ or } j \text{ are MCs}, \\ Q^{-1}\left(P^{th}_e\right) & \text{otherwise}, \end{cases} \tag{12}$$

where the function $Q^{-1}(\cdot)$ corresponds to the inverse of the Q-function, N_0 is the thermal noise power and $I_{\max}$ is the maximum tolerable interference power level. The thermal noise power is set to $N_0 = -114$ dBm, corresponding to a bandwidth of $W = 1$ MHz. Therefore, based on Eqs. (10) and (12)

the transmit power $P_{i,j}^{t,req}$ required for satisfying the BER threshold is equal to:

$$P_{i,j}^{t,req} = L_{i,j}(N_0 + I_{\max})\gamma_{i,j}^{th}. \quad (13)$$

We have imposed a further constraint regarding the actual transmitters' maximum power level $P_{i,j}^{t,act}$. In fact, it is considered to be upper-bounded to $P_{\max}^{t,act} = 20$ dBm, which is a typical value for the IEEE 802.11b/g protocol. Based on this constraint, we can define the *adjacency matrix A* as follows:

$$a_{i,j} = u(P_{i,j}^{t,req} - P_{\max}^{t,act}), \quad (14)$$

where $a_{i,j}$ corresponds to the element of the matrix A located at the i-th row and the j-th column, while $u(\cdot)$ is the Heaviside function defined in [61]. Therefore, the actual transmitted power $P_{i,j}^{t,act}$ required for establishing the link between the nodes i and j is equal to:

$$P_{i,j}^{t,act} = P_{i,j}^{t,req}/a_{i,j}. \quad (15)$$

Based on Eq. (15), the cost in terms of power for the link spanning from the i-th node to the j-th one will be equal to the power required for achieving a BER equal to the threshold value should the required power be less or equal to the maximum transmit power value. Otherwise, the cost is set to $+\infty$, implying that the link cannot be established.

As far as the maximum tolerable interference power level I_{max} is concerned, it is defined as the maximum interference level that allows the MRs to establish at least a single link with the rest of the WMN with a probability of 99%. Therefore, its value can be determined from the CDF of the connectivity of MRs versus the value of I_{max}. The $I_{\max}$ values guaranteeing 99% connectivity and associated with socially-aware networks consisting of 5 to 10 MRs are presented in Table 1 along with the MRs' average connectivity degree. Explicitly, observe in Table 1 that the $I_{\max}$ value decreases as the WMN becomes more densely populated by MRs due to the inherent decrease in the minimum distance between the MRs. As for their degree corresponding to $I_{\max}$, it increases as the number of MRs increases ; however, the WMN becomes more sparsely connected than the fully-connected case scenario. The latter justifies the employment of a routing scheme, since a heuristic method has to be employed for identifying the realizable routes, i.e. routes consisting of links that can be established, based on the adjacency matrix A.

Having defined the physical layer parameters of the WMN layer, let us now proceed by defining our multiple-objective optimization problem. Firstly, let us consider the set of N_r active routes $S = \left[x^{(1)}, \ldots, x^{(i)}, \ldots, x^{(N_r)}\right]$, where $x^{(i)}$ is the i-th active route and corresponds to a unique pair of MCs. Since each MC is associated with a unique MR, each active route is defined as follows:

$$x^{(i)} = [MC_k, MR_l, \ldots, MR_m, MC_n], \quad (16)$$

where the i-th active route corresponds to a transmission from MC_k to MC_n, while the source and destination MCs are associated with MR_l and MR_m, respectively. As our first objective, we will consider the average route delay D, which is quantified as follows:

$$D(S) = \sum_{i=1}^{N_r} \frac{D^{(i)}(S)}{N_r}, \quad (17)$$

where S is the set of the active routes and $D^{(i)}(S)$ corresponds to the delay of the i-th active route. For the sake of simplicity, we have chosen to quantify the latter as the number of hops incorporated by the route $x^{(i)}$. Hence, the route delay $D^{(i)}(S)$ is formulated as follows:

$$D^{(i)}(S) = \sum_{j=1}^{|x^{(i)}|-1} \left(a^{-1}_{x_j^{(i)},\, x_{j+1}^{(i)}}\right) - 1, \quad (18)$$

where the factor $\left|x^{(i)}\right|$ denotes the number of nodes involved by the route $x^{(i)}$, while $x_j^{(i)}$ corresponds to the route's j-th node. Observe in Eq. (18) that the sum of the inverse of the adjacency matrix elements guarantees that all the route's links can be established. Otherwise, the route delay will be set to $D^{(i)}(S) = +\infty$, hence classifying the route $x^{(i)}$ as infeasible. We note that the nodes' specific buffer packet length could be readily encapsulated in Eq. (18) in order to account for delays the imposed by buffered packets.

Apart from the average delay D, we have also considered the routes' average power consumption P, which is quantified as follows:

$$P(S) = \sum_{i=1}^{N_r} \frac{P^{(i)}(S)}{N_r}, \quad (19)$$

where $P^{(i)}(S)$ corresponds to the power consumption of the route $x^{(i)}$, which is in turn formulated based on Eq. (15) as follows:

$$P^{(i)}(S) = \sum_{j=1}^{|x^{(i)}|-1} P^{t,act}_{x_j^{(i)},\, x_{j+1}^{(i)}}. \quad (20)$$

Observe in Eq. (20) that the adjacency matrix elements $a^{-1}_{x_j^{(i)},\, x_{j+1}^{(i)}}$ are taken into account in Eq. (20) with the aid of Eq. (15). Explicitly, a route comprised by links that cannot guarantee satisfying the BER threshold will require a power set to $P^i(S) = +\infty$, based on Eq. (20). This is in line with the route's delay, which is at the same time set to $+\infty$. Therefore, we have encapsulated the BER constraint in both of our optimization objectives, which we will refer to as *Utility Functions* (UF). Based on these UFs let us now define the optimization *Utility Vector* (UV), which we will use for jointly optimizing both the average delay and the average power consumption, as follows:

$$\mathbf{f}(x^{(1)}, \ldots, x^{(N_r)}) \equiv \mathbf{f}(S) = [D(S), P(S)]. \quad (21)$$

C. MULTIPLE-OBJECTIVE OPTIMIZATION MODEL

The evaluation of the UV used for quantifying the performance of the twin-layer network considered can be undertaken with the aid of the *Pareto Dominance* concept [33],

which is encapsulated in Definitions 1 and 2, while the corresponding *Pareto-optimality* conditions are given in Definitions 3 and 4. We note that Definitions 1 and 2 are tailored for jointly minimizing the UFs, since our design objective is to establish the active routes with the minimum possible average delay and power consumption. Nevertheless, they can be readily invoked for maximization problems by substituting the "less (than)" operators by "greater (than)".

Definition 1 (Weak Pareto Dominance [33]): A particular solution x_1, associated with the UV $\mathbf{f}(x_1) = [f_1(x_1), \ldots, f_K(x_1)]$, where K corresponds to the number of optimization objectives, is said to weakly dominate another solution x_2, associated with the UV $\mathbf{f}(x_2) = [f_1(x_2), \ldots, f_n(x_2)]$, iff $\mathbf{f}(x_1) \succeq \mathbf{f}(x_2)$, i.e. we have $f_i(x_1) \leq f_i(x_2)\ \forall i \in \{1, \ldots, K\}$ and $\exists j \in \{1, \ldots, K\}$ such that $f_j(x_1) < f_j(x_2)$.

Definition 2 (Strong Pareto Dominance [33]): A particular solution x_1, associated with the UV $\mathbf{f}(x_1) = [f_1(x_1), \ldots, f_K(x_1)]$, where K corresponds to the number of optimization objectives, is said to strongly dominate another solution x_2, associated with the UV $\mathbf{f}(x_2) = [f_1(x_2), \ldots, f_K(x_2)]$, iff $\mathbf{f}(x_1) \succ \mathbf{f}(x_2)$, i.e. we have $f_i(x_1) < f_i(x_2)\ \forall i \in \{1, \ldots, K\}$.

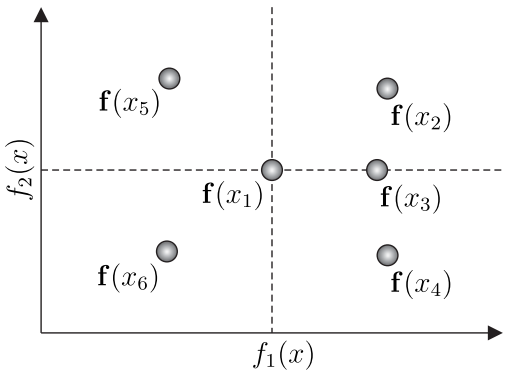

FIGURE 5. A graphical example portraying the dominance relationship of the route-solutions $\{x_i\}_{i=2}^{6}$ with respect to the route-solution x_1 for a generic Pareto-optimality problem with $K = 2$ UFs.

Let us now describe the use of the weak and strong Pareto dominance, encapsulated in Defs. 1 and 2, respectively, with the aid of a graphical example, which is shown in Fig. 5. We note that the example presented in Fig. 5 portrays a Pareto-optimality problem associated with $K = 2$ UFs. As a reference, we use the route-solution x_1, which is associated with the UV $\mathbf{f}(x_1)$, and we will assess its dominance relationship with respect to the route-solutions $\{x_i\}_{i=2}^{6}$, which are associated with the UVs $\{\mathbf{f}(x_i)\}_{i=2}^{6}$. It is clear that the route-solution x_2 is both strongly and weakly dominated by the route-solution x_1, since we have $f_i(x_1) < f_i(x_2)$, $\forall i \in \{1, 2\}$. The difference between strong and weak Pareto dominance becomes visible, when we assess the dominance relationship between the route-solution x_3 and that of x_1. Since we have $f_1(x_1) = f_1(x_3)$, there is no strong dominance relationship between those two route-solutions; however, x_1 weakly dominates x_3, since we have $f_2(x_1) < f_2(x_3)$. Explicitly, the solution x_1 weakly dominates all the potential route-solutions that lie in the plane defined by the boundaries $[f_1(x_1), +\infty]$ and $[f_2(x_1), +\infty]$ including the boundaries, while it does not strongly the boundaries. As for the rest of the route-solutions shown in Fig. 5, there is no dominance relationship among x_1, x_4 and x_5, since we have $f_1(x_5) < f_1(x_1) < f_1(x_4)$, while $f_2(x_5) > f_2(x_1) > f_2(x_4)$. Finally, the route-solution x_6 dominates, both weakly and strongly, the route-solution x_1, since we jointly have $f_1(x_6) < f_1(x_1)$ and $f_2(x_6) < f_2(x_1)$.

Definition 3 (Weak Pareto-Optimality [33]): A particular solution x_i, associated with the UV $\mathbf{f}(x_i) = [f_1(x_i), \ldots, f_N(x_i)]$, where N corresponds to the number of optimization objectives, is considered as strongly (or weakly) Pareto-optimal iff there exist no solution that strongly dominates x_i, i.e. iff $\nexists x_j$ such that $\mathbf{f}(x_j) \succ \mathbf{f}(x_i)$.

Definition 4 (Strong Pareto-Optimality [33]): A particular solution x_i, associated with the UV $\mathbf{f}(x_i) = [f_1(x_i), \ldots, f_N(x_i)]$, where N corresponds to the number of optimization objectives, is considered as strongly Pareto-optimal iff there exist no solution that weakly dominates x_i, i.e. iff $\nexists x_j$ such that $\mathbf{f}(x_j) \succeq \mathbf{f}(x_i)$.

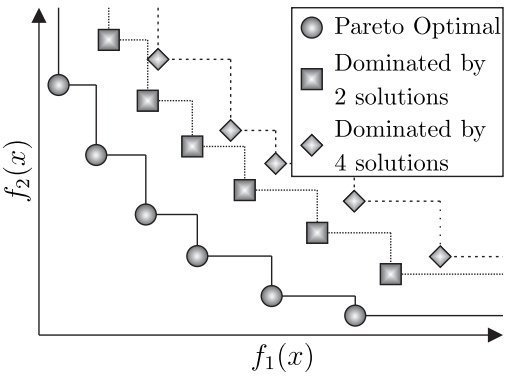

FIGURE 6. Distribution of the route-solutions into fronts based on the number of route-solutions that dominate a specific route-solution for a generic Pareto-optimality problem with $K = 2$ UFs.

Based on Definitions 1 and 2, it is possible to group the route-solutions based on the number of route-solutions that dominate them. Such groups of route-solutions form fronts in the solution space, which are often referred to as *Pareto Fronts* (PF). Naturally, the entire set of Pareto-optimal route-solutions will form a single PF, since all of these route-solutions share the characteristic of being either strongly or weakly dominated by no route-solution, based on Definitions 3 and 4,respectively. We note that this specific front is often referred to as the *Optimal Pareto Front* (OPF). A graphical example of the formation of various PFs is presented in Fig. 6 for a generic minimization Pareto-optimality problem associated with $K = 2$ UFs. Still referring to the same figure, observe that the curves formed by the route-solutions of a specific PF dominate the respective curves associated with higher rank PFs, i.e. PFs formed by route-solutions that are dominated by a higher number of route-solutions.

Explicitly, the OPF is composed by route-solutions having UFs, which cannot be further optimized individually without degrading the fitness of the rest of the UFs, as it can be observed in Fig. 6. As far as our specific application is concerned, when considering weak OPFs, there exist route-solutions classified as Pareto-optimal which may have the same metric, say in terms of their average delay D, yet exhibiting a different performance in terms of their average power consumption P. Nevertheless, the route-solution that exhibits lower average power consumption seems to outperform the other one, since it jointly minimizes both UFs. This specific caveat is rectified by the employment of strong Pareto-optimality, since the route-solution associated with lower average power consumption would dominate the other route-solution and, hence, the latter will not be included in the respective OPF. Based on this observation, we will utilize the concept of strong Pareto-optimality for the sake of constraining the load balancing problem, which is formulated in Eq. (9). Consequently, our optimization problem is formulated as follows:

$$S^{\text{OPF}} = \underset{\forall S_i \in S_{legit}}{\text{argmax}} \ \bar{H}(\bar{B}_{com}(S_i)), \quad \text{subject to } \nexists j: \ \mathbf{f}(S_j) \succeq \mathbf{f}(S_i), \tag{22}$$

where S^{OPF} represents the optimal active route allocation based on our constrained optimization problem and S_{legit} corresponds to the set containing all the potential sets of active routes, which are strictly comprised by individual Hamiltonian routes, i.e. by routes that visit each of the MRs at most once. In a nutshell, the optimization problem of Eq. (22) attempts to distribute the intermediate relay tele-traffic load among the MRs as close as possible to the ideal uniformly distributed load, whist ensuring that the associated network performance is Pareto-optimal in terms of its average delay and power consumption. Assuming a total number of MRs is equal to N_{MR}, the total number N of Hamiltonian routes for a specific pair source and destination MCs is given by [42]:

$$N = \sum_{i=0}^{N_{MR}-2} \frac{(N_{MR}-2)!}{(N_{MR}-2-i)!}. \tag{23}$$

Therefore, for the sake of verifying as to whether a single set of active routes satisfies the optimization problem constraint, we have to perform precisely N Pareto dominance comparisons. Let us now consider that the total number of pairs of source and destination MCs is exactly $N_r = |S|$. Then the total number N_{tot} of sets of active routes is given by:

$$N_{tot} = N^{N_r} = \left[\sum_{i=0}^{N_{MR}-2} \frac{(N_{MR}-2)!}{(N_{MR}-2-i)!} \right]^{N_r}. \tag{24}$$

Since it can be observed in Eq. (24) that the total number of the sets of active routes N_{tot} increases exponentially as the number of MRs N_{MR} increases, our constrained optimization problem defined in Eq. (22) is classified as NP-hard. Consequently, sophisticated quantum-assisted methods are required for the sake of confining the escalating complexity.

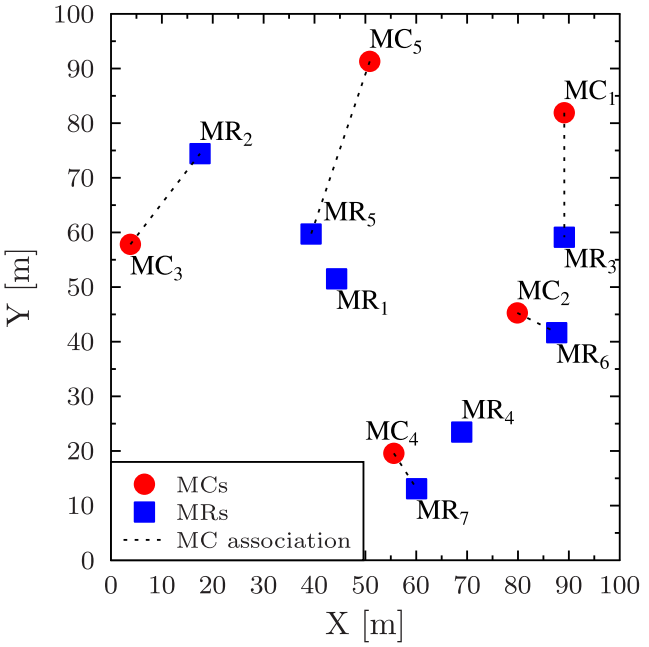

FIGURE 7. Exemplified twin-layer network topology with $N_{\text{MC}} = 5$ MCs and $N_{\text{MR}} = 7$ MRs for a coverage area of (100 × 100) m^2 square block. The association of a specific MC with a specific MR is annotated using the dashed lines. The presence of a central inteligence cluster head node is assumed, albeit not portrayed in this figure.

D. A 12-NODE TUTORIAL EXAMPLE USING EXHAUSTIVE SEARCH

In the context of this tutorial, let us consider the twin-layer network comprised by $N_{\text{MR}} = 7$ MRs and $N_{\text{MC}} = 5$ MCs, which relies on the topology portrayed in Fig. 7, where the association of each of the MCs to their respective MR is represented by the dashed lines connecting each of the MCs to their closest MR. We may consider this topology as a random snapshot of our general network topology, where the MCs are mobile, whilst the MRs are considered to be static.

The transmission power matrix $P^{t,act}$ defined in Eq. (15) for the exemplified topology of Fig. 7 is shown in Table 2, where we can observe that the transmission power levels of several links are set to infinity, indicating that the specific links are infeasible. We note that the elements of the transmission power matrix $P^{t,act}$ in Table 2 are quantified in dBm. Naturally, the transmission power of the links among the MCs is set to infinity, since they cannot directly communicate with each other, only through their associated MRs. Additionally, observe in Table 2 that for the links established between a specific MC and the MRs, there exists only a single link having a finite transmission power, owing to the constraint that a specific MC can only connect to the rest of the network through its closest MR. As far as the links among the MRs are concerned, recall that according to Table 1 the links requiring a transmission power of infinity are unable to satisfying the BER threshold of $P_e^{th} = 10^{-2}$ at the maximum transmission power $P_{\max}^{t,act} = 20$ dBm.

Having presented the specifics of the tutorial example WMN layer, let us now proceed by elaborating on the details

TABLE 2. Transmission power matrix $P^{t,act}$ quantified in dBm for the exemplified topology of Fig. 7.

src \ dst	MC_1	MC_2	MC_3	MC_4	MR_5	MR_1	MR_2	MR_3	MR_4	MR_5	MR_6	MR_7
MC_1	Inf	Inf	Inf	Inf	Inf	Inf	Inf	5.89	Inf	Inf	Inf	Inf
MC_2	Inf	Inf	Inf	Inf	Inf	Inf	Inf	Inf	Inf	Inf	-6.89	Inf
MC_3	Inf	Inf	Inf	Inf	Inf	Inf	5.15	Inf	Inf	Inf	Inf	Inf
MC_4	Inf	Inf	Inf	Inf	Inf	Inf	Inf	Inf	Inf	Inf	Inf	-7.97
MC_5	Inf	Inf	Inf	Inf	Inf	Inf	Inf	Inf	Inf	10.96	Inf	Inf
MR_1	Inf	Inf	Inf	Inf	Inf	Inf	11.59	14.87	12.31	-5.35	14.57	13.71
MR_2	Inf	Inf	5.15	Inf	Inf	11.59	Inf	Inf	Inf	7.77	Inf	Inf
MR_3	5.89	Inf	Inf	Inf	Inf	14.87	Inf	Inf	13.53	16.08	2.48	17.24
MR_4	Inf	Inf	Inf	Inf	Inf	12.31	Inf	13.53	Inf	15.27	7.64	-0.78
MR_4	Inf	Inf	Inf	Inf	10.96	-5.35	7.77	16.08	15.27	Inf	16.53	16.39
MR_6	Inf	-6.89	Inf	Inf	Inf	14.57	Inf	2.48	7.64	16.53	Inf	13.12
MR_7	Inf	Inf	Inf	-7.97	Inf	13.71	Inf	17.24	-0.78	16.39	13.12	Inf

of its OSN layer. As we have mentioned in Subsec. II-A, the MCs exhibit an identical social relationship to that of the members of a Karate Club, which is portrayed Fig. 4. Based on this relationship, we have randomly picked 5 Karate Club members, whose social relationship can be encapsulated in the following MC friendship matrix $\mathcal{F}_{\text{MC}}$:

$$\mathcal{F}_{\text{MC}} = \begin{bmatrix} 0 & 1 & 1 & 1 & 1 \\ 1 & 0 & 0 & 0 & 1 \\ 1 & 0 & 0 & 0 & 0 \\ 1 & 0 & 0 & 0 & 0 \\ 1 & 1 & 0 & 0 & 0 \end{bmatrix}, \tag{25}$$

where we can observe that the MC_1 shares a social relationship with all the remaining MCs, MC_2 shares a social relationship with MC_1 and MC_5, MC_3 and MC_4 share a social relationship solely with MC_1, while MC_5 has a social relationship with both MC_1 as well as MC_2. Based on the friendship relationship $\mathcal{F}_{\text{MC}}$ of Eq. (25), we will consider in this tutorial the following set S^{act} of active source and destination pairs:

$$S^{\text{act}} = \left\{ \begin{matrix} MC_2 \rightarrow MC_1 \\ MC_1 \rightarrow MC_3 \\ MC_4 \rightarrow MC_1 \\ MC_5 \rightarrow MC_1 \\ MC_2 \rightarrow MC_5 \end{matrix} \right\}. \tag{26}$$

In our scenario, there exists $N = 326$ Hamiltonian routes between each specific source and destination MCs, based on Eq. (23), while there exist about $N_{tot} = N^5 \simeq 3.682 \cdot 10^{12}$ legitimate route-combinations in total, based on Eqs. (24) and (55). The exhaustive search method relies upon evaluating each of the legitimate route-combinations for the sake of checking as to whether they are strongly Pareto-optimal, hence satisfying the constraint of Eq. (22). Subsequently, if a specific route-combination is identified as being strongly Pareto-optimal, the value of the normalized entropy of its associated normalized composite betweeness is evaluated as well, aiming for identifying the specific route-combination that maximizes this utility. Therefore, the exhaustive search has to carry out N_{tot}^2 weak Pareto-dominance checks just for identifying the strongly Pareto-optimal route-combinations, plus N_{OPF} single-objective comparisons for determining the maximum normalized entropy route-combination, where N_{OPF} is the number of strongly Pareto-optimal route-combinations.

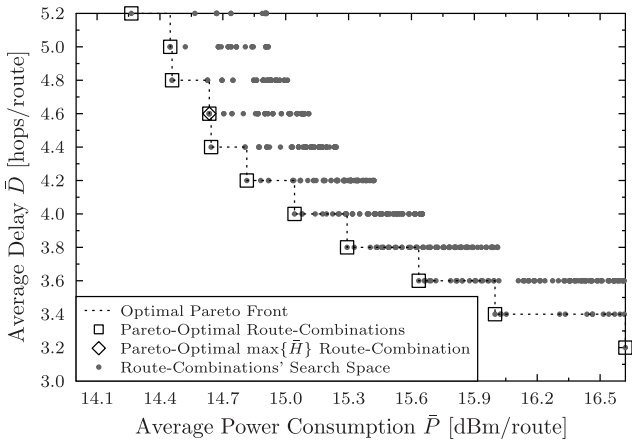

FIGURE 8. Solution space of the route-combinations of the socially-aware network of Fig. 7 in terms of their average power consumtpion $\bar{P}$,quantified in dBm per route, and their average delay $\bar{D}$, quantified in number of hops per route. For the sake of simplicity, we have opted for only portraying the 100 lowest-rank PFs.

The strongly Pareto-optimal routes exported by the exhaustive search are portrayed with the aid of the square markers in Fig. 8 along with the route-combinations belonging to the 100 lowest-rank PFs, which are represented by the dot markers. We note that we have opted for including only the 100 lowest-rank PFs in Fig. 8 for the sake of simplicity. Still referring to the same figure, the specific route-combination that maximizes the normalized entropy of its associated normalized composite betweenness is denoted by the diamond marker. Additionally, a more detailed presentation of the strongly Pareto-optimal route-combinations is included in Table 3, where the Pareto-optimal route-combinations S^{OPF_i}

TABLE 3. Pareto-optimal route-combinations identified by the exhaustive search for the socially-aware network of Fig. 7 corresponding to the OPF seen in Fig. 8. The individual routes $S^{\text{OPF}}_{\text{MC},i,j}$ in the second column are defined in Table 5.

ID	Route-Combination, S	$\bar{D}(S)$	$\bar{P}(S)$	$\bar{H}[\bar{B}_{com}(S)]$	$\max\{\bar{H}[\bar{B}_{com}(S)]\}$	$\text{argmax}\{\bar{H}[\bar{B}_{com}(S)]\}$
S^{OPF}_1	$S^{\text{OPF}}_{\text{MC},1,1}$, $S^{\text{OPF}}_{\text{MC},2,1}$, $S^{\text{OPF}}_{\text{MC},3,1}$, $S^{\text{OPF}}_{\text{MC},4,1}$, $S^{\text{OPF}}_{\text{MC},5,1}$	16.62	3.20	0.000	0.000	S^{OPF}_1
S^{OPF}_2	$S^{\text{OPF}}_{\text{MC},1,1}$, $S^{\text{OPF}}_{\text{MC},2,3}$, $S^{\text{OPF}}_{\text{MC},3,1}$, $S^{\text{OPF}}_{\text{MC},4,1}$, $S^{\text{OPF}}_{\text{MC},5,1}$	16.00	3.40	0.000	0.000	S^{OPF}_1
S^{OPF}_3	$S^{\text{OPF}}_{\text{MC},1,1}$, $S^{\text{OPF}}_{\text{MC},2,3}$, $S^{\text{OPF}}_{\text{MC},3,1}$, $S^{\text{OPF}}_{\text{MC},4,1}$, $S^{\text{OPF}}_{\text{MC},5,1}$	15.63	3.60	0.327	0.327	S^{OPF}_3
S^{OPF}_4	$S^{\text{OPF}}_{\text{MC},1,1}$, $S^{\text{OPF}}_{\text{MC},2,2}$, $S^{\text{OPF}}_{\text{MC},3,3}$, $S^{\text{OPF}}_{\text{MC},4,1}$, $S^{\text{OPF}}_{\text{MC},5,1}$	15.29	3.80	0.534	0.534	S^{OPF}_4
S^{OPF}_5	$S^{\text{OPF}}_{\text{MC},1,1}$, $S^{\text{OPF}}_{\text{MC},2,2}$, $S^{\text{OPF}}_{\text{MC},3,3}$, $S^{\text{OPF}}_{\text{MC},4,1}$, $S^{\text{OPF}}_{\text{MC},5,4}$	15.04	4.00	0.488	0.534	S^{OPF}_4
S^{OPF}_6	$S^{\text{OPF}}_{\text{MC},1,1}$, $S^{\text{OPF}}_{\text{MC},2,2}$, $S^{\text{OPF}}_{\text{MC},3,3}$, $S^{\text{OPF}}_{\text{MC},4,4}$, $S^{\text{OPF}}_{\text{MC},5,4}$	14.81	4.20	0.638	0.638	S^{OPF}_6
S^{OPF}_7	$S^{\text{OPF}}_{\text{MC},1,1}$, $S^{\text{OPF}}_{\text{MC},2,2}$, $S^{\text{OPF}}_{\text{MC},3,3}$, $S^{\text{OPF}}_{\text{MC},4,4}$, $S^{\text{OPF}}_{\text{MC},5,2}$	14.64	4.60	0.679	0.679	S^{OPF}_7
S^{OPF}_8	$S^{\text{OPF}}_{\text{MC},1,1}$, $S^{\text{OPF}}_{\text{MC},2,2}$, $S^{\text{OPF}}_{\text{MC},3,3}$, $S^{\text{OPF}}_{\text{MC},4,2}$, $S^{\text{OPF}}_{\text{MC},5,2}$	14.45	5.00	0.675	0.679	S^{OPF}_7
S^{OPF}_9	$S^{\text{OPF}}_{\text{MC},1,1}$, $S^{\text{OPF}}_{\text{MC},2,2}$, $S^{\text{OPF}}_{\text{MC},3,2}$, $S^{\text{OPF}}_{\text{MC},4,4}$, $S^{\text{OPF}}_{\text{MC},5,4}$	14.64	4.40	0.656	0.679	S^{OPF}_7
S^{OPF}_{10}	$S^{\text{OPF}}_{\text{MC},1,1}$, $S^{\text{OPF}}_{\text{MC},2,2}$, $S^{\text{OPF}}_{\text{MC},3,2}$, $S^{\text{OPF}}_{\text{MC},4,2}$, $S^{\text{OPF}}_{\text{MC},5,4}$	14.46	4.80	0.674	0.679	S^{OPF}_7
S^{OPF}_{11}	$S^{\text{OPF}}_{\text{MC},1,1}$, $S^{\text{OPF}}_{\text{MC},2,2}$, $S^{\text{OPF}}_{\text{MC},3,2}$, $S^{\text{OPF}}_{\text{MC},4,2}$, $S^{\text{OPF}}_{\text{MC},5,2}$	14.26	5.20	0.665	0.679	S^{OPF}_7

are sorted according to their order of being identified as being as Pareto-optimal by the exhaustive method. We note that the database of the route-combinations is constructed by combining the databases combining the individual routes' databases, which are in turn constructed by storing the respective routes in lexicographical ordering using *Lehmer encoding* [42]. Hence, we are able to observe in Table 3 the evolution of the maximum value of the normalized entropy observed by the exhaustive search, which converges to its maximum value for the seventh route-combination S^{OPF_7} of Table 3. Observe in this table that although the maximum value is observed after identifying seven Pareto-optimal route-combinations, the exhaustive search has to identify the entire set of Pareto-optimal route-combinations to classify this value as the maximum observed.

Before delving into the presentation of our proposed algorithm, we provide a brief introduction to the existing quantum search and optimization algorithms, which will constitute the building blocks of our novel algorithm.

III. QUANTUM SEARCH AND OPTIMIZATION ALGORITHMS

In classical computing, the state of a single bit can exclusively be either at the state "0" or at the state "1". By contrast, the state $|\psi\rangle$ of a *quantum bit* (qubit) [47] can be at the superposition of the two basis states, which is formally formulated as $|\psi\rangle = \alpha|0\rangle + \beta|1\rangle$, where $\alpha, \beta \in \mathbb{C}$ and $|\alpha|^2 + |\beta|^2 = 1$. Upon *measurement* [62], the qubit is observed as being in the states of $|0\rangle$ and $|1\rangle$ with probabilities equal to $|\alpha|^2$ and $|\beta|^2$, respectively. However, after the measurement operation the superposition collapses and its *post-mesurement* state becomes equal to the observed state. A qubit's state is manipulated using unitary operators. For instance, the *Hadamard gate* H [47] maps the state $|0\rangle$ to the state $|+\rangle \equiv H|0\rangle = (|0\rangle + |1\rangle)/\sqrt{2}$ and the state $|1\rangle$ to the state $|-\rangle \equiv H|1\rangle = (|0\rangle - |1\rangle)/\sqrt{2}$. Naturally, the employment of these unitary operators combined with the qubits' capability of being at the superposition of their basis states provides a form of parallelism, which is often referred to as *Quantum Parallelism* (QP). Additionally, it is possible to form quantum registers out of individual qubits. Assuming two qubits in the states of $|\psi\rangle_1 = |+\rangle_1$ and $|\psi\rangle_2 = |+\rangle_2$, the resultant composite sytem state $|\psi\rangle_{12}$ is equal to $|\psi\rangle_{12} = |\psi\rangle_1 \otimes |\psi\rangle_2 = (|00\rangle + |01\rangle + |10\rangle + |1\rangle)/2$. If the states of multiple qubits cannot be described separately as in the aforementioned example, the qubits are then termed as *entangled* qubits [47]. Quantum entanglement stems from controlled operators, such as the *Controlled-NOT* (CNOT) gate [47], which has two qubits or registers as its inputs, namely the states $|c\rangle$ and $|t\rangle$, and performs a classical XOR operation of the two inputs, storing the XOR result in the second qubit or register, while leaving the first intact. The CNOT operation is encapsulated by $|c\rangle|t\rangle \xrightarrow{\text{CNOT}} |c\rangle|c \oplus t\rangle$.

Having provided a brief description[6] of the quantum computing postulates [47], let us now proceed with a short introduction to some of the classic *Quantum Search Algorithms* (QSA) [37]–[39], [43], which constitute the building blocks of our novel algorithm.

A. GROVER'S QSA

Grover's QSA [37] is applicable for searching in unsorted or uncorrelated databases, where the value δ sought as well as the number t of solutions are known beforehand. The algorithm is based on a specific unitary operator, namely the so-called *Grover operator* $\mathcal{G}$. This operator is capable of increasing the amplitudes and, hence, the respective probability of finding the valid solutions x, i.e. the solutions that satisfy the condition $f(x) = \delta$, whilst reducing the amplitudes of the invalid solutions. Due to this specific attribute, this operator is invoked in most of the existing QSAs, since it mitigates the deleterious effect of the measurement operation on the QP. The Grover operator $\mathcal{G}$ for a database of $N = 2^n$ elements is defined as follows [37]:

$$\mathcal{G} = H_n P_0 H_n O, \tag{27}$$

where H_n is the n-qubit Hadamard gate [47], P_0 is a unitary operator that flips the phase of all the states apart from the all-zero state, i.e. we have $|x\rangle \xrightarrow{P_0} -|x\rangle$ if $|x\rangle \neq |0\rangle^{\otimes n}$ and the O is

[6]The readers should refer to [62] for a more detailed tutorial.

the so-called *quantum Oracle gate* [47]. The latter "marks" the valid solutions by flipping their phase, while leaving the phase of the invalid solutions intact, i.e. we have $|x\rangle \xrightarrow{O} -|x\rangle$ if $f(x) = \delta$. Grover's QSA initializes the quantum system state $|\psi\rangle_{\text{init}}$ to the equal superposition of all the possible states, i.e. we have $|\psi\rangle_{\text{init}} = \sum_{x=0}^{N-1} |x\rangle/\sqrt{N}$. Then, it applies the Grover operator $\mathcal{G}$ L consecutive times, forming the final state $|\psi\rangle = \mathcal{G}^L |\psi\rangle_{\text{init}}$. Subsequently, the algorithm observes the state ψ and outputs the observed result as the solution.

The optimal number L_{opt} of $\mathcal{G}$ applications has been proven to be equal to [38]:

$$L_{\text{opt}} = \left\lfloor \frac{\pi}{4}\sqrt{\frac{N}{t}} \right\rfloor, \tag{28}$$

yielding a probability of observing a valid solution equal to $P_s = \sin^2[(2L_{opt} + 1)\theta]$, where we have $\theta = \arcsin(\sqrt{t/N})$. Since a single application of the Oracle gate O invokes the comparison $f(x) = \delta$ once, Grover's QSA has a complexity in terms of the number of comparisons, which is on the order of $O(\sqrt{N})$, based on Eq. (28).

B. BOYER-BRASSARD-HØYER-TAPP QSA

The *Boyer-Brassard-Høyer-Tapp* QSA (BBHT-QSA) [38] constitutes an extension of Grovers's QSA, since it is capable of addressing search problems, where the exact number t of valid solutions is unknown to the optimization process, whereas the sought entry δ is known. The only difference with respect to Grover's QSA presented in Sec. III-A is that the optimal number of $\mathcal{G}$ applications is unknown. Therefore, a number of attempts are carried out until a valid solution is observed, where the number of $\mathcal{G}$ applications is generated randomly by obeying a uniform distribution from a range $[0, \lfloor m \rfloor]$ that increases by a factor λ, if no valid solution is observed. Boyer *et al.* [38] have proven that by setting the initial upper bound of the selection range m to $m = 1$ and the exponential expansion factor λ to $\lambda = 6/5$, the BBHT-QSA succeeds in finding a valid solution with $\sim$100% probability, while requiring a maximum of $4.5\sqrt{N}$ Grover operator applications.

As for its associated complexity quantified in terms of upper and lower bounds both in the *Quantum Domain* (QD) and in the *Classic Domain* (CD), they have been proven to be equal to [42]:

$$L_{BBHT}^{\min} = 4.5\sqrt{N} + \log_\lambda\left(4.5\,\frac{\lambda-1}{m}\,\sqrt{N}+1\right) + 1, \tag{29}$$

$$L_{BBHT}^{\max} = 10\sqrt{N} + \log_\lambda \sqrt{N} - 1. \tag{30}$$

Observe in Eqs. (29) and (30) that the complexity quantified in terms of the number of dominance comparisons imposed by the BBHT-QSA is on the order of $O(\sqrt{N})$.

C. Durr-HØYER ALGORITHM

A further extension of the BBHT-QSA of Sec. III-B has been proposed by Durr–Høyer [39] in the form of the so-called *Durr-Høyer Algorithm* (DHA). This algorithm is applicable either to the minimization or to the maximization of single-objective problems, where neither the number t of valid solutions nor the valid solution value δ itself has to be known. Initially, it considers a random solution for the entire search space as the reference solution and invokes the BBHT-QSA for identifying solutions that have a either a high or a lower utility than the reference solution in the context of maximization and minimization problems, respectively. Should a valid solution be observed at the BBHT-QSA's output, the reference route is updated to this output and a new BBHT-QSA process is invoked. This process is repeated until an invalid solution is observed at the BBHT-QSA's output, implying that the reference route is the globally optimum one, which is then exported by the DHA. It has been proven by Durr and Høyer [39] that the DHA succeeds in finding a valid solution with $\sim$100% probability, while requiring a maximum of $22.5\sqrt{N}$ Grover operator applications. Additionally, the DHA's associated complexity quantified in terms of upper and lower bounds both in the QD and in the CD has been proven to be bounded by [43]:

$$L_{DHA}^{\min} = 4.5\sqrt{N} + \log_\lambda\left(4.5\frac{\lambda-1}{m}\sqrt{N}+1\right) + 2 = O(\sqrt{N}), \tag{31}$$

$$L_{DHA}^{\max} = 50\sqrt{N} + 5\log_\lambda(\sqrt{N}). \tag{32}$$

D. NON-DOMINATED QUANTUM ITERATIVE OPTIMIZATION ALGORITHM

The *Non-Dominated Quantum Iterative Optimization* (NDQIO) algorithm [43] constitutes the multi-objective extension of the DHA. It has been designed for identifying the entire OPF in weakly Pareto-optimal routing, where the objectives have to be jointly minimized. Initially, the DHA is invoked once per objective for identifying the global minimum of each objective. These specific route-solutions, which are Pareto-optimal are inserted into the OPF. Subsequently, a BBHT-QSA process, which is termed as *Backward BBHT-QSA* (BW-BBHT-QSA) [43], is activated in order to search for route-solutions that are not dominated by the hitherto generated OPF. Should a valid route-solution be identified by the BW-BBHT-QSA process, this specific valid route-solution is set as the reference route for a new BBHT-QSA process, which searches for route-solutions that dominate the reference one. Should the BBHT-QSA find a valid route-solution that dominates the reference one, the latter is updated to this valid route-solution and a valid new BBHT-QSA is activated. This chain of BBHT-QSAs [42], which resembles the DHA, terminates as soon as a BBHT-QSA iteration fails to identify a valid route-solution, implying that the reference route-solution is Pareto-optimal. Hence, the reference route-solution is included in the OPF and an *OPF repair process* [43] takes place, which successively removes the suboptimal routes that have been erroneously included in the OPF. The series of the BW-BBHT-QSA followed by the BBHT-QSA chain and the

OPF repair process is repeated until the BW-BBHT-QSA fails to observe a route-solution that is not dominated by the hitherto generated OPF. Therefore, the NDQIO algorithm concludes that it has identified the entire OPF and terminates by exporting the OPF.

Finally, the complexity imposed by the NDQIO in terms of the number of dominance comparisons, which from now on will be referred to as *Cost Function Evaluations* (CFEs), can be formulated as a function of the total number N_{OPF} of Pareto-optimal route-solutions as follows [43]:

$$L_{\text{NDQIO}} = \frac{1}{2K}N_{\text{OPF}}^2 + \frac{1}{K}\left(L_{\text{DHA}} + 2L_{\text{BBHT}} - \frac{1}{2}\right)N_{\text{OPF}} + (1-K)\left[\frac{2}{K}L_{\text{BBHT}} + \frac{1}{2}\right], \tag{33}$$

where L_{DHA} and L_{BBHT} correspond to the complexities imposed by the BBHT-QSA and DHA sub-processes, quantified in terms of the number of dominance comparisons, whereas K is the number of utility functions considered. Since both L_{DHA} and L_{BBHT} are on the order of $O(\sqrt{N})$ [38], [39], the NDQIO complexity is on the order of $O(N_{\text{OPF}}\sqrt{N})$, based on Eq. (33), if we have $O(N_{\text{OPF}}) \ll O(N)$; otherwise, it will be on the order of $O(N^2)$ for the sake of providing a full-search-based accuracy [43].

IV. DESIGN METHODOLOGY

Based on the complexity of the NDQIO algorithm quantified in terms of the number of dominance comparisons, which is defined in Eq.(33), invoking the NDQIO algorithm for the optimization problem of Eq. (22) impose a complexity, which is on the order of $O(N_{\text{OPF}}N^{N_r/2})$, where N corresponds to the total number of Hamiltonian routes from a specific pair of source and destination MCs. Naturally, this is significantly lower than $O(N^{2N_r})$ imposed by the exhaustive search. This complexity reduction, albeit substantial, may not be sufficient for near-real-time applications, when the nodes' locations rapidly change over time. In fact, Zalka [48] has proven that Grover's QSA is optimal in terms of the number of CFEs imposed by the algorithm. Since Grover's QSA has been the most popular technique in the family quantum amplitude amplification algorithms [38], [39], [63], which includes the NDQIO algorithm, we cannot achieve a complexity reduction more than that of a factor on the order of $O(\sqrt{N})$.

Having said this, all the QSA-based algorithms are totally oblivious of the optimization problem's structure, and hence they are incapable of exploiting the correlation of the elements in a database. Consequently, our design objective is twofold: on the one hand, we have to transform our composite optimization problem into a series of independent sub-problems, which exhibit a potentially uncorrelated search space; on the other hand, we have to develop a reduced-complexity quantum-assisted process for merging the results of the respective sub-processes, whilst minimizing the potential complexity overhead of the merging process. Naturally, this approach confines the initial search space considered, hence yielding a substantial reduction in complexity.

Having defined our algorithmic design targets in broad terms, let us now proceed with a tutorial example using the exhaustive search for the sake of a better understanding of the the joint routing and loab balancing optimization problem, defined in Eq. (22).

A. WEAK PARETO DOMINANCE OPERATOR

Before delving into the aforementioned transformation specifics, we will introduce the unitary operator U_{g_w}, which carries out a single weak Pareto dominance comparison and will be used as the Oracle gate of the Grover operator $\mathcal{G}$ deployed in our proposed algorithm. Due to the universality of the quantum gate-based computation [47], we have to derive a binary function for implementing the weak Pareto dominance operator. For this reason, let us define the comparison functions $f_k^{\bullet}(x,i)$ in terms of the k-th objective as follows:

$$f_k^{\bullet}(x,i) = \begin{cases} 1, & f_k(x) \bullet f_k(i), \\ 0, & \text{otherwise}, \end{cases} \tag{34}$$

where the operator $\bullet$ is the generic comparison operator corresponding to the operators $\leq, =, <$ etc. This comparison function is implemented by the quantum unitary operator $U_{f_k^{\bullet}}$ defined as follows:

$$|x\rangle\,|i\rangle\,|t\rangle \xrightarrow{U_{f_k^{\bullet}}} |x\rangle\,|i\rangle\,\left|t \oplus f_k^{\bullet}(x,i)\right\rangle, \tag{35}$$

where the quantum registers $|x\rangle$, $|i\rangle$, $|t\rangle$ are often referred to as *Quantum Index Register* (QIR), *Quantum Control Register* (QCR) and *Oracle Workspace* (OW), respectively [42]. The application of $U_{f_k^{\bullet}}$ results in entangling the states of the aforementioned registers.

We may readily create the binary expression of the weak dominance comparison using the generic comparison functions of Eq. (34). Based on Definition 1, the x-th route will be dominated by the reference route associated with the i-th index, provided that we have $f_k^{\leq}(x,1) = 1, \forall k \in \{1,\ldots,K\}$, while at the same time we have $\exists k \in \{1,\ldots,K\}$ so that $f_k^{<}(x,1) = 1$ is satisfied. Explicitly, the second requirement is that we have to exclude the specific route-solutions validated by the first requirement but have their UFs equal to the respective of the i-th route-solution, i.e. we have $f_k^{=}(x,i) = 1, \forall k \in \{1,\ldots,K\}$. Consequently, the weak dominance comparison function $g_w(x,i)$ is defined as follows:

$$g_w(x,i) = \bigcap_{k=1}^{K} f_k^{\leq}(x,i) \oplus \bigcap_{k=1}^{K} f_k^{=}(x,i) \equiv \begin{cases} 1, & \mathbf{f}(x) \succeq \mathbf{f}(i) \\ 0, & \text{otherwise}. \end{cases} \tag{36}$$

Having expressed the weak Pareto dominance comparison function $g_w(x,i)$ as a function of the $f_k^{\bullet}(x,i)$ function, we may readily employ the $U_{f_k^{\bullet}}$ operators for constructing the quantum circuit of the U_{g_w} operator, which is presented in Fig. 9. Observe in this figure that a series of CNOT gates [47] are used for the sake of entangling both the input QIR and input QCR to the respective local quantum registers of each

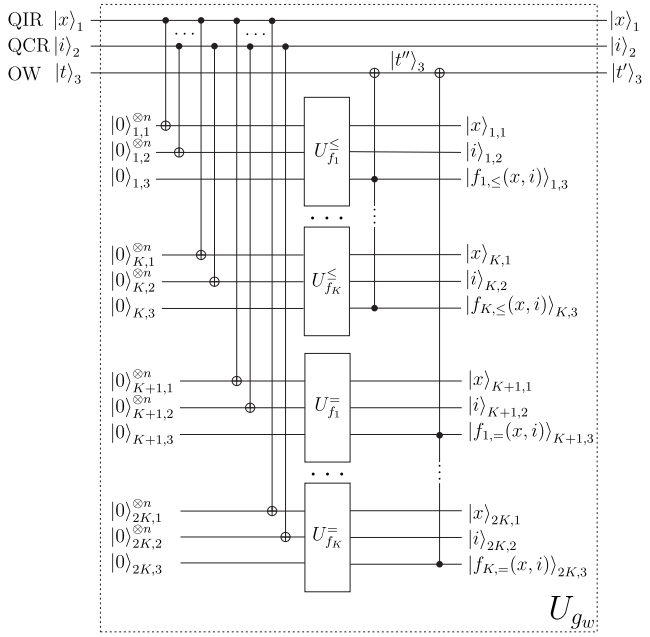

FIGURE 9. **Quantum circuit of the unitary operator U_{g_w} implementing the weak Pareto dominance comparison.**

of the $\{U_{f_k}^{\leq}\}_{k=1}^{K}$ and $\{U_{f_k}^{=}\}_{k=1}^{K}$ operators. Explicitly, the route-solutions' indices are stored in form of their superposition in the input QIR, while the index of the reference route-solution is stored in the QCR. As for the $\{U_{f_k}^{\leq}\}_{k=1}^{K}$ and $\{U_{f_k}^{=}\}_{k=1}^{K}$ operators, they implement the comparison functions defined in Eq. (34) with respect to the k-th UF. Subsequently, all the local OW registers states of the $\{U_{f_k}^{\leq}\}_{k=1}^{K}$ operators are combined by the *Toffoli* gate T [43], [47], which performs an *exclusive-OR* (XOR) between the input OW register $|t\rangle_3$ and the intersection product of the states of all the local OW registers. Therefore, after the first Toffoli gate the composite quantum system state is formulated as:

$$|x\rangle_1 |i\rangle_2 |t''\rangle_3 = |x\rangle_1 |i\rangle_2 \left| t \oplus \bigcap_{k=1}^{K} f^{\leq}(x,i) \right\rangle_3 . \quad (37)$$

A second Toffoli gate is then used for the sake of combining the local OW registers of the $\{U_{f_k}^{=}\}_{k=1}^{K}$ operators. Hence, the resultant composite quantum system state is equal to:

$$\begin{aligned} |x\rangle_1 |i\rangle_2 |t'\rangle_3 &= |x\rangle_1 |i\rangle_2 \left| t \oplus \bigcap_{k=1}^{K} f^{\leq}(x,i) \oplus \bigcap_{k=1}^{K} f^{=}(x,i) \right\rangle_3 , \\ &= |x\rangle_1 |i\rangle_2 |t \oplus g_w(x,i)\rangle_3 . \end{aligned} \quad (38)$$

Explictly, Eq. (38) proves that the circuit of Fig. 9 implements the weak dominance comparison function $g_w(x,i)$.

As for the circuit's complexity quantified in terms of the number of CFEs, we will define a single CFE as the complexity imposed by the strong Pareto dominance operator proposed in [42], which constists of a series of $U_{f_k^<}$ operators serially connected, for the sake of continuity. Therefore, assuming that both the CNOT and the Toffoli gates have an instant responce as in [43] and that the $U_{f_k^\bullet}$ comparison operators impose identical complexity, the complexity imposed by the quantum circuit of Fig. 9 is equal to $1/K$ CFEs. This is justified by the parallel activation of the $U_{f_k^\bullet}$ operator through the employment of the synergistic framework between the QP and the HP, which was introduced in [43] and it is comprised by the series of CNOT gates and the Toffoli gates at the $U_{f_k^\bullet}$ comparison operators' input and output, respectively.

At this point, let us emphasize that in the context of this treatise the proposed U_{g_w} operator will be used as the Oracle gate in the NDQIO algorithm's sub-processes, so that the algorithm becomes capable of identifying the OPF formed by strongly Pareto-optimal route-solutions.

B. MULTI-OBJECTIVE DECOMPOSITION QUANTUM OPTIMIZATION

As we mentioned in the introduction of this section, our design objective for the proposed algorithm is to transform the problem to a series of sub-problems having databases exhibiting the minimum amount of correlation among their elements. By a close inspection of Eqs. (17) and (19), which correspond to the average route delay and power consumption, respectively, we can conclude that both UFs considered in the constraint of Eq. (22) share the same generic form of:

$$f_k(S) = f_k(x^{(1)}, x^{(2)}, \ldots, x^{(N_r)}) = \sum_{n=1}^{N_r} a_{k,n} f_k(x^{(n)}), \quad (39)$$

where S denotes the set of N_r active routes, $x^{(n)}$ corresponds to the n-th active route and $a_{k,n}$ is a constant, which may be different for each UF but obeys the constraint $a_{k,i} > 0$. In our scenario, we have $a_{k,i} = N_r^{-1}$ for both UFs and $\forall i \in \{1, \ldots, N_r\}$. This specific form of the UFs can be exploited in the context of Pareto-optimality problems for reducing the search space, based on Proposition 1.

Proposition 1: Let us assume having N_r independent strong Pareto-optimality problems, each associated with the UVs $\mathbf{f}_n(x^{(n)}) = [f_1(x^{(n)}), \ldots, f_K(x^{(n)})]$, where K corresponds to the number of UFs, and that their OPF solutions form the sets $\{S_n^{OPF}\}_{n=1}^{N_r}$. Let us furthermore consider the composite Pareto-optimality problem of their convex combination, which is associated with the utility vector $\mathbf{f}(S) = \mathbf{f}(x^{(1)}, \ldots, x^{(N_r)}) = \left[\sum_{n=1}^{N_r} a_{1,n} f_1(x^{(n)}), \ldots, \sum_{n=1}^{N_r} a_{K,n} f_K(x^{(n)}) \right]$, with $a_{k,n} > 0$ $\forall n \in \{1, \ldots, N_r\}$ and $\forall k \in \{1, \ldots, K\}$, and that the OPF solutions of this problem form the set S^{OPF}. The set S^{OPF} is a subset of the union of the sets $\{S_n^{OPF}\}_{n=1}^{N_r}$, i.e. we have:

$$S^{OPF} \subseteq \bigcup_{n=1}^{N_r} S_n^{OPF}. \quad (40)$$

We note that the inverse of Proposition 1 does not apply, since there may exist solutions, which are composed by Pareto-optimal solutions in all the respective independent problems, but are suboptimal in the composite problem. Despite this limitation, Proposition 1 provides us with useful

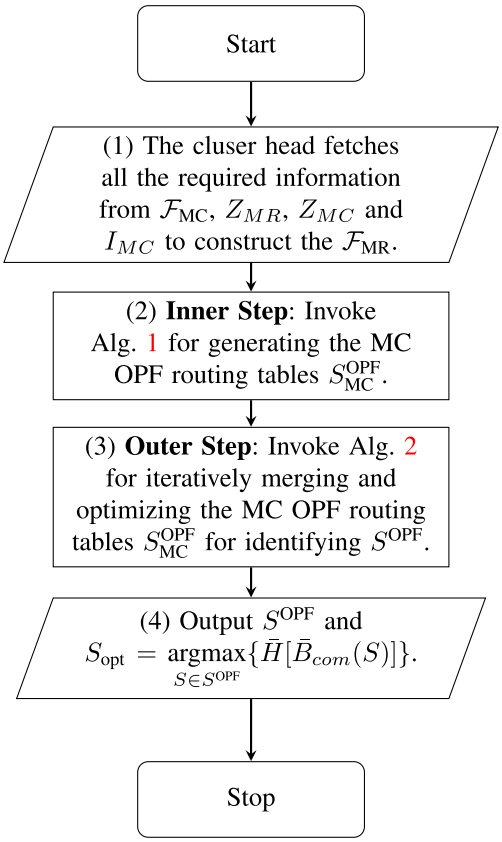

FIGURE 10. Multi-Objective Decomposition Quantum Optimization (MODQO) algorithm flowchart. We note that the in parentheses numbers at the begining of each block correspond to the identification number of each block.

insight into a potential transformation of our search space for sake of reducing the total number N_{tot} of sets of active routes considered, which was defined in Eq. (24).

Explicitly, we do not have to consider all the possible sets of active routes S; instead, we only have to identify the routes belonging to the union of the OPFs of all the active pairs of source and destination MCs. This actually constitutes a *divide and conquer* approach, since the sub-problems created for finding the OPF of a specific pair of source and destination MCs are independent of each other, yielding a reduction in the total complexity required by the exhaustive search, which is on the order of $O(N_r N^2)$, down from $O(N^{2N_r})$. Nevertheless, the solutions identified are not Pareto-optimal as yet, as we know based on Proposition 1; we still need a process for identifying the composite OPF S^{OPF} from the union of the OPFs of the independent sub-problems $\{S_n^{\text{OPF}}\}_{n=1}^{N_r}$, which yields an additional overhead on the order of $O(\bar{N}_{\text{OPF}}^{2N_r})$ in terms of complexity imposed by the exhaustive search, where $\bar{N}_{\text{OPF}}$ corresponds to average number of Pareto-optimal routes for each of the sub-problems. Therefore, the total complexity imposed by the exhaustive search using this transformation method is on the order of $O(N_r N^2 + \bar{N}_{\text{OPF}}^{2N_r})$, which is far less than $O(N^{2N_r})$, assuming that $O(\bar{N}_{\text{OPF}}) \ll O(N)$.

Explicitly, the exhaustive search method is far from efficient, despite the use of the search space transformation method, which was analyzed in the previous paragraph. For this reason, we will exploit the hybrid hardware and quantum parallelism offered by the NDQIO algorithm for further reducing the complexity of both the search space transformation step and the merging step, which will be referred to from now on as the *inner step* and *outer step*, respectively. The flowchart of our proposed algorithm, namely the *Multi-Objective Decomposition Quantum Optimization* (MODQO) algorithm, is shown in Fig. 10, where it can be observed that the execution of the algorithm is comprised by four distinct sub-processes or blocks.

To elaborate further, since our routing algorithm requires a centralized quantum-computer the presence of a cluster head is assumed, which monitors and controls the dissemination of the packets throughout the network. For the sake of performing optimal joint routing and load balancing, the cluster head needs to gather all the necessary data for constructing $\mathcal{F}_{\text{MR}}$, $\mathcal{F}_{\text{MC}}$, Z_{MR}, Z_{MC} and I_{MC}, corresponding to the MRs' friendship matrix, the MCs' friendship matrix, the MR locations, the MC locations and the MC to MR association vector, respectively. This information is essential for accurately evaluating the routes' UVs and, in the context of this treatise, we will assume perfect estimation of the aforementioned parameters at the cluster head. This process is shown in Block 1 of Fig. 10.

Subsequently, the cluster head performs the inner step optimization, as described by Block 2 of Fig. 10, where the routing table $S_{\text{MC}}^{\text{OPF}}$ containing the Pareto-optimal routes of all the active source and destination MC pairs, which are identified independently through a NDQIO sub-process, based on Alg. 1. The routes contained in $S_{\text{MC}}^{\text{OPF}}$ are then combined through several iterations for producing the S^{OPF} set, which contains the Pareto-optimal route-combinations in terms of the network's average delay and average power consumption. This process constitutes the outer step of the MODQO algorithm and it is denoted by Block 3 of Fig. 10 and it is detailed in Alg. 2. Finally, the MODQO algorithm outputs the identified OPF routing table S^{OPF} along with the solution $S_{\text{opt}} \in S^{\text{OPF}}$ that maximizes the normalized entropy of the normalized composite betweenness distribution. We note that we do not have to invoke a new search process for the latter; instead, during the last iteration of Alg. 2, the normalized entropy value of the normalized composite betweenness distribution of each S^{OPF} element is evaluated as long as the specific set of active routes is identified as Pareto-optimal. It is then compared to the maximum hitherto observed value and this value is updated, should the observed value be greater than the maximum value observed so far. This process imposes a further overhead in terms of complexity equal to the number $\left|S^{\text{OPF}}\right|$ of elements comprising the OPF.

Having presented an overview of the MODQO algorithm let us now provide some further discussions regarding

Algorithm 1 Inner Step of the Multi-Objective Decomposition Quantum Optimization (MODQO) Algorithm, Introduced in Block 2 of Fig. 10

Building MR Routing Table $S_{\mathrm{MR}}^{\mathrm{OPF}}$:
Set $S_{\mathrm{MR}}^{\mathrm{OPF}} \leftarrow [\,]$.
for $i = 0$ **to** N_{MR} **do**
  for $j = i + 1$ **to** N_{MR} **do**
    if $\mathcal{F}_{\mathrm{MR},i,j} \neq 0$ **then**
      Invoke the NDQIO process of [43, Alg. 4] with source node the MR_i and destination node the MR_j and store the OPF routes to $S_{\mathrm{MR},i,j}^{\mathrm{OPF}}$ and the reciprocal of these routes to $S_{\mathrm{MR},j,i}^{\mathrm{OPF}}$.
    end if
  end for
end for
# Building MC Routing Table $S_{\mathrm{MC}}^{\mathrm{OPF}}$:
Set $S_{\mathrm{MC}}^{\mathrm{OPF}} \leftarrow [\,]$ and $n \leftarrow 0$.
for $i = 0$ **to** N_{MC} **do**
  for $j = i + 1$ **to** N_{MC} **do**
    if $\mathcal{F}_{\mathrm{MC},i,j} \neq 0$ **then**
      Set $n \leftarrow n + 1$, $l \leftarrow I_{\mathrm{MC},i}$ and $m \leftarrow I_{\mathrm{MC},j}$.
      if $l \neq m$ **then**
        for $k = 1$ **to** $\left|S_{\mathrm{MR},i,j}^{\mathrm{OPF}}\right|$ **do**
          Set $S_{\mathrm{MC},n,k}^{\mathrm{OPF}} = [\mathrm{MC}_i, S_{\mathrm{MR},l,m,k}^{\mathrm{OPF}}, \mathrm{MC}_j]$.
        end for
      else
        Set $S_{\mathrm{MC},n}^{\mathrm{OPF}} \leftarrow [\mathrm{MC}_i, \mathrm{MR}_l, \mathrm{MC}_j]$.
      end if
    end if
  end for
end for
Export the $S_{\mathrm{MC}}^{\mathrm{OPF}}$ and exit.

Algorithm 2 Outer Step of the Multi-Objective Decomposition Quantum Optimization (MODQO) Algorithm, Introduced in Block 3 of Fig. 10

Sort $S_{\mathrm{MC}}^{\mathrm{OPF}}$ in terms of their number of OPF routes in ascending order.
Initialize $S^{\mathrm{OPF}} \leftarrow S_{\mathrm{MC},1}^{\mathrm{OPF}}$ and remove $S_{\mathrm{MC},1}^{\mathrm{OPF}}$ from $S_{\mathrm{MC}}^{\mathrm{OPF}}$.
repeat
  Calculate $L_{\mathrm{CM}}(n)$, $L_{\mathrm{QM,min}}^{\mathrm{ref}}(n)$ and $L_{\mathrm{QM,max}}^{\mathrm{ref}}(n)$, defined in (49), (50) and (51) respectively, $\forall n \in \left\{1, \ldots, \left|S_{\mathrm{MC}}^{\mathrm{OPF}}\right|\right\}$.
  Evaluate n_{opt} from Eq (53).
  if $L_{\mathrm{QM\,min}}^{\mathrm{ref}}(n_{\mathrm{opt}}) < L_{\mathrm{CM}}^{\mathrm{ref}}(n_{\mathrm{opt}})$ **then**
    Consider jointly the solutions formed by merging S^{OPF} and $\{S_{\mathrm{MC},n}^{\mathrm{OPF}}\}_{n=1}^{n_{\mathrm{opt}}}$ and activate a NDQIO process of [43, Alg. 4] storing the identified OPF to S^{OPF} and removing the elements $\{S_{\mathrm{MC},n}^{\mathrm{OPF}}\}_{n=1}^{n_{\mathrm{opt}}}$ from $S_{\mathrm{MC}}^{\mathrm{OPF}}$.
  else
    Consider jointly the solutions formed by merging S^{OPF} and $S_{\mathrm{MC},1}^{\mathrm{OPF}}$ and store the identified OPF by exhaustive search to S^{OPF}, removing $S_{\mathrm{MC},1}^{\mathrm{OPF}}$ from $S_{\mathrm{MC}}^{\mathrm{OPF}}$.
  end if
until $\left|S_{\mathrm{MC}}^{\mathrm{OPF}}\right| > 0$.
Export the S^{OPF} and exit.

the inner (Block 2) and the outer (Block 3) steps in Subsections IV-C and IV-D, respectively.

C. BUILDING THE MC ROUTING TABLES

During the inner step, our design objective is to construct the routing table $S_{\mathrm{MC}}^{\mathrm{OPF}}$ for all the active pairs of source and destination MCs. The formal statement of the inner process introduced in Block 2 of Fig. 10 is presented in Alg. 1. We note that the n-th element $S_{\mathrm{MC},n}^{\mathrm{OPF}}$ of the routing table $S_{\mathrm{MC}}^{\mathrm{OPF}}$, which appears in Alg. 1, contains the Pareto-optimal routes of the n-th pair of source and destination MCs, while $S_{\mathrm{MC},n,k}^{\mathrm{OPF}}$ corresponds to the k-th identified Pareto-optimal route of $S_{\mathrm{MC},n}^{\mathrm{OPF}}$.

Based on the assumption that the MRs operate in full-duplex with the aid of a sufficient number of orthogonal spreading codes and channels both in the frequency domain, we are ready to independently address each of the routing sub-problems for a specific pair of source and destination MCs. Explicitly, this specific assumption provides us with the upper bounds of the twin-layer network's achievable performance. Additionally, we can achieve a further reduction in the complexity imposed by the inner step, if we exploit the fact that each of the MCs is assigned to its closest MR. Based on this allocation scheme, different source MCs assigned to the same MR have identical sets of Pareto-optimal routes leading to the specific destination MCs that are also assigned to the same MR. Therefore, we can directly perform the routing optimization directly among the MRs based on their friendship matrix $\mathcal{F}_{\mathrm{MR}}$, hence constructing the respective routing table $S_{\mathrm{MR}}^{\mathrm{OPF}}$. This process is performed in Steps 3-9 of Alg. 1, where the NDQIO process of [43, Algorithm 4] is activated in Step 6 of Alg. 1, as long as the source MR_i and destination MR_j share a social relationship, i.e. we have $\mathcal{F}_{\mathrm{MR},i,j} \neq 0$. In this way, we have managed to reduce the number of NDQIO activations to $||\mathcal{F}_{\mathrm{MR}}||_2\,/2$ from $||\mathcal{F}_{\mathrm{MC}}||_2\,/2$, where the $||\cdot||_2$ operator corresponds to the power-2 norm of a matrix [61].

After successfully constructing the MR routing table $S_{\mathrm{MC}}^{\mathrm{OPF}}$, the cluster can readily construct the respective MC routing table $S_{\mathrm{MC}}^{\mathrm{OPF}}$ from $S_{\mathrm{MC}}^{\mathrm{OPF}}$, the active MC association vector I_{MC} to MRs and the MC friendship $\mathcal{F}_{\mathrm{MC}}$ in Steps 11-25 of Alg. 1. The exception of the source and destination MCs that are associated with the same MR is examined in Step 16 of Alg. 1. Naturally, should the source and destination MCs be associated with different MRs, the MODQO algorithm will rely on the MR routing table to construct the Pareto-optimal set of MC routes, as shown in Step 18 of Alg. 1. Otherwise, the two MCs are directly connected through their associated MR without the inclusion of intermediate MRs based on Step 21

of Alg. 1, since there exists no other valid Hamiltonian route that does not traverse the specific MR twice.

Finally, we note that should half-duplex and a finite number of either orthogonal codes or orthogonal channels be considered, our MODQO algorithm will still be applicable; however, a further constraint has to be imposed regarding the priority of each active route. This leads to a modified inner step, where the MC routing table is directly constructed, rather than exported from the respective MR routing table $S_{\mathrm{MR}}^{\mathrm{OPF}}$.

D. MERGING THE MC ROUTES

Having identified the Pareto-optimal routes $S_{\mathrm{MC},i}^{\mathrm{OPF}}$ for each individual active pair of source and destination MCs, we now have to combine the routes for identifying the network's Pareto-optimal sets of routes in terms of the network's average delay and its average power dissipation. Naturally, the conceptually simplest method of combining the individual routes would be to consider them jointly. Therefore, assuming N_r active pairs of source and destination MCs having on average $\bar{N}_{\mathrm{OPF}}$ Pareto-optimal routes, the resultant complexity imposed by the exhaustive search is equal to:

$$L_{\mathrm{ES}}^{\mathrm{outer}} = \bar{N}_{\mathrm{OPF}}^{2N_r}. \tag{41}$$

Observe in Eq. (41) that the complexity imposed by the exhaustive search increases exponentially, as the number of active routes increases. By contrast, when an NDQIO process is utilized, the resultant complexity quantified in terms of the number of CFEs will be on the order of $O(\bar{N}_{\mathrm{OPF}}^{N_r})$, owing to the complexity reduction offered by the QP, based on Eqs. (29)-(33). Explicitly, this problem is NP-hard, since it belongs to the class of *Multi-Objective Knapsack Problems* [64]. Hence, for the sake of efficiently identifying the Pareto-optimal route-combinations, a heuristic approach has to be adopted.

In fact, the solution space formed by the combinations of the independent of the sub-problems Pareto-optimal routes can be portrayed as the *irregular trellis* diagram [65] of Fig. 11a. Explicitly, an irregular trellis diagram is utilized, since the trellis paths can reach different total number of states at the n-th stage, which is denoted by $\left|S_{\mathrm{MC},n}^{\mathrm{OPF}}\right|$. Still referring to Fig. 11a, a specific trellis path representing a particular route-combination is formed once a trellis transition traverses a specific trellis node, which correspods to a specific route. For instance, at the 3rd stage of Fig. 11a a trellis path visiting the trellis nodes $S_{\mathrm{MC},1,2}^{\mathrm{OPF}}$, $S_{\mathrm{MC},2,1}^{\mathrm{OPF}}$ and $S_{\mathrm{MC},3,5}^{\mathrm{OPF}}$ represents the particular route-combination formed by the second identified Pareto-optimal route of the first active pair of source and destination MCs, the first identified Pareto-optimal route of the second active pair of source and destination MCs and the fifth identified Pareto-optimal route of the third active pair of source and destination MCs.

Owing to the irregular trellis structure of the outer problem, we may readily employ the classic *Viterbi Algorithm* [66]. However, we have to modify it so that it becomes applicable for multi-objective *Cost Functions* (CF), since it has been initially designed for single-objective CFs in the context of decoding *Forward Error Correction* (FEC) schemes [67]. Explicitly, we have proven in Proposition 1 that a route-combination is potentially Pareto-optimal, when all of the routes comprising the route-combination are Pareto-optimal in their respective individual sub-problems. Naturally, due to the specific form of the utility functions of the UV defined in Eq. (39) it is possible to group n sub-problems into a smaller composite sub-problem $\mathbf{x}$, which is defined as follows:

$$\mathbf{x} = \left[x^{(1)}, \ldots, x^{(n)}\right], \tag{42}$$

while its k-th respective UF is given by:

$$f_k(\mathbf{x}) = \sum_{i=1}^{n} a_{k,n} f_k(x^{(i)}). \tag{43}$$

Based on Eq. (42) the composite problem's solution S is now defined as follows:

$$S = \left[\mathbf{x}, x^{(n+1)}, \ldots, x^{(N_r)}\right], \tag{44}$$

and based on Eq. (43), the route-combination S has a k-th UF that attains the form of Eq. (39). This is the critical condition for Proposition 1 to be valid and, hence, we have:

$$S^{\mathrm{OPF}} \subseteq S_{(n)}^{\mathrm{OPF}} \cup \left(\bigcup_{i=n+1}^{N_r} S_{\mathrm{MC},i}^{\mathrm{OPF}} \right), \quad \forall n, N_r \in \mathbb{N}^*, \tag{45}$$

where we have $n \leq N_r$ and $S_{(n)}^{\mathrm{OPF}}$ corresponds to the OPF of the Pareto-optimality routing sub-problem with route solutions having the form $\mathbf{x} = \left[x^{(1)}, \ldots, x^{(n)}\right]$. Naturally, if we have $n = N_r$, Eq. (45) is reduced to $S^{\mathrm{OPF}} = S_{(N_r)}^{\mathrm{OPF}}$, while if we set $N_r = n+1$, Eq. (45) is transformed into the following recursive closed form:

$$S_{(n+1)}^{\mathrm{OPF}} \subseteq S_{(n)}^{\mathrm{OPF}} \cup S_{\mathrm{MC},n+1}^{\mathrm{OPF}}, \tag{46}$$

where the equality of the sets is satisfied, as long as the set $S_{\mathrm{MC},n+1}^{\mathrm{OPF}}$ consists of a single Pareto-optimal route, i.e. we have $\left|S_{\mathrm{MC},n+1}^{\mathrm{OPF}}\right| = 1$.

Explicitly, Eq. (46) provides us with a reduced-complexity optimal merging method for the sake of iteratively combining the OPF $S_{\mathrm{MC},n}^{\mathrm{OPF}}$ of each stage to form the network's overall OPF S^{OPF}. To elaborate further, at the n-th horizontal step or stage of Fig. 11a we only have to consider the arrival of hitherto Pareto-optimal route-combinations for the previous $(n-1)$ stages, i.e. the route-combinations belonging to the set $S_{(n-1)}^{\mathrm{OPF}}$. Subsequently, these routes visit each of the nodes of the n-th stage, thus constructing the set $S_{(n-1)}^{\mathrm{OPF}} \cup S_{\mathrm{MC},n}^{\mathrm{OPF}}$ of route-combinations. Since the OPF of the n-th stage route-combinations $S_{(n-1)}^{\mathrm{OPF}}$ is a subset of $S_{(n-1)}^{\mathrm{OPF}} \cup S_{\mathrm{MC},n}^{\mathrm{OPF}}$ we will have to identify the new OPF for the sake of discarding the sub-optimal routes and, thus, confining the search space for the sake of reducing the complexity imposed without degrading the associated accuracy. As far as the initialization of the OPF of route-combinations is concerned, it is set to $S_{(0)}^{\mathrm{OPF}} = [\,]$,

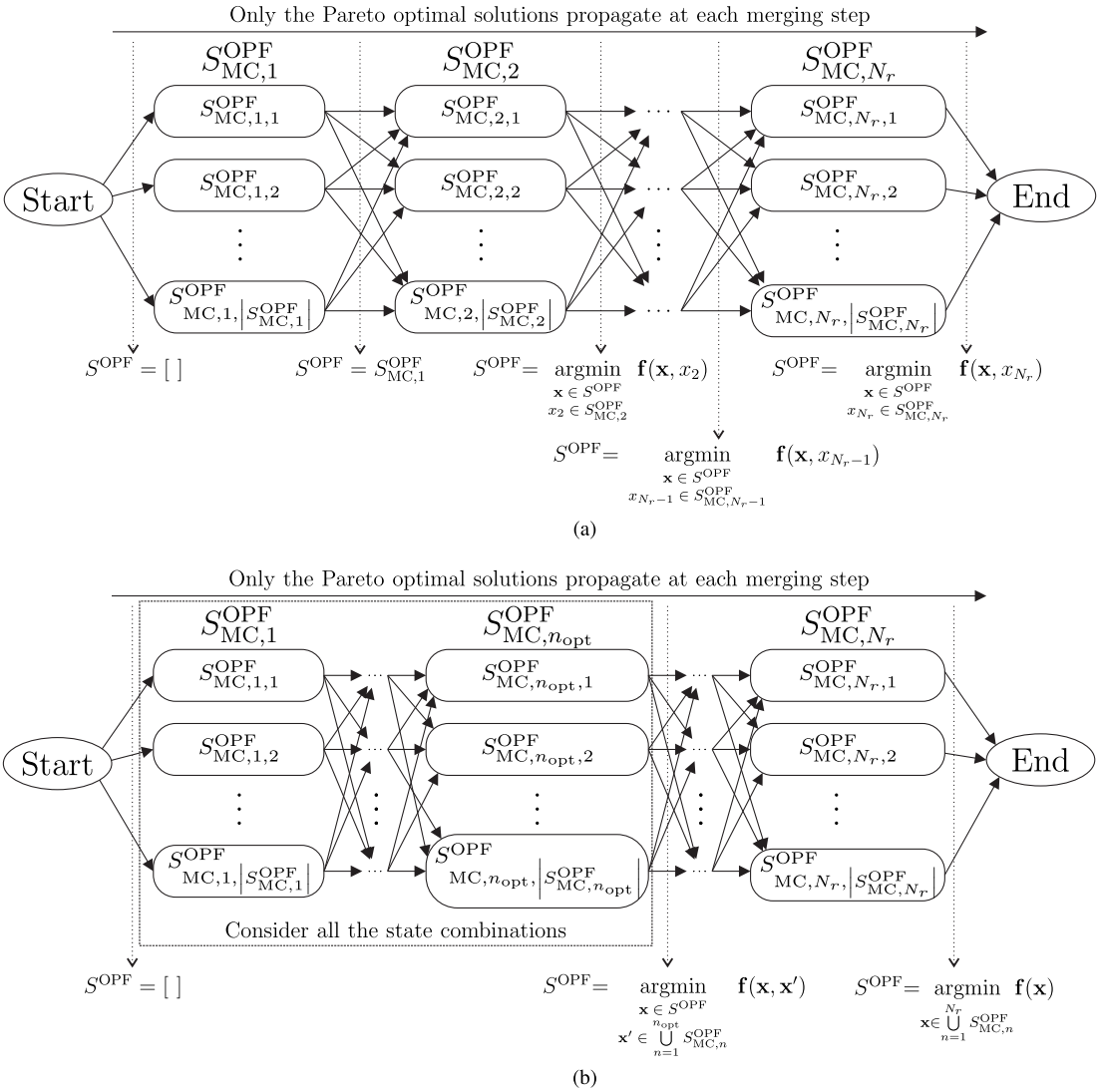

FIGURE 11. **Trellis diagram of the merging process solely using (a) CM and (b) QM methods for the outer step optimization. We note that at each stage only $\left|S^{\mathrm{OPF}}\right|$ routes continue propagating towards the End node, as denoted by the dotted arrows, while traversing precisely $\left|S^{\mathrm{OPF}}_{\mathrm{MC},i}\right|$ nodes at the i-th step.**

which represents an empty set. The aforementioned iterative process is repeated until the route-combinations have encapsulated routes from all the active pairs of source and destination MCs. The intermediate products of this iterative process are portrayed in Fig. 11a with the aid of dotted arrows; these arrows demonstrate the routes that horizontally propagate at the next stage.

In a nutshell, this iterative process resembles the classic Viterbi Algorithm, since they both attempt to reduce the search space using a series of iterations. The most notable difference in our approach compared to the classic Viterbi Algorithm is that the number of propagating routes in our scenario is variable and it depends on the number $\left|S^{\mathrm{OPF}}_{(n)}\right|$ of the Pareto-optimal route-combinations at the n-th stage. Therefore, the complexity of this method, which will be referred to from now on as *Classical Merging* (CM), is bounded by:

$$L^{\mathrm{outer}}_{\mathrm{CM,min}} = (N_r - 1)\bar{N}^4_{\mathrm{OPF}} = O(N_r \bar{N}^4_{\mathrm{OPF}}), \tag{47}$$

$$L^{\mathrm{outer}}_{\mathrm{CM,max}} = \sum_{n=2}^{N_r} \bar{N}^{2n}_{\mathrm{OPF}} = \frac{\bar{N}^{2(N_r+2)}_{\mathrm{OPF}} - \bar{N}^4_{\mathrm{OPF}}}{\bar{N}^2_{\mathrm{OPF}} - 1} = O(\bar{N}^{2(N_r+1)}_{\mathrm{OPF}}), \tag{48}$$

where $\bar{N}_{\mathrm{OPF}}$ corresponds to the average number of OPF in the independent sub-problems, while $L^{\mathrm{outer}}_{\mathrm{CM,min}}$ and $L^{\mathrm{outer}}_{\mathrm{CM,max}}$ are the lower and upper bounds of the CM method. The lower bound of Eq. (47) corresponds to the best-case scenario, where the number of route-combinations that propagate across the irregular trellis stages is equal to the number of the respective states at the specifc trellis stage, i.e. equal to $\left|S^{\mathrm{OPF}}_{\mathrm{MC,n}}\right|$ for the n-th stage, while the upper bound of Eq. (48) is

encountered in the worst-case scenario, where all the possible route-combinations are Pareto-optimal. Observe in Eqs. (47) and (48) that although the CM method imposes a substantially lower amount of complexity in the best-case scenario than the exhaustive search, in the worst-case scenario the CM method actually imposes a higher complexity, owing to the design assumption of having sub-optimal route-combinations that will be eliminated during the intermediate stages. In the next section we will provide the critical condition for the CM to outperform the exhaustive search.

Furthermore, we can readily empower the CM method with the quantum-aided framework of [43], which was invoked in the inner step, for the sake of achieving a further reduction in the complexity imposed by the outer step. A naive approach would be to invoke the NDQIO algorithm at each stage; however, this approach would only be efficient for a high number of route-combinations, whilst its potential application would impose a higher complexity than the convetional CM method. For the sake of circumventing this problem, we have introduced an additional degree of freedom for the NDQIO process. In particular, we have designed the NDQIO sub-process to be capable of jointly considering multiple stages of the irregular trellis, set to an optimal number of stages n_{opt}, as it is portrayed in Fig. 11b. We note that from this point on this process will be referred to as the *Quantum Merging* (QM) process. Observe in Fig. 11b that the NDQIO process jointly considers the route-combinations formed by the OPF sets $\left\{S^{\text{OPF}}_{\text{MC},n}\right\}_{n=1}^{n_{\text{opt}}}$, as marked by the dashed-line-bordered rectangle.

Based on this, we have to define the selection criterion regarding the value of the parameter n_{opt}, which would allow the NDQIO sub-process to impose a lower complexity than the CM method. For this reason, let us first define a metric for quantifying the complexity imposed by the CM. Explicitly, for accurately quantifying the complexity imposed by the CM method, the number of Pareto-optimal route-combinations has to be known prior to the optimization. Since the optimization process is incapable of estimating the number of Pareto-optimal route-combinations at each stage without actually solving the respective Pareto-optimality sub-problems, we will attempt to approximate the complexity imposed by the CM method using its lower bound. Hence, we set the number of Pareto-optimal route-combinations at each stage equal to the number of nodes of that stage. Based on this assumption, the reference complexity $L^{\text{ref}}_{\text{CM}}$ imposed by the CM method quantified in terms of the trelis stage index n is equal to:

$$L^{\text{ref}}_{\text{CM}}(n) = \sum_{n=2}^{|S^{\text{OPF}}_{\text{MC}}|} \left|S^{\text{OPF}}_{\text{MC},n-1}\right|^2 \left|S^{\text{OPF}}_{\text{MC},n}\right|^2. \tag{49}$$

Based on the same assumption and Eq. (33), we are capable of deriving the upper and lower bounds of the complexity imposed by the NDQIO algorithm, when n stages are considered jointly. Explicitly, the aforementioned bounds of complexity quantified in terms of the number of CFEs are equal to:

$$\begin{aligned} L^{\text{ref}}_{\text{QM,min}}(n) = {} & (2K)^{-1}\left|S^{\text{OPF}}_{\text{MC},n}\right|^2 + K^{-1}\left\{L^{\min}_{\text{DHA}}[\hat{N}(n)]\right. \\ & \left. + 2L^{\min}_{\text{BBHT}}[\hat{N}(n)] - \frac{1}{2}\right\}\left|S^{\text{OPF}}_{\text{MC},n}\right| \\ & + (1-K)\left\{\frac{2}{K}L^{\min}_{\text{BBHT}}[\hat{N}(n)] + \frac{1}{2}\right\}, \end{aligned} \tag{50}$$

$$\begin{aligned} L^{\text{ref}}_{\text{QM,max}}(n) = {} & (2K)^{-1}\left|S^{\text{OPF}}_{\text{MC},n}\right|^2 + K^{-1}\left\{L^{\max}_{\text{DHA}}[\hat{N}(n)]\right. \\ & \left. + 2L^{\max}_{\text{BBHT}}[\hat{N}(n)] - \frac{1}{2}\right\}\left|S^{\text{OPF}}_{\text{MC},n}\right| \\ & + (1-K)\left\{\frac{2}{K}L^{\max}_{\text{BBHT}}[\hat{N}(n)] + \frac{1}{2}\right\}, \end{aligned} \tag{51}$$

where $L^{\min}_{\text{BBHT}}[\hat{N}(n)]$ and $L^{\max}_{\text{BBHT}}[\hat{N}(n)]$ correspond to the lower and upper bounds of the complexity imposed by the BBHT-QSA for a database of $\hat{N}(n)$ elements, as defined in Eqs. (29) and (30), respectively, whereas $L^{\min}_{\text{DHA}}[\hat{N}(n)]$ and $L^{\max}_{\text{DHA}}[\hat{N}(n)]$ are the respective complexity bounds of the DHA, which are defined in Eqs. (31) and (32), respectively. Additionally, recall that the parameter K represents the number of utility functions considered, which is set equal to $K = 2$ utility functions in our scenario. We note that the database length $\hat{N}(n)$ is quantified in terms of the number n of joint stages considered by the NDQIO algorithm as follows:

$$\hat{N}(n) = \prod_{i=1}^{n}\left|S^{\text{OPF}}_{\text{MC},i}\right|. \tag{52}$$

We note that we are using the upper and lower bounds of complexity for the NDQIO algorithm due to the stochastic nature of both the DHA and of the BBHT-QSA. Having derived these bounds, we may now assess the criteria for an efficient deployment of the NDQIO algorithm. Our ultimate design target is to determine at each iteration the optimal number n_{opt} of joint stages for ensuring that the NDQIO algorithm outperforms the CM method, while imposing the lowest possible complexity. Therefore, the optimal value n_{opt} occurs at the specific trellis stage, where the lower bound of the complexity reduction with respect to the CM is maximized. This can be formulated as follows:

$$n_{\text{opt}} = \underset{n\in\{1,\ldots,|S^{\text{OPF}}_{\text{MC}}|\}}{\arg\max}\left\{\frac{L^{\text{ref}}_{\text{CM}}(n)}{L^{\text{ref}}_{\text{QM,max}}(n)}\right\}. \tag{53}$$

Nonetheless, we should also ensure that the NDQIO process achieves a beneficial complexity reduction compared to the partial CM method, for this optimal value of n_{opt}. Explicitly, this can be verified by comparing the lower bound $L^{\text{ref}}_{\text{QM,max}}(n_{\text{opt}})$ of the complexity imposed by the NDQIO algorithm to the respective value $L^{\text{ref}}_{\text{CM}}(n_{\text{opt}})$ of the CM method: should the NDQIO lower bound for the specific value of n_{opt} derived by Eq. (53) be lower than that of the CM method, then we may conclude that the NDQIO process is potentially capable of outperforming the CM method. Otherwise, it is clear that the CM method should be invoked. At this

point, we would like to point out that we have opted for utilizing the lower bound of the NDQIO's average complexity, since it tends to be closer to average case, when compared to its upper bound counterpart, as presented in [43].

Based on this framework, which relies on a synergistic hybrid of classical and quantum optimization, let us now describe the outer step of the MODQO algorithm, which is formally presented in Alg 2. Prior to constructing the irregular trellis structure of Fig. 11b, we have to sort the MC Pareto-optimal routing tables $\{S^{\text{OPF}}_{\text{MC},n}\}^{N_r}_{n=1}$ based on their number $\left|S^{\text{OPF}}_{\text{MC},n}\right|$ of the independent Pareto-optimal routes, as it is shown in Step 1 of Alg. 2. This can be justified by the fact that the number of route-combinations will eventually increase, as more stages of the trellis diagram are examined. Naturally, this sorting is consistent with the design assumption that the number of Pareto-optimal routes at the end of each stage is equal to the number of the specific states at that trellis stage. Subsequently, the set of Pareto-optimal route-combinations S^{OPF} is initialized to the first set $S^{\text{OPF}}_{\text{MC},1}$ of Pareto-optimal routes in the MC routing table, which is then removed from $S^{\text{OPF}}_{\text{MC}}$ in Step 2 of Alg. 2 followed by the iterative process of Steps 3-11 of Alg. 2. This iterative process is invoked for the sake of determining as to whether a single NDQIO activation is capable of imposing a lower complexity than the CM method for the same number of trellis stages. Hence, the more efficient method is activated at each iteration. To elaborate further, the respective reference complexities are quantified in terms of the trellis stage index n and the its optimal value n_{opt} with respect to the maximum complexity reduction achieved by the QM over the CM method in Steps 4-5 of Alg. 2, respectively. Should the algorithm conclude that the QM method is potentially capable of operating at a lower complexity than the CM, n_{opt} stages are considered jointly with the Pareto-optimal route-combinations S^{OPF} gleaned from the previous iterations in Step 7 of Alg. 2; it then updates the OPF route-combinations S^{OPF} and removes the encapsulated stages from the MC routing table. Otherwise, a single CM iteration is applied, i.e. the first set $S^{\text{OPF}}_{\text{MC},1}$ of the MC routing table is jointly considered with the S^{OPF} gleaned from the previous iterations and Alg. 2 removes the set $S^{\text{OPF}}_{\text{MC},1}$ from the MC routing table after updating the OPF of route-combinations S^{OPF} in Step 9 of Alg. 2. We note that a single CM is applied, rather than n_{opt} for the sake of allowing the algorithm to iteratively calibrate itself for all the potential outcomes of all Pareto-optimal route-combinations.

For the sake of simplicity, we have not included the specific process, appearing in Block 4 of Fig. 10, which identifies the specific Pareto-optimal route-combination S_{opt} exhibiting the maximum value of the normalized entropy of the normalized composite betweenness. In fact, this specific process can be incorporated during the last iteration of Alg. 2, where the normalized entropy $\bar{H}[\bar{B}_{com}(S)]$ of the normalized composite betweenness is evaluated, when a route-combination is identified as being Pareto-optimal. This value of $\bar{H}[\bar{B}_{com}(S)]$ is then compared to the maximum observed $\bar{H}_{\max}$ value, which is updated depending on the comparison outcome. In this way, we can reach the optimal route-combination S_{opt} with respect to the optimization problem of Eq. (22) by imposing a modest overhead of $\left|S^{\text{OPF}}\right|$ CFEs.

E. A 12-NODE TUTORIAL EXAMPLE USING MODQO

Having fully described the MODQO algorithm's the inner and the outer sub-processes, let us now elaborate on its function with the aid of a low-paced tutorial example. We note that the following tutorial assumes knowledge of the NDQIO algorithm. Therefore, the readers new to this subject should refer to the tutorial section of [43]. Additionally, we will assume an identical twin-layer network to that of the tutorial using the Exhaustive Search presented in Sec. II-D.

Based on the friendship matrix $\mathcal{F}_{\text{MC}}$ of Eq. (25), the MCs' locations Z_{MC}, the MRs' locations Z_{MR} and the MCs to MRs association vector I_{MC}, which are shown in Fig. 7, the cluster head invokes the MODQO algorithm seen in Fig. 10. Firstly, based on Block 1 of the MODQO flowchart seen in Fig. 10 the MR friendship matrix $\mathcal{F}_{\text{MR}}$ is constructed, whose elements indicate which pairs of MRs are associated with MCs that share a social relationship. In our scenario, the MR friendship matrix $\mathcal{F}_{\text{MR}}$ is equal to:

$$\mathcal{F}_{\text{MR}} = \begin{bmatrix} 0 & 0 & 0 & 0 & 0 & 0 & 0 \\ 0 & 0 & 1 & 0 & 0 & 0 & 0 \\ 0 & 1 & 0 & 0 & 1 & 1 & 1 \\ 0 & 0 & 0 & 0 & 0 & 0 & 0 \\ 0 & 0 & 1 & 0 & 0 & 1 & 0 \\ 0 & 0 & 1 & 0 & 1 & 0 & 0 \\ 0 & 0 & 1 & 0 & 0 & 0 & 0 \end{bmatrix}, \tag{54}$$

where we can observe that the MR_1 and MR_4 share no social relationship with the rest of the MRs, since they are not associated with any of the MCs. To elaborate further, MR_2 and MR_7 shares a social relationship only with MC_3, MR_3 in turn shares a friendship relationship with MR_2, MR_5, MR_6 and MR_7, since it is associated with the social by-minded MC_1, while MR_5 and MR_6 share a social relationship both with each other and with MR_3.

After the construction of the MR friendship matrix $\mathcal{F}_{\text{MR}}$, the MODQO algorithm proceeds with its inner step, according to Block 2 of the MOQDO flowchart seen in Fig. 10. In this step, the MODQO algorithm initializes the MR routing table to an empty matrix based on Step 2 of Alg. 1. It then acts on the upper triangular part of the $\mathcal{F}_{\text{MR}}$ matrix by activating a NDQIO sub-process in Steps 3-9 of Alg. 1 for the sake of identifying the entire set of Pareto-optimal routes between MR_i and MR_j as long as $\mathcal{F}_{\text{MR},i,j} = 1$, i.e. MR_i and MR_j have a social relationship. We note that the NDQIO sub-process activates the weak Pareto dominance operator U_{g_w} portrayed in Fig. 9. Based on Eq. (54) for our scenario, the NDQIO sub-process will be activated $||\mathcal{F}_{\text{MR}}||_2/2 = 6$ times, namely for the elements $\mathcal{F}_{\text{MR},2,3}$, $\mathcal{F}_{\text{MR},2,3}$, $\mathcal{F}_{\text{MR},3,5}$, $\mathcal{F}_{\text{MR},3,6}$, $\mathcal{F}_{\text{MR},3,7}$ and $\mathcal{F}_{\text{MR},5,6}$, thus exporting the sets of

TABLE 4. MR routing table $S_{\text{MR}}^{\text{OPF}}$ exported by Alg. 1.

ID	Route, x	$D(x)$	$P(x)$
$S_{\text{MR},2,3}^{\text{OPF}}$			
$S_{\text{MR},2,3,1}^{\text{OPF}}$	$\text{MR}_2 \rightarrow \text{MR}_1 \rightarrow \text{MR}_3$	2.00	16.55
$S_{\text{MR},2,3,2}^{\text{OPF}}$	$\text{MR}_2 \rightarrow \text{MR}_5 \rightarrow \text{MR}_1 \rightarrow \text{MR}_4 \rightarrow \text{MR}_6 \rightarrow \text{MR}_3$	5.00	14.90
$S_{\text{MR},2,3,3}^{\text{OPF}}$	$\text{MR}_2 \rightarrow \text{MR}_5 \rightarrow \text{MR}_1 \rightarrow \text{MR}_6 \rightarrow \text{MR}_3$	4.00	15.65
$S_{\text{MR},2,3,4}^{\text{OPF}}$	$\text{MR}_2 \rightarrow \text{MR}_5 \rightarrow \text{MR}_1 \rightarrow \text{MR}_3$	3.00	15.68
$S_{\text{MR},3,5}^{\text{OPF}}$			
$S_{\text{MR},3,5,1}^{\text{OPF}}$	$\text{MR}_3 \rightarrow \text{MR}_5$	1.00	16.08
$S_{\text{MR},3,5,2}^{\text{OPF}}$	$\text{MR}_3 \rightarrow \text{MR}_6 \rightarrow \text{MR}_4 \rightarrow \text{MR}_1 \rightarrow \text{MR}_5$	4.00	13.96
$S_{\text{MR},3,5,3}^{\text{OPF}}$	$\text{MR}_3 \rightarrow \text{MR}_6 \rightarrow \text{MR}_1 \rightarrow \text{MR}_5$	3.00	14.88
$S_{\text{MR},3,5,4}^{\text{OPF}}$	$\text{MR}_3 \rightarrow \text{MR}_1 \rightarrow \text{MR}_5$	2.00	14.92
$S_{\text{MR},3,6}^{\text{OPF}}$			
$S_{\text{MR},3,6,1}^{\text{OPF}}$	$\text{MR}_3 \rightarrow \text{MR}_6$	1.00	2.48
$S_{\text{MR},3,7}^{\text{OPF}}$			
$S_{\text{MR},3,7,1}^{\text{OPF}}$	$\text{MR}_3 \rightarrow \text{MR}_7$	1.00	17.24
$S_{\text{MR},3,7,2}^{\text{OPF}}$	$\text{MR}_3 \rightarrow \text{MR}_6 \rightarrow \text{MR}_4 \rightarrow \text{MR}_7$	3.00	9.25
$S_{\text{MR},3,7,3}^{\text{OPF}}$	$\text{MR}_3 \rightarrow \text{MR}_6 \rightarrow \text{MR}_7$	2.00	13.48
$S_{\text{MR},5,6}^{\text{OPF}}$			
$S_{\text{MR},5,6,1}^{\text{OPF}}$	$\text{MR}_5 \rightarrow \text{MR}_6$	1.00	16.53
$S_{\text{MR},5,6,2}^{\text{OPF}}$	$\text{MR}_5 \rightarrow \text{MR}_1 \rightarrow \text{MR}_4 \rightarrow \text{MR}_6$	3.00	13.64
$S_{\text{MR},5,6,3}^{\text{OPF}}$	$\text{MR}_5 \rightarrow \text{MR}_1 \rightarrow \text{MR}_6$	2.00	14.62

Pareto-optimal routes $S_{\text{MR},2,3}^{\text{OPF}}$, $S_{\text{MR},2,3}^{\text{OPF}}$, $S_{\text{MR},3,5}^{\text{OPF}}$, $S_{\text{MR},3,6}^{\text{OPF}}$, $S_{\text{MR},3,7}^{\text{OPF}}$ and $S_{\text{MR},5,6}^{\text{OPF}}$, respectively. The aforementioned OPFs constituting the MR routing table along with their associated utility functions, namely their delay $D(x)$ quantified in terms of the number of established hops and their power consumption $P(x)$ quantified in dBm, are presented in Table 4. Recall that the notation $S_{\text{MR},i,j,k}^{\text{OPF}}$ of Table 4 represents the k-th Pareto-optimal route identified by the NDQIO sub-process for producing the OPF $S_{\text{MR},i,j}^{\text{OPF}}$, which in turn corresponds to the set of Pareto-optimal routes spanning from MR_i to MR_j and vice versa.

Subsequently, the inner process of the MODQO algorithm builds up the respective MC routing table $S_{\text{MC}}^{\text{OPF}}$ based on the MR routing table $S_{\text{MR}}^{\text{OPF}}$ of Table 4, on the MC to MR association vector I_{MC} and on the MC friendship matrix $\mathcal{F}_{\text{MR}}$, which in our scenario is quantified in Eq. (25). We note that in the context of this current treatise, we have assumed that only the routes spanning from a specific MC_i to another specific MC_j are active during a transmission period, but not the reverse of these routes. The latter are considered to be activated during the next transmission period, when the first ones are inactive. In our scenario, the set S^{act} of active source and destination pairs considered is equal to:

$$S^{\text{act}} = \left\{ \begin{matrix} \text{MC}_2 \rightarrow \text{MC}_1 \\ \text{MC}_1 \rightarrow \text{MC}_3 \\ \text{MC}_4 \rightarrow \text{MC}_1 \\ \text{MC}_5 \rightarrow \text{MC}_1 \\ \text{MC}_2 \rightarrow \text{MC}_5 \end{matrix} \right\}, \tag{55}$$

TABLE 5. MC routing table $S_{\text{MC}}^{\text{OPF}}$ after Step 1 of Alg. 2.

ID	Route, x	$D(x)$	$P(x)$
$S_{\text{MC},1}^{\text{OPF}}$			
$S_{\text{MC},1,1}^{\text{OPF}}$	$\text{MC}_2 \rightarrow \text{MR}_6 \rightarrow \text{MR}_3 \rightarrow \text{MC}_1$	3.00	7.68
$S_{\text{MC},2}^{\text{OPF}}$			
$S_{\text{MC},2,1}^{\text{OPF}}$	$\text{MC}_4 \rightarrow \text{MR}_7 \rightarrow \text{MR}_3 \rightarrow \text{MC}_1$	3.00	17.56
$S_{\text{MC},2,2}^{\text{OPF}}$	$\text{MC}_4 \rightarrow \text{MR}_7 \rightarrow \text{MR}_4 \rightarrow \text{MR}_6 \rightarrow \text{MR}_3 \rightarrow \text{MC}_1$	5.00	10.95
$S_{\text{MC},2,3}^{\text{OPF}}$	$\text{MC}_4 \rightarrow \text{MR}_7 \rightarrow \text{MR}_6 \rightarrow \text{MR}_3 \rightarrow \text{MC}_1$	4.00	14.20
$S_{\text{MC},3}^{\text{OPF}}$			
$S_{\text{MC},3,1}^{\text{OPF}}$	$\text{MC}_2 \rightarrow \text{MR}_6 \rightarrow \text{MR}_5 \rightarrow \text{MC}_5$	3.00	17.61
$S_{\text{MC},3,2}^{\text{OPF}}$	$\text{MC}_2 \rightarrow \text{MR}_6 \rightarrow \text{MR}_4 \rightarrow \text{MR}_1 \rightarrow \text{MR}_5 \rightarrow \text{MC}_5$	5.00	15.54
$S_{\text{MC},3,3}^{\text{OPF}}$	$\text{MC}_2 \rightarrow \text{MR}_6 \rightarrow \text{MR}_1 \rightarrow \text{MR}_5 \rightarrow \text{MC}_5$	4.00	16.20
$S_{\text{MC},4}^{\text{OPF}}$			
$S_{\text{MC},4,1}^{\text{OPF}}$	$\text{MC}_1 \rightarrow \text{MR}_3 \rightarrow \text{MR}_1 \rightarrow \text{MR}_2 \rightarrow \text{MC}_3$	4.00	17.19
$S_{\text{MC},4,2}^{\text{OPF}}$	$\text{MC}_1 \rightarrow \text{MR}_3 \rightarrow \text{MR}_6 \rightarrow \text{MR}_4 \rightarrow \text{MR}_1 \rightarrow \text{MR}_5 \rightarrow \text{MR}_2 \rightarrow \text{MC}_3$	7.00	15.80
$S_{\text{MC},4,3}^{\text{OPF}}$	$\text{MC}_1 \rightarrow \text{MR}_3 \rightarrow \text{MR}_6 \rightarrow \text{MR}_1 \rightarrow \text{MR}_5 \rightarrow \text{MR}_2 \rightarrow \text{MC}_3$	6.00	16.42
$S_{\text{MC},4,4}^{\text{OPF}}$	$\text{MC}_1 \rightarrow \text{MR}_3 \rightarrow \text{MR}_1 \rightarrow \text{MR}_5 \rightarrow \text{MR}_2 \rightarrow \text{MC}_3$	5.00	16.45
$S_{\text{MC},5}^{\text{OPF}}$			
$S_{\text{MC},5,1}^{\text{OPF}}$	$\text{MC}_5 \rightarrow \text{MR}_5 \rightarrow \text{MR}_3 \rightarrow \text{MC}_1$	3.00	17.55
$S_{\text{MC},5,2}^{\text{OPF}}$	$\text{MC}_5 \rightarrow \text{MR}_5 \rightarrow \text{MR}_1 \rightarrow \text{MR}_4 \rightarrow \text{MR}_6 \rightarrow \text{MR}_3 \rightarrow \text{MC}_1$	6.00	16.16
$S_{\text{MC},5,3}^{\text{OPF}}$	$\text{MC}_5 \rightarrow \text{MR}_5 \rightarrow \text{MR}_1 \rightarrow \text{MR}_6 \rightarrow \text{MR}_3 \rightarrow \text{MC}_1$	5.00	16.73
$S_{\text{MC},5,4}^{\text{OPF}}$	$\text{MC}_5 \rightarrow \text{MR}_5 \rightarrow \text{MR}_1 \rightarrow \text{MR}_3 \rightarrow \text{MC}_1$	4.00	16.76

where we can observe that the number N_r of active pairs of source and destination MCs is equal to:

$$N_r = \frac{||\mathcal{F}_{\text{MC}}||_2}{2} = \left|S^{\text{act}}\right| = 5. \tag{56}$$

Based on the active set S^{act} defined in Eq (55) and on the association vector I_{MC}, which is portrayed with the aid of the dashed lines in Fig. 7, the MODQO algorithm attempts to construct the respective MC routing table $S_{\text{MC}}^{\text{OPF}}$ in Steps 11-25 of Alg. 1. In particular, for the routes from MC_2 to MC_1 associated with MR_6 and MR_3, respectively, the set $S_{\text{MC},3,6}^{\text{OPF}}$ consisting of a single route will be utilized, with the order of its nodes reversed, and the source and destination MCs are appended at the start and the end of the Pareto-optimal route, as stated in Step 18 of Alg. 1. The same process is repeated until the Pareto-optimal routes of the entire set of active source and destination pairs have been constructed forming the MR routing table $S_{\text{MC}}^{\text{OPF}}$.

The construction the MC routing table $S_{\text{MC}}^{\text{OPF}}$ denotes the end of the MODQO inner step presented in Alg. 1. Then, the MODQO algorithm then invokes its outer step, which is formally defined in Alg. 2. Initially, the MODQO outer step sortsthe elements $\{S_{\text{MC},n}^{\text{OPF}}\}_{n=1}^{5}$ of the MC routing in ascending order according to their number $\left|S_{\text{MC},n}^{\text{OPF}}\right|$ of the Pareto-optimal

routes in Step 1 of Alg. 2. The sorted MC routing table associated with our scenario along with the routes' delay and power consumption is presented in Table 5, where the notation $S^{\text{OPF}}_{\text{MC},i,j}$ is used, denoting the j-th Pareto-optimal route of the set $S^{\text{OPF}}_{\text{MC},i}$, which in turn corresponds to the Pareto-optimal routes' set for the i-th active pair of source and destination MCs. The MODQO algorithm then initializes the set S^{OPF} of Pareto-optimal route-combinations to the first set of element in the MC routing table, i.e. we have $S^{\text{OPF}} = S^{\text{OPF}}_{\text{MC},1}$, and it then removes this element from the MC routing table, according to Step 2 of Alg. 2.

Subsequently, observe for the MODQO outer step's iterative process of Steps 3-11 of Alg. 2 that the route-combinations' OPF S^{OPF} contains routes from all the active pairs of source and destination MCs, as encapsulated by Step 11 of Alg. 2. During the first iteration, the MODQO outer procedure assesses the maximum achievable complexity reduction offered by the NDQIO algorithm by jointly considering multiple stages. After the initialization the MC routing table consists of four elements, namely the elements $\{S^{\text{OPF}}_{\text{MC},n}\}^{5}_{n=2}$ of Table 5. According to Step 4 of Alg. 2, the reference complexity $L^{\text{ref}}_{\text{CM}}(n)$ quantified in terms of the number of CFEs as a function of n encapsulated stages imposed by the CM method based on Eq. (49) is equal to:

$$L^{\text{ref}}_{\text{CM}}(n) = \begin{cases} 9, & n = 1, \\ 90, & n = 2, \\ 234, & n = 3, \\ 490, & n = 4, \end{cases} \tag{57}$$

while the upper bound of the reference complexity $L^{\text{ref}}_{\text{QM,max}}(n)$ quantified in terms of the number of CFEs as a function of n encapsulated stages imposed by the QM method based on Eq. (51) is equal to:

$$L^{\text{ref}}_{\text{QM,max}}(n) = \begin{cases} 59, & n = 1, \\ 405, & n = 2, \\ 777, & n = 3, \\ 2016, & n = 4. \end{cases} \tag{58}$$

Therefore, based on Eqs. (57) and (58) the lower bound of the complexity reduction offered by the NDQIO with respect to the CM method as a function of n encapsulated stages is equal to:

$$\frac{L^{\text{ref}}_{\text{CM}}(n)}{L^{\text{ref}}_{\text{QM,max}}(n)} = \begin{cases} 0.1525, & n = 1, \\ 0.2222, & n = 2, \\ \mathbf{0.3012}, & n = 3, \\ 0.2431, & n = 4. \end{cases} \tag{59}$$

Therefore, it is clear from Eq. (59) that the lower bound of the complexity reduction offered by the NDQIO algorithm with respect to the CM method is maximized for $n_{\text{opt}} = 3$ joint stages.

Having exported the optimal number n_{opt} of the joint stages to be considered by the NDQIO algorithm, the MODQO outer step has to assess as to whether the NDQIO algorithm is indeed capable of outperforming the CM method for this specific optimal value. This action is undertaken by Step 6 of Alg. 2, where the lower bound of the complexity imposed by the NDQIO algorithm is compared to that of the CM method. More particularly, for our scenario we have:

$$L^{\text{ref}}_{\text{QM,min}}(n_{\text{opt}}) = 123 < 234 = L^{\text{ref}}_{\text{CM}}(n_{\text{opt}}). \tag{60}$$

Therefore, based on Eq. (60) the MODQO outer step concludes that NDQIO may potentially impose a lower number of CFEs than the CM method, and activates it for $n_{\text{opt}} = 3$ stages, according to Step 7 of Alg. 2, thus invoking the process portrayed in Fig. 11b and the stages examined are then removed from the MC routing table. At the end of the NDQIO process the MODQO outer step reaches the end of the fourth stage in Fig. 11b and, thus, the set S^{OPF} of the route-combinations is updated to the OPF exported by the NDQIO process, which in turn constitutes the set[7] $S^{\text{OPF}}_{(4)}$ of the surviving route-combinations of the fourth stage in the irregular trellis of Fig. 11b. These eight route-combinations along with their respective average delay and their respective average power consumption are presented in Table 6, where the route-combinations are represented using the IDs from the first column of Table 5 containing the MC routing table. For instance, the first surviving route-combination $S^{\text{OPF}}_{(4),1}$ of the fourth stage is translated using Table 5 as follows:

$$S^{\text{OPF}}_{(4),1} = \left\{ \begin{array}{c} \text{MC}_2 \rightarrow \text{MR}_6 \rightarrow \text{MR}_3 \rightarrow \text{MC}_1, \\ \text{MC}_4 \rightarrow \text{MR}_7 \rightarrow \text{MR}_3 \rightarrow \text{MC}_1, \\ \text{MC}_2 \rightarrow \text{MR}_6 \rightarrow \text{MR}_5 \rightarrow \text{MC}_5, \\ \text{MC}_1 \rightarrow \text{MR}_3 \rightarrow \text{MR}_1 \rightarrow \text{MR}_2 \rightarrow \text{MC}_3 \end{array} \right\}. \tag{61}$$

Subsequently, the eight surviving route-combinations contained in the set $S^{\text{OPF}}_{(4)}$ continue their propagation to the final stage of the irregular trellis diagram of Fig. 11b. A new iteration of the MODQO outer step is invoked and the reference complexities quantified in terms of the number of CFEs are evaluated during Step 4 of Alg. 2, as follows:

$$L^{\text{ref}}_{\text{CM}}(n) = 1024, \quad n = 1, \tag{62}$$

$$L^{\text{ref}}_{\text{QM,max}}(n) = 1563 \quad n = 1, \tag{63}$$

$$L^{\text{ref}}_{\text{QM,min}}(n) = 291 \quad n = 1, \tag{64}$$

where the maximum complexity reduction offered by the NDQIO algorithm with respect to the CM method is achieved for $n_{\text{opt}} = 1$, in the absence of any other stages. Additionally, since the lower bound of the NDQIO reference complexity $L^{\text{ref}}_{\text{QM,min}}$ is lower than that of the CM method, a NDQIO process is activated for encapsulating the final stage into the eight surviving route-combinations and, thus, updating the OPF of the route combinations to $S^{\text{OPF}} = S^{\text{OPF}}_{(5)}$. Naturally, since we have $n_{\text{opt}} = \left|S^{\text{OPF}}_{\text{MC}}\right| = 1$, the outer step concludes that this is the final stage. Hence, the normalized entropy of the normalized composite betweenness $\bar{H}[\bar{B}_{com}(S)]$ is calculated after the identification of a Pareto-optimal route-combination by the NDQIO algorithm and a record of the route-combination exhibiting the highest $\bar{H}[\bar{B}_{com}(S)]$ value is kept. For this

[7]In general, the notation $S^{\text{OPF}}_{(n)}$ corresponds to the surviving route-combinations of the n-th trellis stage.

TABLE 6. Surviving route-combinations S of the outer step.

ID	Pareto-optimal Route-combinations	$\bar{P}(S)$	$\bar{D}(S)$	$\bar{H}[\bar{B}_{com}(S)]$	$\max\{\bar{H}[\bar{B}_{com}(S)]\}$	$\text{argmax}\{\bar{H}[\bar{B}_{com}(S)]\}$
Initialization $S^{\text{OPF}}_{(1)}$						
$S^{\text{OPF}}_{(1),1}$	$S^{\text{OPF}}_{\text{MC},1,1}$	7.68	3.00	N/A		
Iteration 1: NDQIO encapsulates 3 joint stages						
$S^{\text{OPF}}_{(4),1}$	$S^{\text{OPF}}_{\text{MC},1,1}$, $S^{\text{OPF}}_{\text{MC},2,1}$, $S^{\text{OPF}}_{\text{MC},3,1}$, $S^{\text{OPF}}_{\text{MC},4,1}$	16.35	3.25	N/A		
$S^{\text{OPF}}_{(4),2}$	$S^{\text{OPF}}_{\text{MC},1,1}$, $S^{\text{OPF}}_{\text{MC},2,2}$, $S^{\text{OPF}}_{\text{MC},3,2}$, $S^{\text{OPF}}_{\text{MC},4,2}$	13.63	5.00			
$S^{\text{OPF}}_{(4),3}$	$S^{\text{OPF}}_{\text{MC},1,1}$, $S^{\text{OPF}}_{\text{MC},2,2}$, $S^{\text{OPF}}_{\text{MC},3,3}$, $S^{\text{OPF}}_{\text{MC},4,1}$	14.48	4.00			
$S^{\text{OPF}}_{(4),4}$	$S^{\text{OPF}}_{\text{MC},1,1}$, $S^{\text{OPF}}_{\text{MC},2,2}$, $S^{\text{OPF}}_{\text{MC},3,3}$, $S^{\text{OPF}}_{\text{MC},4,4}$	14.15	4.25			
$S^{\text{OPF}}_{(4),5}$	$S^{\text{OPF}}_{\text{MC},1,1}$, $S^{\text{OPF}}_{\text{MC},2,2}$, $S^{\text{OPF}}_{\text{MC},3,3}$, $S^{\text{OPF}}_{\text{MC},4,2}$	13.89	4.75			
$S^{\text{OPF}}_{(4),6}$	$S^{\text{OPF}}_{\text{MC},1,1}$, $S^{\text{OPF}}_{\text{MC},2,3}$, $S^{\text{OPF}}_{\text{MC},3,1}$, $S^{\text{OPF}}_{\text{MC},4,1}$	15.51	3.50			
$S^{\text{OPF}}_{(4),7}$	$S^{\text{OPF}}_{\text{MC},1,1}$, $S^{\text{OPF}}_{\text{MC},2,2}$, $S^{\text{OPF}}_{\text{MC},3,2}$, $S^{\text{OPF}}_{\text{MC},4,4}$	13.90	4.50			
$S^{\text{OPF}}_{(4),8}$	$S^{\text{OPF}}_{\text{MC},1,1}$, $S^{\text{OPF}}_{\text{MC},2,3}$, $S^{\text{OPF}}_{\text{MC},3,3}$, $S^{\text{OPF}}_{\text{MC},4,1}$	14.99	3.75			
Final Iteration: NDQIO encapsulates 1 stage						
$S^{\text{OPF}}_{(5),1}$	$S^{\text{OPF}}_{\text{MC},1,1}$, $S^{\text{OPF}}_{\text{MC},2,1}$, $S^{\text{OPF}}_{\text{MC},3,1}$, $S^{\text{OPF}}_{\text{MC},4,1}$, $S^{\text{OPF}}_{\text{MC},5,1}$	16.62	3.20	0.000	0.000	$S^{\text{OPF}}_{(5),1}$
$S^{\text{OPF}}_{(5),2}$	$S^{\text{OPF}}_{\text{MC},1,1}$, $S^{\text{OPF}}_{\text{MC},2,2}$, $S^{\text{OPF}}_{\text{MC},3,2}$, $S^{\text{OPF}}_{\text{MC},4,2}$, $S^{\text{OPF}}_{\text{MC},5,2}$	14.26	5.20	0.665	0.665	$S^{\text{OPF}}_{(5),2}$
$S^{\text{OPF}}_{(5),3}$	$S^{\text{OPF}}_{\text{MC},1,1}$, $S^{\text{OPF}}_{\text{MC},2,2}$, $S^{\text{OPF}}_{\text{MC},3,3}$, $S^{\text{OPF}}_{\text{MC},4,1}$, $S^{\text{OPF}}_{\text{MC},5,4}$	15.04	4.00	0.488	0.665	$S^{\text{OPF}}_{(5),2}$
$S^{\text{OPF}}_{(5),4}$	$S^{\text{OPF}}_{\text{MC},1,1}$, $S^{\text{OPF}}_{\text{MC},2,2}$, $S^{\text{OPF}}_{\text{MC},3,2}$, $S^{\text{OPF}}_{\text{MC},4,4}$, $S^{\text{OPF}}_{\text{MC},5,4}$	14.64	4.40	0.656	0.665	$S^{\text{OPF}}_{(5),2}$
$S^{\text{OPF}}_{(5),5}$	$S^{\text{OPF}}_{\text{MC},1,1}$, $S^{\text{OPF}}_{\text{MC},2,3}$, $S^{\text{OPF}}_{\text{MC},3,1}$, $S^{\text{OPF}}_{\text{MC},4,1}$, $S^{\text{OPF}}_{\text{MC},5,1}$	16.00	3.40	0.000	0.665	$S^{\text{OPF}}_{(5),2}$
$S^{\text{OPF}}_{(5),6}$	$S^{\text{OPF}}_{\text{MC},1,1}$, $S^{\text{OPF}}_{\text{MC},2,2}$, $S^{\text{OPF}}_{\text{MC},3,3}$, $S^{\text{OPF}}_{\text{MC},4,4}$, $S^{\text{OPF}}_{\text{MC},5,2}$	14.64	4.60	**0.679**	0.679	$S^{\text{OPF}}_{(5),6}$
$S^{\text{OPF}}_{(5),7}$	$S^{\text{OPF}}_{\text{MC},1,1}$, $S^{\text{OPF}}_{\text{MC},2,3}$, $S^{\text{OPF}}_{\text{MC},3,1}$, $S^{\text{OPF}}_{\text{MC},4,1}$, $S^{\text{OPF}}_{\text{MC},5,1}$	15.63	3.60	0.327	0.679	$S^{\text{OPF}}_{(5),6}$
$S^{\text{OPF}}_{(5),8}$	$S^{\text{OPF}}_{\text{MC},1,1}$, $S^{\text{OPF}}_{\text{MC},2,2}$, $S^{\text{OPF}}_{\text{MC},3,3}$, $S^{\text{OPF}}_{\text{MC},4,1}$, $S^{\text{OPF}}_{\text{MC},5,1}$	15.29	3.80	0.534	0.679	$S^{\text{OPF}}_{(5),6}$
$S^{\text{OPF}}_{(5),9}$	$S^{\text{OPF}}_{\text{MC},1,1}$, $S^{\text{OPF}}_{\text{MC},2,2}$, $S^{\text{OPF}}_{\text{MC},3,2}$, $S^{\text{OPF}}_{\text{MC},4,2}$, $S^{\text{OPF}}_{\text{MC},5,4}$	14.46	4.80	0.674	0.679	$S^{\text{OPF}}_{(5),6}$
$S^{\text{OPF}}_{(5),10}$	$S^{\text{OPF}}_{\text{MC},1,1}$, $S^{\text{OPF}}_{\text{MC},2,2}$, $S^{\text{OPF}}_{\text{MC},3,3}$, $S^{\text{OPF}}_{\text{MC},4,4}$, $S^{\text{OPF}}_{\text{MC},5,4}$	14.81	4.20	0.638	0.679	$S^{\text{OPF}}_{(5),6}$
$S^{\text{OPF}}_{(5),11}$	$S^{\text{OPF}}_{\text{MC},1,1}$, $S^{\text{OPF}}_{\text{MC},2,2}$, $S^{\text{OPF}}_{\text{MC},3,3}$, $S^{\text{OPF}}_{\text{MC},4,2}$, $S^{\text{OPF}}_{\text{MC},5,2}$	14.45	5.00	0.675	0.679	$S^{\text{OPF}}_{(5),6}$

reason, the normalized entropy of the normalized composite betweenness values of the Pareto-optimal route-combinations are exclusively included in the last three columns of Table 6, where we can observe that the Pareto-optimal route-combination is the $S^{\text{OPF}}_{(5),6}$ one, which is translated using Table 5 as follows:

$$S^{\text{OPF}}_{(5),6} = \left\{ \begin{array}{c} \text{MC}_2 \rightarrow \text{MR}_6 \rightarrow \text{MR}_3 \rightarrow \text{MC}_1, \\ \text{MC}_4 \rightarrow \text{MR}_7 \rightarrow \text{MR}_4 \rightarrow \text{MR}_6 \rightarrow \text{MR}_3 \rightarrow \text{MC}_1 \\ \text{MC}_2 \rightarrow \text{MR}_6 \rightarrow \text{MR}_1 \rightarrow \text{MR}_5 \rightarrow \text{MC}_5 \\ \text{MC}_1 \rightarrow \text{MR}_3 \rightarrow \text{MR}_1 \rightarrow \text{MR}_5 \rightarrow \text{MR}_2 \rightarrow \text{MC}_3 \\ \text{MC}_5 \rightarrow \text{MR}_5 \rightarrow \text{MR}_1 \rightarrow \text{MR}_4 \rightarrow \text{MR}_6 \rightarrow \text{MR}_3 \rightarrow \text{MC}_1 \end{array} \right\}. \tag{65}$$

Finally, the MOQDO algorithm outputs the specific route-combination $S^{\text{OPF}}_{(5),6}$ that exhibits the highest load balancing metric along with the entire set S^{OPF} of Pareto-optimal route-combinations, as described in Block 4 of the MODQO flowchart seen in Fig. 10. By a close inspection, the eight routes of the last stage are identical to those of Table 3 exported by the exhaustive search.

V. ACCURACY VERSUS COMPLEXITY DISCUSSIONS

Having provided a detailed description of the MODQO algorithm in the previous section, let us now assess it performance in terms of both its complexity imposed and its accuracy in terms of the optimization metrics considered.

A. COMPLEXITY

As it can be observed in the MODQO flowchart of Fig. 10, the MODQO algorithm's operation is constituted by two distinct steps, namely the *inner* and *outer steps*. Therefore, we have to characterize the complexity associated with each step independently for the sake of characterizing the total complexity imposed by the MODQO algorithm. Let us commence with the characterization of the MODQO inner step complexity.

1) INNER STEP

As far as the inner step is concerned, the NDQIO algorithm, defined in [43, Algorithm 4], is activated by the cluster head in Step 6 of Alg. 1 precisely $||\mathcal{F}_{MR}||_2/2$ times, namely once per two friendly MRs. This is justified by the fact that we can utilize the Pareto-optimal routes spanning from MR_i to MR_j for constructing the Pareto-optimal routes emerging from MR_j to MR_i by inverting the sequence of the nodes at the cost of no additional CFEs. Therefore, the total number N_{NDQIO} of the NDQIO process activations is equal to:

$$N_{\text{NDQIO}} = \frac{||\mathcal{F}_{MR}||_2}{2}, \tag{66}$$

while the respective lower and upper bounds are equal to:

$$N^{\min}_{\text{NDQIO}} = 1, \tag{67}$$

$$N^{\max}_{\text{NDQIO}} = \frac{N_{\text{MR}}(N_{\text{MR}}-1)}{2}, \tag{68}$$

where the lower bound $N^{\min}_{\text{NDQIO}}$ corresponds to the best-case scenario, and the MCs are associated with only two different MR. By contrast, the upper bound $N^{\max}_{\text{NDQIO}}$ occurs

in the worst-case scenario, where each of the MRs shares a friendship relationship with all the rest of the MRs. Therefore, the complexity $L^{\text{inner}}_{\text{MODQO}}$ quantified in terms of the number of CFEs imposed by the MODQO inner step is equal to:

$$L^{\text{inner}}_{\text{MODQO}} = \frac{||\mathcal{F}_{MR}||_2 \, L_{\text{NDQIO}}}{2}, \tag{69}$$

where the complexity L_{NDQIO} imposed by a single NDQIO algorithm activation has been quantified in Eq. (33) in terms of the number of CFEs. We note that the Eq. (69) corresponds to the general case of the complexity imposed by the MODQO algorithm inner step. Explicitly, we can readily derive its lower and upper bounds using Eqs. (67) and (68) as follows:

$$\begin{aligned} L^{\text{inner,min}}_{\text{MODQO}}(N_{\text{OPF}}) &= L^{\text{min}}_{\text{NDQIO}}(N_{\text{OPF}}) = O(N_{\text{OPF}}\sqrt{N}), \quad (70) \\ L^{\text{inner,max}}_{\text{MODQO}}(N_{\text{OPF}}) &= \frac{N_{\text{MR}}(N_{\text{MR}}-1)}{2} L^{\text{max}}_{\text{NDQIO}}(N_{\text{OPF}}), \\ &= O(N^2_{\text{MR}} N_{\text{OPF}}\sqrt{N}), \quad (71) \end{aligned}$$

where N_{OPF} corresponds to the number of Pareto-optimal route-solutions of each independent sub-problem and N is the total number of legitimate routes between two MRs as defined in Eq. (23). We note that the minimum complexity imposed by the NDQIO algorithm can be derived by considering that both the BBHT-QSA and the DHA sub-processes impose the minimum possible amount of complexity, namely $L^{\text{min}}_{\text{DHA}}$ and $L^{\text{min}}_{\text{BBHT}}$ defined in Eqs. (29) and (31), respectively . Equivalently, the NDQIO algorithm's maximum complexity is derived by considering that both the BBHT-QSA and the DHA sub-processes impose the maximum amount of complexity, namely $L^{\text{max}}_{\text{DHA}}$ and $L^{\text{max}}_{\text{BBHT}}$ defined in Eqs. (30) and (32), respectively.

Observe in Eq. (75) that the upper bound of the complexity imposed by the MODQO algorithm becomes independent of the number N_{MC} of MCs, since it solely depends on the number N_{MR} of MRs. Naturally, as the number of MCs increases the number of friendly MRs per MR also increases up to a maximum of the total number of MRs.

Additionally, it is possible to derive the upper and lower bounds of the number N_{OPF} of Pareto-optimal routes specifically for our scenario. Explicitly, the lower bound corresponds to the best-case scenario, where a single Pareto-optimal route exists for all the possible pairs of source and destination MCs. By contrast, the upper bound of the number N_{OPF} of Pareto-optimal routes corresponds to the worst-case scenario, where a single Pareto-optimal route exists for all the possible values of the delay due to the utilization of the weak Pareto dominance operator of Definition 1. Since the delay has been quantified in terms of the number of hops, its maximum value is encountered when all the MRs participate in the route establishment, i.e. we have $D_{\max}(x) = N_{\text{MR}} + 2$ hops, while its minimum value corresponds to the case where there are no intermediate MR involved in the route construction, i.e. we have $D_{\min}(x) = 3$ hops. This range provides us with at most $D_{\max}(x) - D_{\min}(x) = N_{\text{MR}} - 1$ possible delay values. Therefore the upper and lower bounds of the number of Pareto-optimal routes are quantified as follows:

$$N^{\text{min}}_{\text{OPF}} = 1, \tag{72}$$

$$N^{\text{max}}_{\text{OPF}} = N_{\text{MR}} - 1. \tag{73}$$

Consequently, we may readily derive the strict upper and lower bounds of the MODQO inner step complexity by substituting the bounds of Eqs. (72) and (73) into Eqs. (70) and (71), respectively. Hence, the resultant strict MODQO inner step lower bound is equal to:

$$L^{\text{inner,min}}_{\text{MODQO}} = L^{\text{min}}_{\text{NDQIO}}(1) = O(\sqrt{N}), \tag{74}$$

while the respective strict upper bound is equal to:

$$\begin{aligned} L^{\text{inner,max}}_{\text{MODQO}} &= \frac{N_{\text{MR}}(N_{\text{MR}}-1)}{2} L^{\text{max}}_{\text{NDQIO}}(N_{\text{MR}}-1), \\ &= O(N^3_{\text{MR}}\sqrt{N}). \quad (75) \end{aligned}$$

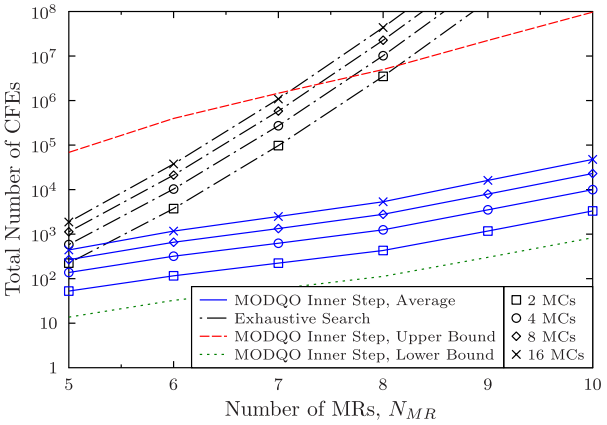

FIGURE 12. Average MODQO inner step complexity quantified as a function of the number of CFEs for twin-layer networks consisting of $N_{\text{MR}} = \{5, 6, \ldots, 10\}$ MRs and $N_{\text{MR}} = \{2, 4, 8, 16\}$ MCs. The MODQO inner step complexity is compared to that of the exhaustive search and to its respective upper and lower bounds. The results have been averaged over 10^8 runs.

Based on this analysis, let us now proceed by presenting the average MODQO inner step complexity results quantified as a function of the number of CFEs for twin-layer networks consisting of $N_{\text{MR}} = \{5, 6, \ldots, 10\}$ MRs and $N_{\text{MR}} = \{2, 4, 8, 16\}$ MCs, which is shown in Fig. 12, where the MODQO algorithm's average inner step complexity is compared both to its lower and upper bounds, as they were quantified in Eqs. (74) and (75), and that of to the exhaustive search. We note that both the exhaustive search and the MODQO algorithm have been deployed and their complexity was averaged over identical twin-layer network structures. Observe in Fig. 12 that the MODQO algorithm's average complexity increases exponentially with the number N_{MR} of MRs. Nevertheless, it increases with a substantially lower gradient than that of the average complexity imposed by the exhaustive search. In fact, the MODQO inner step achieves a significant complexity reduction even for twin-layer networks comprised by as few as $N_{\text{MR}} = 5$ MRs,

where the MODQO algorithm imposes a complexity, which is four times lower than that of the exhaustive search, while the complexity imposed by the MODQO algorithm's inner step becomes about six orders of magnitude lower than that of the exhaustive search for twin-layer networks consisting of $N_{\mathrm{MR}} = 10$ MRs.

Additionally, the complexity quantified in terms of the number of CFEs imposed both by the MODQO inner step and by the exhaustive search increases almost proportionally to number of MCs as the the number N_{MC} of MCs increases. Naturally, as N_{MC} increases, the average number of friends of each of the MRs increases, since the associated number of active pairs of source and destination MCs increases. This results, in turn, in an increase in the number of the NDQIO process activations, hence yielding an increase in the MODQO's inner step complexity. Nevertheless, this rate of increase slows down as the network becomes more densely populated by MCs, slowly approaching the upper bound of Eq. (75), where all the MRs share a social relationship with all the rest of the MRs.

2) OUTER STEP

As far as the complexity imposed by the MODQO outer step is concerned, we first quantify that of the CM method, which constitutes the upper bound of our proposed QM process. For this reason, let us make the additional assumption that the number of Pareto-optimal route-combinations increases by a factor ρ after each state. This can be formally formulated as follows:

$$\left|S_{(n)}^{OPF}\right| = \rho^{n-1}\bar{N}_{\mathrm{OPF}}, \tag{76}$$

where $\bar{N}_{\mathrm{OPF}}$ corresponds to the average number of Pareto-optimal routes on the independent sub-problems, while $S_{(n)}^{\mathrm{OPF}}$ is the set of Pareto-optimal route-combinations after n stages of the irregular trellis diagram. We note that it is possible to fully characterize $\bar{N}_{\mathrm{OPF}}$ with the aid of statistical analysis of offline data. Thus, we can estimate the complexity imposed. Based on Eq. (76), we can quantify the complexity in terms of the number of CFEs imposed by the CM method as follows:

$$\begin{aligned} L_{\mathrm{CM}}^{\mathrm{outer}} &= \sum_{n=2}^{N_r} \rho^{2(n-1)}\bar{N}_{\mathrm{OPF}}^4 = \bar{N}_{\mathrm{OPF}}^4 \frac{\rho^{2N_r}-\rho^2}{\rho^2-1}, \\ &= O(\rho^{2N_r}\bar{N}_{\mathrm{OPF}}^4). \end{aligned} \tag{77}$$

Explicitly, the upper bound of the factor ρ, for which the CM method is capable offering beneficial complexity reduction compared to the exhaustive search, is given by:

$$\rho < \bar{N}_{\mathrm{OPF}}^{\frac{2N_r-2}{2N_r-1}}. \tag{78}$$

Consequently, the CM method is capable of offering a complexity reduction, as long as the number of Pareto-optimal route-combinations increases by a factor that is slightly less than $\bar{N}_{\mathrm{OPF}}$, based on Eq. (78).

Having characterized the CM method in terms of its complexity, let us now proceed with the characterization of our proposed QM method. To begin with, we will assess the complexity reduction achieved by the QM method compared to that of the CM one at a single iteration of the QM method. For this reason, we ought to investigate the dynamics behind the selection of the number n_{opt} of joint stages. In general, the complexity quantified in terms of the number of CFEs imposed by the NDQIO process during a single iteration is equal to:

$$\begin{aligned} L_{\mathrm{QM}}^{\mathrm{outer}}(n, n_{\mathrm{opt}}) = (2K)^{-1}\rho^{2(n+n_{\mathrm{opt}}-1)}\bar{N}_{\mathrm{OPF}}^2 + K^{-1} \\ \cdot\left[L_{\mathrm{DHA}}(\rho^{n-1}\bar{N}_{\mathrm{OPF}}^{n_{\mathrm{opt}}+1}) \right. \\ \left. + 2L_{\mathrm{BBHT}}(\rho^{n-1}\bar{N}_{\mathrm{OPF}}^{n_{\mathrm{opt}}+1}) - \frac{1}{2}\right] \\ \cdot\rho^{n+n_{\mathrm{opt}}-1}\bar{N}_{\mathrm{OPF}} \\ + (1-K)\left\{\frac{2}{K}L_{\mathrm{BBHT}}(\rho^{n-1}\bar{N}_{\mathrm{OPF}}^{n_{\mathrm{opt}}+1}) + \frac{1}{2}\right\}, \end{aligned} \tag{79}$$

with its order being equal to:

$$\begin{aligned} &L_{\mathrm{QM}}^{\mathrm{outer}}(n, n_{\mathrm{opt}}) \\ &\quad = \begin{cases} O(\rho^{2n}\bar{N}_{\mathrm{OPF}}^2), & n_{\mathrm{opt}} = 1, \\ O\left[\rho^{(3n+2n_{\mathrm{opt}}-3)/2}\bar{N}_{\mathrm{OPF}}^{(n_{\mathrm{opt}}+3)/2}\right], & n_{\mathrm{opt}} > 1. \end{cases} \end{aligned} \tag{80}$$

Futhermore, the respective complexity imposed by the CM method, based on Eq. (77), is equal to:

$$\begin{aligned} L_{\mathrm{CM}}^{\mathrm{outer}}(n, n_{\mathrm{opt}}) &= \sum_{n'=n}^{n+n_{\mathrm{opt}}-1} \rho^{2(n'-1)}\bar{N}_{\mathrm{OPF}}^4 \\ &= \bar{N}_{\mathrm{OPF}}^4 \frac{\rho^{2(n+n_{\mathrm{opt}})}-\rho^{2n}}{\rho-1}, \\ &= O(\rho^{2(n+n_{\mathrm{opt}})}\bar{N}_{\mathrm{OPF}}^4). \end{aligned} \tag{81}$$

Explicitly, we have to estimate the value of the optimal number n_{opt} of stages to be considered by the QM method. Naturally, we can derive the orders of the respective reference complexities by setting $\rho = 1$ in Eqs. (81) and (80), yielding:

$$L_{\mathrm{QM}}^{\mathrm{ref}}(n, n_{\mathrm{opt}}) = O\left[\bar{N}_{\mathrm{OPF}}^{(n_{\mathrm{opt}}+3)/2}\right], \tag{82}$$

$$L_{\mathrm{CM}}^{\mathrm{ref}}(n, n_{\mathrm{opt}}) = O(\bar{N}_{\mathrm{OPF}}^4), \tag{83}$$

where it is clear that the CM method's order of reference complexity is constant, whilst the QM method's complexity increases as the number n_{opt} of joint stages increases. In fact, after $n_{\mathrm{opt}} = 5$ stages the order of the QM method reference complexity becomes equal to that of the CM method, implying that the NDQIO process will no longer offer any complexity reduction. Based on this dynamic, we can conclude that the optimal value of the number of joint stages considered by the NDQIO process, which provides the maximum possible complexity reduction is $n_{\mathrm{opt}} = 1$ stage. Therefore, the total

complexity $L^{\text{outer}}_{\text{MODQO}}$ imposed by the QM method of Alg. 2 is equal to:

$$\begin{aligned} L^{\text{outer}}_{\text{MODQO}} &= \sum_{n=2}^{N_r} L^{\text{outer}}_{\text{QM}}(n,1), \\ &= \sum_{n=1}^{N_r} O(\rho^{2n}\bar{N}^2_{\text{OPF}}), \\ &= O\left[\bar{N}^2_{\text{OPF}} \frac{\rho^{2(Nr+1)}-\rho^4}{\rho^2-1}\right] \\ &= O\left[\rho^{2(Nr+1)}\bar{N}^2_{\text{OPF}}\right]. \end{aligned} \tag{84}$$

Hence, based on Eqs. (77) and (84) the QM method achieves a complexity reduction, which is on the the order of $O\left(\rho^{-2}\bar{N}^2_{\text{OPF}}\right)$, when compared to the CM method, as long as $\rho < \bar{N}_{\text{OPF}}$. We note that if we have $\rho = \bar{N}_{\text{OPF}}$, then the QM method will match the complexity order of the CM method. Additionally, a single NDQIO iteration invoked for all the stages would result in a complexity that is equal to:

$$\begin{aligned} L^{\text{outer}}_{\text{NDQIO}} &= L^{\text{outer}}_{\text{QM}}(1, N_r), \\ &= O\left[\rho^{N_r}\bar{N}^{(N_r+3)/2}_{\text{OPF}}\right], \end{aligned} \tag{85}$$

where we can clearly observe that the QM method offers a complexity reduction on order of $O(N^{Nr/2}_{\text{OPF}}\rho^{-Nr})$, when compared to that of a single NDQIO activation that jointly considers all the stages. Consequently, the QM method outperforms the NDQIO algorithm that considers jointly all the trellis stages, as long as we strictly have the following asymptotic bound for the surviving route-combinations' growth factor ρ:

$$\rho < \sqrt{N_{\text{OPF}}}. \tag{86}$$

For the sake of demonstrating the benefits of the QM method against the single NDQIO algorithm activation for all the stages, we have to statistically characterize the factor ρ for our scenario considered. Explicitly, the average number $\bar{N}_{\text{OPF}}$ of Pareto-optimal routes in the MC routing quantified as a function of the number N_{MR} of MRs is shown in Fig. 13. Observe in this figure that the average number lies far below the asymptotic bound of Eq. (86) and it is inversely proportional both to the number of MCs and to the number of MRs. This is justified by the fact that the number of Pareto-optimal route-combinations increases at a lower rate compared to the number of active routes, i.e. compared to the number of stages in the irregular trellis diagram of Figs. 11a and 11b, both of which increase proportionally to the number of MCs. Additionally, an increase in the number of MRs results in an increase in the value of $\bar{N}_{\text{OPF}}$ and, thus, the number of states per trellis stage; however, the number of Pareto-optimal route-combinations tends to grow slower, hence, reducing the order of the factor ρ with respect to $\bar{N}_{\text{OPF}}$ as the number of MRs increase.

Moving on to the upper and lower bounds of the complexity imposed by the MODQO algorithm's outer step, we

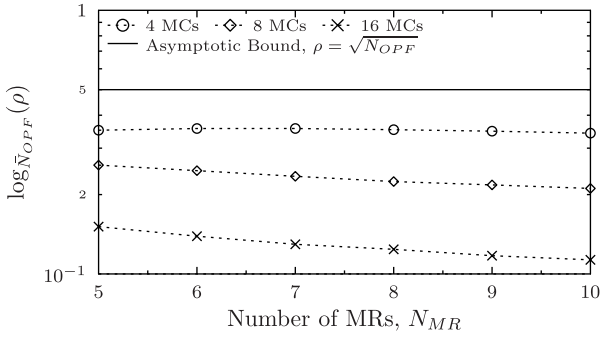

FIGURE 13. Order of the surviving route-combinations' growth factor ρ with respect to the average number $\bar{N}_{\text{NOPF}}$ of Pareto-optimal routes in the MC routing table for twin-layer networks comprised by $N_{\text{MC}} = \{4, 8, 16\}$ MCs and $N_{\text{MR}} = \{5, \ldots, 10\}$ MRs. The results have been averaged over 10^8 runs.

will consider two extreme scenarios. In the best-case scenario, we assume that the number of Pareto-optimal route-combinations at the n-th stage is equal to the average number of Pareto-optimal routes per stage, hence, we have $\rho = 1$. We have assumed furthermore that all the quantum processes impose the minimum possible complexity in terms of CFEs. As for the lower bound of the number N_r of active routes, since we have assumed that all of the MCs share a social relationship with at least another MC, we have:

$$N^{\min}_r = N_{\text{MC}}. \tag{87}$$

Therefore, the lower bound of the complexity imposed by a single iteration using the QM method as a function of the average number $\bar{N}_{\text{OPF}}$ of Pareto-optimal routes may be expressed as follows:

$$\begin{aligned} L^{\text{outer}}_{\text{QM,min}}(\bar{N}_{\text{OPF}}) &= (2K)^{-1}\bar{N}^2_{\text{OPF}} + K^{-1}\left\{L^{\min}_{\text{DHA}}(\bar{N}^2_{\text{OPF}}) \right. \\ &\quad \left. + 2L^{\min}_{\text{BBHT}}(\bar{N}^2_{\text{OPF}}) - \frac{1}{2}\right\}\bar{N}_{\text{OPF}} \\ &\quad + (1-K)\left\{\frac{2}{K}L^{\min}_{\text{BBHT}}(\bar{N}^2_{\text{OPF}}) + \frac{1}{2}\right\}, \\ &= O(\bar{N}^2_{\text{OPF}}). \end{aligned} \tag{88}$$

Hence, based on Eq. (88) the lower bound of the MODQO outer step's complexity, quantified in terms of the number of CFEs and as a function of the average number $\bar{N}_{\text{OPF}}$ of Pareto-optimal routes, is equal to:

$$\begin{aligned} L^{\text{outer}}_{\text{MODQO,min}}(\bar{N}_{\text{OPF}}) &= \sum_{n=2}^{N^{\min}_r} L^{\text{outer}}_{\text{QM,min}}(\bar{N}_{\text{OPF}}), \\ &= (N_{\text{MC}}-1)L^{\text{outer}}_{\text{QM,min}}(\bar{N}_{\text{OPF}}), \\ &= O(N_{\text{MC}}\bar{N}^2_{\text{OPF}}). \end{aligned} \tag{89}$$

Consequently, the lower bound $L^{\text{outer}}_{\text{MODQO,min}}$ of the MODQO outer step occurs when the average number of Pareto-optimal routes is strictly equal to $N_{\text{OPF}} = 1$ for all the routes, based on Eq. (72). However, in this particular case no CFEs are

required for constructing the single Pareto-optimal route-combination, since there is only a single possible route-combination, yielding:

$$L^{\text{outer}}_{\text{MODQO,min}} = 0. \tag{90}$$

We note that the same lower bound is valid for the CM method as well, yielding:

$$L^{\text{outer}}_{\text{CM,min}} = 0. \tag{91}$$

Subsequently, let us now derive the strict upper bound of the MODQO outer step complexity. For this reason, we will consider the worst case scenario, where all the potential route-combinations identified by the MODQO inner step are Pareto-optimal. In this scenario, the surviving route-combinations' growth factor is set to $\rho = \bar{N}_{\text{OPF}}$. Additionally, the maximum number $N_r^{\max}$ of the active pairs of source and destination MCs occurs in the case, where all the MCs share a friendship relationship with each other. Nevertheless, as the number N_{MC} of MCs increases, so does the probability of two MCs being associated with the same MR. This results in a single Pareto-optimal route and, thus, in a single state in the respective stage of the irregular trellis diagram, where no CFEs are required for encapsulating it in the set of Pareto-optimal route-combinations. Therefore, the upper bound of the number of active pair of source and destination MCs that require at least a single CFE for their processing and for their inclusion in the Pareto-optimal route combinations is derived as follows:

$$N_r^{\max} = \frac{1}{2}\left[(N_{\text{MC}}(N_{\text{MC}}-1) - \left\lfloor \frac{N_{\text{MC}}}{N_{\text{MR}}} \right\rfloor\right] = O(N_{\text{MC}}^2). \tag{92}$$

As for the upper bound $L^{\text{outer}}_{\text{QM,max}}(n, \bar{N}_{\text{OPF}})$ of the complexity imposed by a single iteration using the QM method as a function of the average number $\bar{N}_{\text{OPF}}$ of Pareto-optimal routes at the n-th stage of the irregular trellis diagram, it is derived a follows:

$$\begin{aligned} L^{\text{outer}}_{\text{QM,max}}(n, \bar{N}_{\text{OPF}}) &= (2K)^{-1}\bar{N}_{\text{OPF}}^{2n} + K^{-1}\left\{L^{\max}_{\text{DHA}}(\bar{N}^n_{\text{OPF}}) \right. \\ &\quad \left. + 2L^{\max}_{\text{BBHT}}(\bar{N}^n_{\text{OPF}}) - \frac{1}{2}\right\}\bar{N}_{\text{OPF}} \\ &\quad + (1-K)\left\{\frac{2}{K}L^{\max}_{\text{BBHT}}(\bar{N}^n_{\text{OPF}}) + \frac{1}{2}\right\}, \\ &= O(\bar{N}^{2n}_{\text{OPF}}). \end{aligned} \tag{93}$$

Based on Eq. (93), the upper bound $L_{\text{MODQO,max}}(\bar{N}_{\text{OPF}})$ of the MODQO outer step complexity, quantified in terms of the number of CFEs and as a function of the average number $\bar{N}_{\text{OPF}}$ of Pareto-optimal routes, is derived as follows:

$$\begin{aligned} L^{\text{outer}}_{\text{MODQO,max}}(\bar{N}_{\text{OPF}}) &= \sum_{n=2}^{N_r^{\max}} L^{\text{outer}}_{\text{QM,min}}(n, \bar{N}_{\text{OPF}}), \\ &= O\left[\frac{\bar{N}^{2(N_r^{\max}+1)}_{\text{OPF}} - \bar{N}^4_{\text{OPF}}}{\bar{N}^2_{\text{OPF}} - 1}\right], \\ &= O(\bar{N}^{2N^2_{\text{MC}}}_{\text{OPF}}). \end{aligned} \tag{94}$$

Consequently, the upper bound $L^{\text{outer}}_{\text{MODQO,max}}$ of the MODQO outer step's complexity is encountered when the average number of Pareto-optimal routes is strictly equal to $N_{\text{OPF}} = N_{\text{MR}} - 1$ for all the routes. Then, based on Eq. (73), we have:

$$L^{\text{outer}}_{\text{MODQO,max}} = O\left(N_{\text{MR}}^{2N^2_{\text{MC}}}\right). \tag{95}$$

The respective upper bound of the CM method is derived by setting $\rho = \bar{N}_{\text{OPF}} = N_{MR} - 1$ in Eq. (77), yielding:

$$L^{\text{outer}}_{\text{CM,max}} = O\left(N_{\text{MR}}^{2N^2_{\text{MC}}}\right). \tag{96}$$

Consequently, both the MODQO QM method and the CM method impose the same order of complexity in the worst-case scenario, matching the exhaustive search complexity. Explicitly, in the worst-case scenario there will be no complexity reduction for either of these methods. We note though that this specific scenario hardly occurs due to the trend of the ρ parameter shown in Fig 13, which decreases as the number N_{MC} of MCs increases.

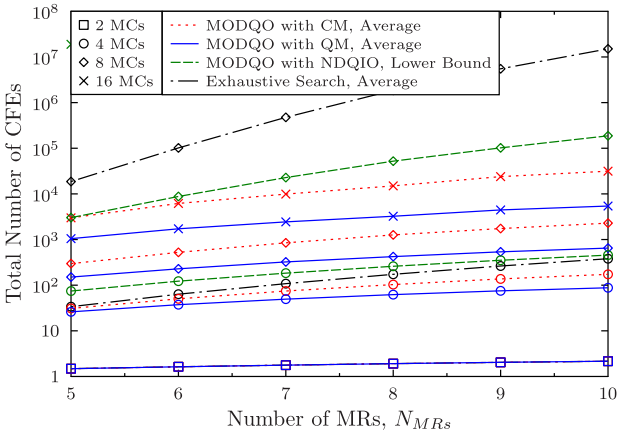

FIGURE 14. Average MODQO outer step complexity quantified as a function of the number of CFEs for twin-layer networks consisting of $N_{\text{MR}} = \{5, 6, \ldots, 10\}$ MRs and $N_{\text{MR}} = \{2, 4, 8, 16\}$ MCs. The MODQO outer step complexity is compared to that of the exhaustive search, that of the CM method and to the lower bound of the NDQIO algorithm invoked jointly for all the available stages. The portrayed results have been averaged over 10^8 runs.

The average complexity quantified in terms of the number of CFEs of the MODQO outer step is shown in Fig. 14 for twin-layer networks consisting of 5 to 10 MRs and of 2, 4, 8, and 16 MCs. The MODQO outer step complexity, which is represented by the solid lines in Fig. 14 and denoted as "MODQO with QM", is compared both to the average complexity of the CM method, corresponding to the dotted dotted lines and referred to as "MODQO with CM", as well as to the lower bound of the NDQIO process considering all the trellis stages jointly, which is marked by dashed lines and finally to the average complexity imposed by the exhaustive search, which is represented by the dashed and dotted lines. In general, observe that the outer step complexity of all the methods examined increases exponentially, as the number of

MCs increases, whereas the respective gradient is substantially reduced with number of MRs increases. This is justified by the fact that the average number of Pareto-optimal routes increases almost linearly with the number of MRs, while the total number N_r of active source and destination MCs, which is the exponent of the complexity function, increases almost quadratically with the number of MCs, as it may be inferred based on Eqs. (41), (77), (84) and (85).

For networks having 2 MCs, we can observe in Fig. 14 that all the methods considered impose an identical complexity, since a single stage is encountered and no merging takes place. Explicitly, this specific complexity is directly determined by the number of Pareto-optimal routes between the two MCs, since the algorithm has to identify the particular route that exhibits the highest value in terms of the normalized entropy of its associated composite betweenness. Naturally, the merging process imposes non-negligible complexity for networks having 3 or more MCs. For the scenario of $N_{\text{MC}} = 4$ MCs, we can clearly observe in Fig. 14 that the proposed MODQO outer step design, namely the one that invokes the QM method, imposes a lower number of CFEs that its counterparts. More specifically, for networks consisting of $N_{\text{MR}} = 10$ MRs the MODQO outer step relying on the QM method imposes about half the complexity imposed by the CM method and less than a third of the exhaustive search as well as a thrid of the NDQIO algorithm's lower bound. We note that for this N_{MC} value, the exhaustive search imposes a lower complexity than the minimum required by the NDQIO, which is indeed expected owing to the rather low total number of route combinations, hence not allowing the QP to excel. This trend is reversed however for networks with a higher number of MCs. More specifically for $N_{\text{MC}} = 8$, the MODQO outer step operates at a 2 times to 3.5 times lower complexity than that of the CM method for larger networks having 5 and 10 MRs, respectively, as seen in Fig 14. More dramatically, it imposes a complexity that is two and four orders of magnitude lower than the lower bound of the NDQIO algorithm and than the average exhaustive search complexity. Finally, for networks having $N_{\text{MC}} = 16$ MCs, the MODQO outer step imposes almost 6 times lower number of CFEs than that of the CM method for $N_{\text{MR}} = 10$ MRs and several orders of magnitude less than the exhaustive search and the lower bound of the NDQIO algorithm.

In a nutshell, we expect the complexity reduction offered by the QM method of the MODQO outer step to increase even further, as the number of MCs increases. Recall that this complexity reduction offered by the QM method of the MODQO outer step is on the order of $O\left(\rho^{-2}\bar{N}_{\text{OPF}}^2\right)$ when compared to the CM method, based on Eqs. (77) and (84). Explicitly, as the numbers of MRs and MCs increase, the average number $\bar{N}_{\text{OPF}}$ of Pareto-optimal routes increases, while the surviving route-combinations' growth factor ρ decreases with respect to $\bar{N}_{\text{OPF}}$, as we demonstrated in Fig. 13, which drives the associated complexity reduction to even higher levels.

3) TOTAL COMPLEXITY

Having characterized both the inner and the outer steps of the MODQO algorithm, let us now provide some further insights into the total complexity trends quantified in terms of the number of CFEs. Explicitly, the MODQO algorithm's total complexity as a function of the average number $\bar{N}_{\text{OPF}}$ of Pareto-optimal routes and of the surviving route-combinations' growth factor ρ is derived as follows:

$$L_{\text{MODQO}}^{\text{tot}} = L_{\text{MODQO}}^{\text{inner}} + L_{\text{MODQO}}^{\text{outer}} + \rho^{Nr-1}\bar{N}_{\text{OPF}}, \quad (97)$$

where $L_{\text{MODQO}}^{\text{inner}}$ and $L_{\text{MODQO}}^{\text{outer}}$ correspond to the complexity imposed by the MODQO algorithm's inner and outer steps, respectively, while the last factor $\rho^{Nr-1}\bar{N}_{\text{OPF}}$ is equal to the number of Pareto-optimal route-combinations at the termination of the QM procedure. This specific factor accounts for the selection of the route-combination S exhibiting the highest value of normalized entropy for its normalized composite betweenness $\bar{H}[\bar{B}_{com}(S)]$ at the very last iteration of the QM method. Consequently, we may readily derive the lower and upper bounds associated with the best- and worst-case scenarios, respectively, as follows:

$$L_{\text{MODQO,min}}^{\text{tot}} = O(\sqrt{N}), \quad (98)$$

$$L_{\text{MODQO,max}}^{\text{tot}} = O(N_{\text{MR}}^3\sqrt{N} + N_{\text{MR}}^{2N_{\text{MC}}^2}), \quad (99)$$

where Eq. (98) is derived by substituting Eqs. (74) and (90) into Eq. (97), while Eq. (99) is derived by substituting Eqs. (75) and (95) into Eq. (97). Therefore, a significant complexity reduction is achieved even for the worst-case scenario as opposed to the naive exhaustive search, which would check every legitimate route-combination, constituted by all the possible Hamiltonian routes, and would impose a complexity on the order of $O(N^{2N_{\text{MC}}^2})$ with $O(N) \gg O(N_{\text{MR}})$. Additionally, the MODQO-CM method, which incorporates first the MODQO inner step and then the CM method as its outer step, exhibits the same upper and lower bounds as those of the MODQO algorithm, based on Eqs. (48) and (47). Nevertheless, since the MODQO algorithm's lower bound complexity is based on no complexity being imposed by its outer step, the MODQO algorithm's total complexity is upper bounded by that of the MODQO-CM algorithm.

Both the MODQO and the MODQO-CM algorithms' average complexities quantified in terms of their imposed number of CFEs are presented in Fig. 15 for networks consisting of 5 to 10 MRs and of 2, 4, 8, and 16 MCs. The complexities of these two algorithms are compared to that of the exhaustive search, which carries out two separate exhaustive search procedures, namely one for the inner and one for the outer step as represented by the black dashed and dotted lines. We note that in Fig. 15 the MODQO algorithm is labeled as ''MODQO using QM'' and its average total complexity portrayed with a blue solid line, whilst the MODQO-CM algorithm is labelled ''MODQO using CM'' and its average total complexity is portrayed by a dotted line. For networks having $N_{\text{MC}} = 2$ MCs, there will be a single active source and destination MC pair, hence the MODQO and the MODQO-CM algorithms

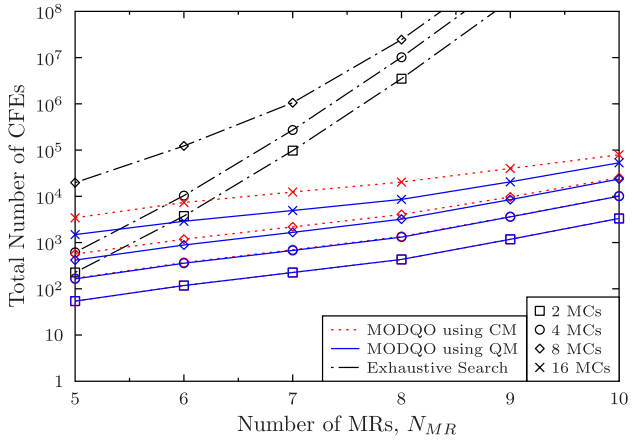

FIGURE 15. Average MODQO outer step complexity quantified as a function of the number of CFEs for twin-layer networks consisting of $N_{\mathrm{MR}} = \{5, 6, \ldots, 10\}$ MRs and $N_{\mathrm{MR}} = \{2, 4, 8, 16\}$ MCs. The MODQO average complexity is compared to that of the exhaustive search and that of the MODQO using the CM method. The portrayed results have been averaged over 10^8 runs.

impose an identical number of CFEs, which is more than four orders of magnitude below the exhaustive search procedure's average total complexity. Indeed, this complexity advantage increases even further as the number of MRs increases. This is justified by the fact that their respective outer step requires no CFEs to identify the Pareto-optimal route-combinations in the presence of a single trellis stage. As the number of MCs increases, the complexity reduction offered by the MODQO algorithm with respect to the MODQO-CM increases. More specifically, observe in Fig. 15 that for networks having $N_{\mathrm{MC}} = 4$ MCs, our proposed MODQO algorithm imposes 3% fewer CFEs than the MODQO-CM. Explicitly, in this case the order of both algorithms' complexities is governed by that of the inner step, which is one order of magnitude higher than that of the algorithms' outer steps, as seen in Figs. 12 and 14.

This effect can be observed for networks comprised by a higher number of MCs as well, yielding an interesting trade-off. Explicitly, for networks having $N_{\mathrm{MC}} = 16$ MCs, observe in Fig. 15 that the MODQO algorithm offers an almost constant complexity reduction factor of 2.5 compared to the MODQO-CM alg. for N_{MR} values up to 8 MRs. However, for larger networks the complexity reduction is gradually eroded due to the steep rise in the inner step's complexity, which dominates the total complexity. This drives the MODQO total complexity to an asymptotic convergence woth that of the MODQO-CM, as the number of MRs increases. However, based on Fig. 15, in practical scenarios, where the total number N_{MC} of MCs is significantly higher than N_{MR}, the MODQO algorithm will outperform the MODQO-CM in terms of the required number of CFEs and the complexity reduction offered by the MODQO will increase as the number of MCs increases, which is owing to a better exploitation of the QP.

B. ACCURACY

Having fully characterized the MODQO algorithm in terms of its complexity, let us now proceed by assessing its accuracy. Explicitly, we have analytically proven that the search space transformation relying on Proposition 1 attains a full-search-based accuracy and it has been demonstrated in [43] that the NDQIO algorithm approaches a full-search-based accuracy as well. Consequently, we can surmise that the MODQO also algorithm exhibits a full-search-based accuracy. Therefore, instead of comparing the MODQO algorithm's accuracy to that of the naive exhaustive search, we will use as a benchmark algorithm the state-of-the-art multi-objective evolutionary algorithm, namely the NSGA-II [32], [49]. Explicitly, our accuracy case study will examine as to whether the MODQO algorithm strikes an efficient accuracy versus complexity trade-off when compared to the NSGA-II. For this reason, we will compare these algorithms' accuracy to each other, when both operate at the same complexity, quantified in terms of CFEs.

1) BENCHMARKING ALGORITHM

Prior to proceeding with the MODQO algorithm and NSGA-II accuracy comparison, let us provide a brief introduction to the NSGA-II algorithm. In a nutshell, the NSGA-II initializes a population of $N_{\mathrm{pop}}/2$ individuals, corresponding to our route-combinations. Then a mating pool is constructed using a binary tournament selection method for determining, which of the individuals mate with each other. In total $N_{\mathrm{pop}}/4$ pairs of parent individuals are formed for producing $N_{\mathrm{pop}}/2$ offspring individuals by applying the classic crossover operation to the chromosome of the parent individual with a probability of P_c. The $N_{\mathrm{pop}}/2$ individuals have their chromosomes mutated with a probability of P_m and they are incorporated into the initial population. Subsequently, an ascending-order non-dominated sorting is performed in the initial population, where the individuals are sorted based on the number of individuals that dominate them. For individuals that are dominated by an identical number of route-combinations they are sorted according to their so-called *crowding distance*[8] [49] in descending order. Based on this sorting scheme, the first $N_{\mathrm{pop}}/2$ individuals are then selected for initializing the population of the next generation. This process is repeated for N_{gen} generations and the OPF of route-combinations is then exported.

We note that we have adapted the NSGA-II used in [42] so that it can benefit from the search space transformation of Proposition 1. To elaborate further, we have assumed that each of the individuals is constituted by multiple chromosomes, each corresponding to a Hamiltonian route for a specific pair of source and destination MCs. Furthermore, during the mating process independent crossover and mutation operations are performed for each of the chromosomes.

[8]The *crowding distance* of a specific route-combination determines its distance with respect to its neighboring route-solutions in the hyper-space defined by their utility vectors. The readers should refer to [49] for a more detailed description of this metric.

For the sake of simplicity, we have assumed that the number N_{pop} of individuals per generation is equal to the number N_{gen} of generetions, i.e. we have:

$$N_{\text{pop}} = N_{\text{gen}}, \tag{100}$$

yielding a total complexity in terms of the number of CFEs, which is equal to:

$$L_{\text{NSGA-II}} = N_{\text{pop}}^3, \tag{101}$$

since the non-dominated sort requires precisely N_{pop}^2 CFEs for N_{pop} generations. The simulation parameters considered for the NSGA-II are presented in Table 7,[9] where the number N_{pop} of individuals was set to match the maximal total complexity of MODQO algorithm observed throughout the simulations that produced Fig. 15. The rest of the parameters values used have been optimized through extensive simulations.

TABLE 7. NSGA-II simulation parameters.

Parameter	Value
N_{pop}	$\{24, 26, 28, 32, 34, 36\}$
P_c	0.8
P_m	0.1

2) ACCURACY COMPARISON

Ideally we would have to compare the MODQO algorithm and the NSGA-II in terms of the average of the identified OPF formed by the Pareto-optimal route combinations as far as the average network delay and the average network power consumption are concerned. However, the visualization of the OPF would complicate the representation of the results rendering the related trends rather opaque. For the sake of simplifying the presentation of the results, we will assess both algorithms' performance by providing the simulation results for the Pareto-optimal solutions having four distinct characteristics. First, we have to assess the networks' limits in terms of the WMN QoS criteria considered, namely the average minimum network delay $\min\{\bar{D}(S)\}$ and the average minimum network power consumption $\min\{\bar{P}(S)\}$. In addition to these metrics, we will provide the Pareto-optimal solutions of the maximum normalized entropy of the normalized composite betweenness $\max\{\bar{H}[\bar{B}_{com}(S)]\}$ and compare it to the one exhibiting the minimum standard deviation of the normalized composite betweenness $\min\{\sigma_{\bar{B}_{com}}\}$ for the sake of assessing the proposed load balancing strategy.

Let us now proceed by jointly assessing the MODQO performance in terms of the QoS criteria considered for the WMN layer, namely the average network delay performance $\bar{D}$ per route quantified in terms of the number of established hops and average network power consumption $\bar{P}$ per route in dBm. The aforementioned metrics are portrayed in Fig. 16 for

[9]Solely for $N_{\text{MC}} = 16$ MCs.

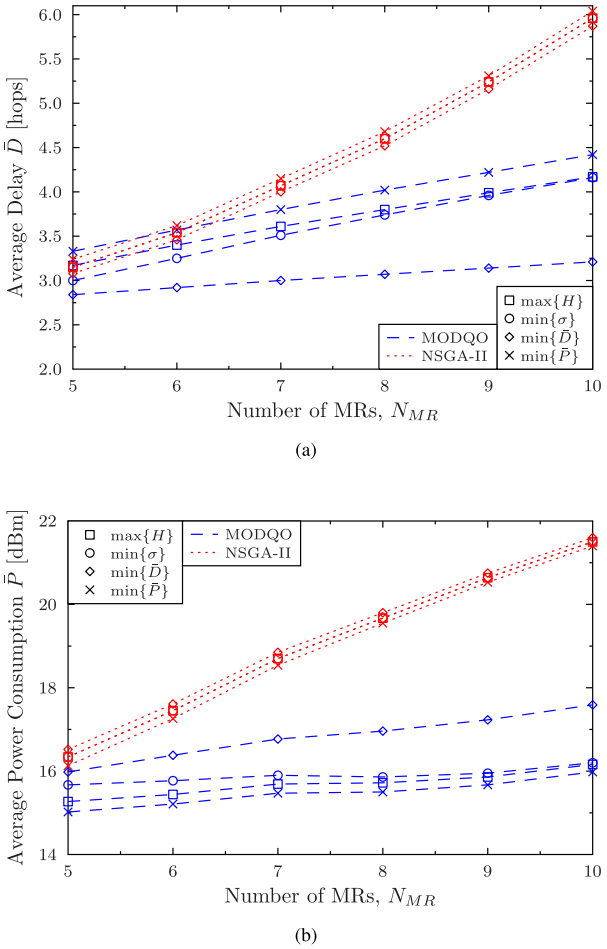

FIGURE 16. Average network delay performance $\bar{D}$ per route in terms of the number of established hops (a) and average network power consumption $\bar{P}$ per route in dBm (b) for both the MODQO algorithm and the NSGA-II for networks having from 5 to 10 MRs and 16 MCs. The NSGA-II initialization parameters are presented in Table 7. The results have been averaged over 10^8 runs.

networks having 5 to 10 MRs for 16 MCs. As far as the delay is concerned, observe in Fig. 16a that the minimum delay achieved by the MODQO algorithm slightly increases, as the number N_{MR} of MRs increases. This is justified by the fact that as the number of MRs increases, the probability of two specific MCs being associated with the same MR decreases, hence reducing the probability of establishing a connection with the minimum possible delay of two hops. On the other hand, the minimum power consumption portrayed in Fig. 16b is governed by a pair of conflicting dynamics. To elaborate further, as the number N_{MR} of MRs the distances between the MRs decrease, hence the shorter links require a lower power, while if the probability of two MCs being associated with the same MR decreases, this virtually increases the average distance among the MCs quantified in terms of the number of hops. The latter is justified by the fact that the MCs tend to be associated with their closest MRs; however, this does not necessarily imply that the MR association is optimal in terms of the routes' power consumption, since an MR that is closest

to the source MC can potentially be located further away from the destination MC, hence increasing in the average power consumption.

As for the load balancing metrics, namely the maximum normalized entropy of the normalized composite betweenness distribution and minimum standard deviation of the specific distribution, which are denoted by $\max\{\bar{H}\}$ and $\min\{\sigma\}$, respectively, observe in Fig. 16 that they both lie between the two extreme strategies. Additionally, we can observe in Fig. 16a that the specific $\min\{\sigma\}$-strategy that minimizes the standard deviation of the composite betweenness distribution seems to be biased towards the minimum-delay solution. This is justified by the fact that this strategy considers to be optimal the specific route-combination that utilizes no intermediate MRs in the construction of all the routes, while in its absence it will identify as optimal the same route-combination as the strategy aiming for maximizing the normalized entropy, yielding $\max\{\bar{H}\}$. This explains the trend that the $\min\{\sigma\}$-strategy exhibits lower average delay in Fig. 16a and a higher average power consumption in Fig. 16b than those of the $\max\{\bar{H}\}$-strategy for networks having less than 8 MRs. By contrast, for a higher number of MRs the performance of the $\min\{\sigma\}$-strategy asymptotically converges to that of the $\max\{\bar{H}\}$-strategy. Explicitly, as the number N_{MR} of MRs increases, the probability of forming a Pareto-optimal route-combination without the involvement of intermediate MRs decreases, since the MCs tend to become more distant in terms of the number of hops, as the network becomes populated by more MRs.

Additionally, we can observe both in Fig. 16a and in 16b that the proposed maximum-entropy strategy yielding $\max\{\bar{H}\}$ exhibits an average delay that is about 0.3 hops lower that of the strategy minimizing the average power consumption, namely $\min\{\bar{P}\}$, for networks having $N_{\mathrm{MR}} = 5$ MRs. This performance-discrepancy widens, as the number of MRs increases, reaching a reduction of 0.5 hops for networks having $N_{\mathrm{MR}} = 10$ MRs. Naturally, this reduction comes at a cost of about 0.3 dB in terms of the average power consumption, as observed in Fig. 16b. Explicitly, this delay reduction exhibits an underlying trade-off among the $\max\{\bar{H}\}$, the $\min\{\bar{P}\}$ and the $\min\{\bar{D}\}$ strategies: the normalized composite entropy asymptotically converges to the uniform distribution, as and when more MRs become involved as intermediate relays and reaches its minimum divergence for the route-combination of the $\max\{\bar{H}\}$ strategy. From this point onwards, an increase in the number of MRs results in the central MRs becoming bottlenecks, hence driving the normalized composite entropy further away from the uniform distribution.

As for the NSGA-II performance we can observe that it fails to converge to the Pareto-optimal route-combinations of the MODQO algorithm owing to the latter's extremely low complexity. More specifically, based on Figs. 16a and 16b, we can clearly observe that the route-combinations of all four strategies identified by the NSGA-II are dominated by the respective ones identified by the MODQO algorithm for networks having more than $N_{\mathrm{MR}} = 7$ MRs. More specifically

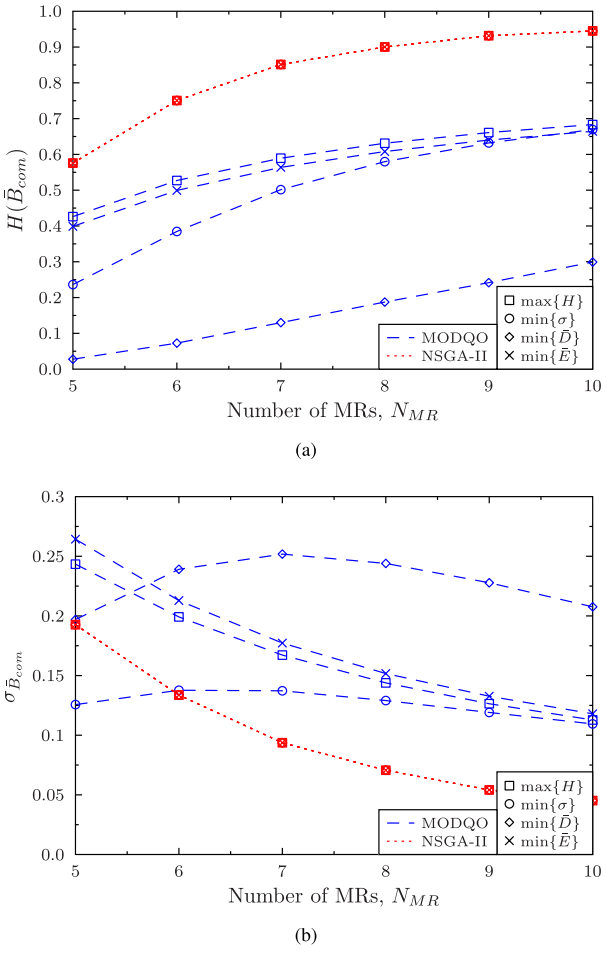

FIGURE 17. Average normalized entropy of the normalized composite betweenness $\bar{H}[B_{com}(S)]$ (a) and standard deviation of the normalized composite betweenness $\sigma_{\bar{B}_{com}}$ (b) for both the MODQO algorithm and the NSGA-II for networks having from 5 to 10 MRs and 16 MCs. The NSGA-II initialization parameters are presented in Table 7. The results have been averaged over 10^8 runs.

for networks having $N_{\mathrm{MR}} = 10$ MRs, the MODQO algorithm achieves a power-reduction of at least 4 dB and a delay-reduction of at least 1.5 hops at the same number of CFEs. Therefore, we can conclude that our proposed MODQO algorithm exhibits a better performance versus complexity trade-off associated with identifying the Pareto-optimal solutions.

Subsequently, the evaluation to the networks' load balancing performance is characterized in Figs. 17a and 17b in terms of the normalized entropy of the normalized composite betweenness distribution and the distribution's standard deviation, respectively. In a nutshell, we can observe that a more efficient load balancing is performed, as the number of MRs increases. The strategy minimizing the average network delay constitutes an exception. On the one hand it exhibits the lowest value of $\bar{H}(\bar{B}_{com})$ yielding that its respective route-combinations' $\bar{B}_{com}$ distribution deviates more substantially from the uniform distribution, based on Fig 17a. On the other hand, as we can observe in Fig. 17b, this specific strategy exhibits a lower standard deviation for the $\bar{B}_{com}$ distribution

in networks having $N_{\mathrm{MR}} = 5$ MRs, owing to the inclusion of direct routes relying on no intermediate relays, which in turn exhibit zero standard deviation. However, as the number N_{MR} of MRs increases, the probability of these specific routes being identified as Pareto-optimal decreases, yielding an increase in the associated standard deviation, which then obeys the trend of the rest of the strategies. This standard deviation trend is observed in Fig. 17b for the $\min\{\sigma\}$ strategy, where the standard deviation is seen to increase for networks having $N_{\mathrm{MR}} = 7$ up to MRs and then decreases as the number of MRs increases further. We note that the respective value of $\bar{H}(\bar{B}_{com})$ seen in Fig. 17a for the route-combinations exported by this strategy is lower than those of both the $\max\{\bar{H}\}$ and $\max\{\bar{P}\}$ strategies. This exhibits a poorer resemblance to the uniform distribution of the $\min\{\sigma\}$ as well as to the $\max\{\bar{H}\}$ and $\max\{\bar{P}\}$ strategies.

Finally, as far as the NSGA-II algorithm is concerned, we can observe in both Figs. 17a and 17b that they exhibit a far better load balancing performance than the MODQO algorithm for all the strategies examined. This is justified by the fact that the route-combinations exported by the NSGA-II do not comply with the constraint of Eq. (22), since the Pareto-optimal route-combinations identified the NSGA-II are sub-optimal in comparison to the respective ones identified by the MODQO algorithm. This results in an excessive involvement of MRs for the sake of approximating the uniform distribution, which leads to both an excessive delay and an excessive power consumption. Based on this fact, we can infer that load balancing tends to degrade both the average network delay and the average power consumption. Naturally, based on the problem formulation in Eq. (22), load balancing is imposed as a secondary optimization objective, whilst the constraint of Eq. (22) constitutes the primary optimization criterion, since it forces the optimization to additionally perform load balancing, while explicitly considering Pareto-optimal route-combinations.

VI. CONCLUSIONS

In this treatise, we have proposed an optimal quantum-assisted algorithm, namely the MODQO algorithm, for addressing the joint multi-objective routing and load balancing problem in socially-aware networks. The MODQO algorithm benefits from both a framework exploiting the synergies between the QP and HP, which is inherited by the NDQIO algorithm as well as from the novel database transformation framework advocated. The latter succeeds in transforming the strongly correlated database into a series of weakly correlated ones, where the QP and HP synergistic framework exploits the optimality of Grover's QSA [48]. Additionally, we have analytically proven that this transformation has no negative impact on the MODQO accuracy. Furthermore, we have introduced a novel socially-aware metric for characterizing the load balancing, namely the normalized entropy of the normalized composite betweenness distribution. We have also demonstrated that it succeeds in mitigating the biasing towards the minimum delay solution incurred by the employment of the standard deviation of the respective distribution. Furthermore, we have characterized the computational complexity in terms of the number of CFEs imposed by the MODQO algorithm, which is on the order of $O(\sqrt{N})$ and $O(N_{\mathrm{MR}}^{2N_{\mathrm{MC}}^2})$ for networks having N_{MR} MRs and N_{MC} MCs in the best- and the worst-case scenarios, respectively. Explicitly, we have achieved a significant complexity reduction compared to the exhaustive search, which is on the order of $O(N^{2N_{\mathrm{MC}}^2})$, with $N \gg N_{\mathrm{MR}}$ being the total number of Hamiltonian routes between a pair of specific users. Additionally, we demonstrated using extensive simulations that the average complexity of the MODQO algorithm is multiple orders of magnitude lower than that of the exhaustive search. Finally, we have compared the MODQO algorithm's accuracy to that of the NSGA-II [32], [49], which constitutes the state-of-the-art for socially-oblivious networks, for a scenario where the network is sufficiently densely populated by MCs, i.e. we have $N_{\mathrm{MC}} = 16$ MCs and have demonstrated that our proposed MODQO algorithm is capable of improving both the delay and the power consumption by about 2 hops and 4 dB, respectively, for networks having 10 routers, when compared to the NSGA-II. This trend suggests that the MODQO algorithm exhibits a better complexity versus accuracy trade-off than the NSGA-II.

APPENDIX
PROOF OF PROPOSITION 1

Proof: Let us assume that the solution $S = [x^{(1)}, \ldots, x^{(j)}, \ldots, x^{(N_r)}]$ of the composite Pareto-optimality problem is Pareto-optimal and that the independent solutions $\{x^{(n)}\}$ are Pareto-optimal in their respective independent problems except for the solution $x^{(j)}$, which is suboptimal in its respective independent problem. Hence, there exits a solution $x'^{(j)}$ such that $\mathbf{f}_j(x'^{(j)}) \succeq \mathbf{f}_j(x^{(j)})$, i.e. we have:

$$f_k(x^{(j)}) \geq f_k(x'^{(j)}), \quad \forall n \in \{1, \ldots, K\}. \tag{102}$$

Therefore, if we multiply Eq. (102) by the factor $a_{k,j}$ and add the terms $a_{k,n}f_k(x^{(n)})$ associated with $n \neq j$, we will have $\forall k \in \{1, \ldots, K\}$:

$$\sum_{n=1}^{N_r} a_{k,n}f_k(x^{(n)}) \geq \sum_{\substack{n=1 \\ n \neq j}}^{N_r} a_{k,n}f_k(x^{(n)}) + a_{k,j}f_k(x'^{(j)}), \tag{103}$$

which can be written in the following compact form:

$$f_k(S) \geq f_k(S'), \quad \forall k \in \{1, \ldots, K\} \tag{104}$$

where $S' = [x^{(1)}, \ldots, x'^{(j)}, \ldots, x^{(N_r)}]$. Additionally, since $x'^{(j)}$ strongly dominates the solution $x^{(j)}$, we have that $\exists k' \in \{1, \ldots, K\}$ such that:

$$f_{k'}(x^{(j)}) > f_{k'}(x'^{(j)}). \tag{105}$$

If we now multiply Eq. (105) by the factor $a_{k',j}$ and add the terms $a_{k',n}f_{k'}(x^{(n)})$ with $n \neq j$, we will have for this

specific k':

$$\sum_{n=1}^{N_r} a_{k',n} f_{k'}(x^{(n)}) > \sum_{\substack{n=1 \\ n \neq j}}^{N_r} a_{k',n} f_{k'}(x^{(n)}) + a_{k',j} f_{k'}(x'^{(j)}), \quad (106)$$

which can be written in the following compact form:

$$\exists k' \in \{1, \ldots, K\} : f_{k'}(S) > f_{k'}(S'). \quad (107)$$

Hence, observe that Eqs. (104) and (107) encapsulate the two critical conditions so that $\mathbf{f}(S') \succeq \mathbf{f}(S)$, based on Definition 1, yielding that the initial assumption of having $S \in S^{\text{OPF}}$ is invalid. Hence, we have $S = [x^{(1)}, \ldots, x^{(N_r)}] \in S^{\text{OPF}}$ only if $x^{(n)} \in S_n^{\text{OPF}}$, $\forall n \in \{1, \ldots, N_r\}$. Therefore, all members of S^{OPF} are contained in the union of the sets $\{S_n^{\text{OPF}}\}_{n=1}^{N_r}$, hence proving the claim of Eq. (40). ■

Acknowledgment

The use of the IRIDIS High Performance Computing Facility at the University of Southampton is also acknowledged. The research data for this paper is available at http://doi.org/10.5258/SOTON/403120.

REFERENCES

[1] M. Weiser, "The computer for the 21st century," *Sci. Amer.*, vol. 265, no. 3, pp. 94–104, 1991.
[2] L. Atzori, A. Iera, and G. Morabito, "The Internet of Things: A survey," *Comput. Netw.*, vol. 54, no. 15, pp. 2787–2805, Oct. 2010.
[3] D. Evans, "The Internet of Things: How the next evolution of the Internet is changing everything," Cisco Syst., San Jose, CA, USA, Tech. Rep. IoT-IBSG-0411, 2011.
[4] J. Fry "The intelligent flexible cloud," ARM Ltd., Cambridge, U.K., Tech. Rep. DOC-9981, 2015.
[5] L. Atzori, A. Iera, and G. Morabito, "SIoT: Giving a social structure to the Internet of Things," *IEEE Commun. Lett.*, vol. 15, no. 11, pp. 1193–1195, Nov. 2011.
[6] L. Atzori, A. Iera, G. Morabito, and M. Nitti, "The social Internet of Things (SIoT)—When social networks meet the Internet of Things: Concept, architecture and network characterization," *Comput. Netw.*, vol. 56, no. 16, pp. 3594–3608, Nov. 2012.
[7] K.-C. Chen, M. Chiang, and H. V. Poor, "From technological networks to social networks," *IEEE J. Sel. Areas Commun.*, vol. 31, no. 9, pp. 548–572, Sep. 2013.
[8] C. Y. Lin *et al.*, "Social network analysis in enterprise," *Proc. IEEE*, vol. 100, no. 9, pp. 2759–2776, Sep. 2012.
[9] C. Boldrini, M. Conti, and A. Passarella, "The stability region of the delay in Pareto opportunistic networks," *IEEE Trans. Mobile Comput.*, vol. 14, no. 1, pp. 180–193, Jan. 2015.
[10] J. Wu and Y. Wang, "Hypercube-based multipath social feature routing in human contact networks," *IEEE Trans. Comput.*, vol. 63, no. 2, pp. 383–396, Feb. 2014.
[11] Z. Li and H. Shen, "SEDUM: Exploiting social networks in utility–based distributed routing for DTNs," *IEEE Trans. Comput.*, vol. 62, no. 1, pp. 83–97, Jan. 2013.
[12] K. Chen and H. Shen, "SMART: utilizing distributed social map for lightweight routing in delay-tolerant networks," *IEEE/ACM Trans. Netw.*, vol. 22, no. 5, pp. 1545–1558, Oct. 2014.
[13] E. Bulut and B. K. Szymanski, "Exploiting friendship relations for efficient routing in mobile social networks," *IEEE Trans. Parallel Distrib. Syst.*, vol. 23, no. 12, pp. 2254–2265, Dec. 2012.
[14] L. Yao, Y. Man, Z. Huang, J. Deng, and X. Wang, "Secure routing based on social similarity in opportunistic networks," *IEEE Trans. Wireless Commun.*, vol. 15, no. 1, pp. 594–605, Jan. 2016.
[15] P. Hui, J. Crowcroft, and E. Yoneki, "BUBBLE rap: Social-based forwarding in delay-tolerant networks," *IEEE Trans. Mobile Comput.*, vol. 10, no. 11, pp. 1576–1589, Nov. 2011.
[16] F. Xia, L. Liu, J. Li, A. M. Ahmed, L. T. Yang, and J. Ma, "BEEINFO: Interest-based forwarding using artificial bee colony for socially aware networking," *IEEE Trans. Veh. Technol.*, vol. 64, no. 3, pp. 1188–1200, Mar. 2015.
[17] M. E. J. Newman, "The structure and function of complex networks," *SIAM Rev.*, vol. 45, no. 2, pp. 167–256, 2003.
[18] P. Hui, E. Yoneki, S. Y. Chan, and J. Crowcroft, "Distributed community detection in delay tolerant networks," in *Proc. 2nd ACM/IEEE Int. Workshop Mobility Evolving Internet Archit. (MobiArch)*, New York, NY, USA, Aug. 2007, pp. 7:1–7:8.
[19] E. Stai, V. Karyotis, and S. Papavassiliou, "Exploiting socio-physical network interactions via a utility-based framework for resource management in mobile social networks," *IEEE Wireless Commun.*, vol. 21, no. 1, pp. 10–17, Feb. 2014.
[20] B. Azimdoost, H. R. Sadjadpour, and J. J. Garcia-Luna-Aceves, "Capacity of wireless networks with social behavior," *IEEE Trans. Wireless Commun.*, vol. 12, no. 1, pp. 60–69, Jan. 2013.
[21] D. Liben-Nowell, J. Novak, R. Kumar, P. Raghavan, and A. Tomkins, "Geographic routing in social networks," *Proc. Nat. Acad. Sci. USA*, vol. 102, no. 33, pp. 11623–11628, 2005.
[22] J. Hu, L.-L. Yang, H. V. Poor, and L. Hanzo, "Bridging the social and wireless networking divide: Information dissemination in integrated cellular and opportunistic networks," *IEEE Access*, vol. 3, pp. 1809–1848, 2015.
[23] Z. Zhang, H. Wang, C. Wang, and H. Fang, "Modeling epidemics spreading on social contact networks," *IEEE Trans. Emerg. Topics Comput.*, vol. 3, no. 3, pp. 410–419, Sep. 2015.
[24] H. Sun and C. Wu, "Epidemic forwarding in mobile social networks," in *Proc. IEEE Int. Conf. Commun. (ICC)*, Jun. 2012, pp. 1421–1425.
[25] O. Yagan, D. Qian, J. Zhang, and D. Cochran, "Conjoining speeds up information diffusion in overlaying social-physical networks," *IEEE J. Sel. Areas Commun.*, vol. 31, no. 6, pp. 1038–1048, Jun. 2013.
[26] Y. Zhu, B. Xu, X. Shi, and Y. Wang, "A survey of social-based routing in delay tolerant networks: Positive and negative social effects," *IEEE Commun. Surveys Tut.*, vol. 15, no. 1, pp. 387–401, 1st Quart., 2013.
[27] Y. Li, P. Hui, D. Jin, L. Su, and L. Zeng, "Evaluating the impact of social selfishness on the epidemic routing in delay tolerant networks," *IEEE Commun. Lett.*, vol. 14, no. 11, pp. 1026–1028, Nov. 2010.
[28] Y. Li, G. Su, D. O. Wu, D. Jin, L. Su, and L. Zeng, "The impact of node selfishness on multicasting in delay tolerant networks," *IEEE Trans. Veh. Technol.*, vol. 60, no. 5, pp. 2224–2238, Jun. 2011.
[29] Z. Wang, C. Wu, L. Sun, and S. Yang, "Peer-assisted social media streaming with social reciprocity," *IEEE Trans. Netw. Service Manage.*, vol. 10, no. 1, pp. 84–94, Mar. 2013.
[30] G. Xue, Q. He, H. Zhu, T. He, and Y. Liu, "Sociality-aware access point selection in enterprise wireless LANs," *IEEE Trans. Parallel Distrib. Syst.*, vol. 24, no. 10, pp. 2069–2078, Oct. 2013.
[31] A. Turk, R. O. Selvitopi, H. Ferhatosmanoglu, and C. Aykanat, "Temporal workload-aware replicated partitioning for social networks," *IEEE Trans. Knowl. Data Eng.*, vol. 26, no. 11, pp. 2832–2845, Nov. 2014.
[32] H. Yetgin, K. Cheung, and L. Hanzo, "Multi-objective routing optimization using evolutionary algorithms," in *Proc. IEEE Wireless Commun. Netw. Conf. (WCNC)*, Apr. 2012, pp. 3030–3034.
[33] K. Deb, "Multi-objective optimization," in *Search Methodologies*, E. K. Burke and G. Kendall, Eds. New York, NY, USA: Springer, 2005, pp. 273–316.
[34] M. Camelo, C. Omaña, and H. Castro, "QoS routing algorithm based on multi-objective optimization for wireless mesh networks," in *Proc. IEEE Latin-Amer. Conf. Commun. (LATINCOM)*, Sep. 2010, pp. 1–6.
[35] F. V. C. Martins, E. G. Carrano, E. F. Wanner, R. H. C. Takahashi, and G. R. Mateus, "A hybrid multiobjective evolutionary approach for improving the performance of wireless sensor networks," *IEEE Sensors J.*, vol. 11, no. 3, pp. 545–554, Mar. 2011.
[36] E. Masazade, R. Rajagopalan, P. K. Varshney, C. K. Mohan, G. K. Sendur, and M. Keskinoz, "A multiobjective optimization approach to obtain decision thresholds for distributed detection in wireless sensor networks," *IEEE Trans. Syst., Man B, Cybern.*, vol. 40, no. 2, pp. 444–457, Apr. 2010.
[37] L. K. Grover, "A fast quantum mechanical algorithm for database search," in *Proc. 28th Annu. ACM Symp. Theory Comput.*, 1996, pp. 212–219.
[38] M. Boyer, G. Brassard, P. Høyer, and A. Tapp. (1996). "Tight bounds on quantum searching." [Online]. Available: https://arxiv.org/abs/quant-ph/9605034
[39] C. Durr and P. Høyer. (1996). "A quantum algorithm for finding the minimum." [Online]. Available: https://arxiv.org/abs/quant-ph/9607014

[40] P. Botsinis, D. Alanis, Z. Babar, S. X. Ng, and L. Hanzo, "Iterative quantum-assisted multi-user detection for multi-carrier interleave division multiple access systems," *IEEE Trans. Commun.*, vol. 63, no. 10, pp. 3713–3727, Oct. 2015.
[41] P. Botsinis, D. Alanis, Z. Babar, S. X. Ng, and L. Hanzo, "Noncoherent quantum multiple symbol differential detection for wireless systems," *IEEE Access*, vol. 3, pp. 569–598, 2015.
[42] D. Alanis, P. Botsinis, S. X. Ng, and L. Hanzo, "Quantum-assisted routing optimization for self-organizing networks," *IEEE Access*, vol. 2, pp. 614–632, 2014.
[43] D. Alanis, P. Botsinis, Z. Babar, S. X. Ng, and L. Hanzo, "Non-dominated quantum iterative routing optimization for wireless multihop networks," *IEEE Access*, vol. 3, pp. 1704–1728, 2015.
[44] S. Imre and L. Gyongyosi, *Advanced Quantum Communications: An Engineering Approach*. Hoboken, NJ, USA: Wiley, 2013.
[45] Z. Babar, P. Botsinis, D. Alanis, S. X. Ng, and L. Hanzo, "The road from classical to quantum codes: A hashing bound approaching design procedure," *IEEE Access*, vol. 3, pp. 146–176, 2015.
[46] Z. Babar *et al.*, "Fully-Parallel Quantum Turbo Decoder," *IEEE Access*, vol. 4, pp. 6073–6085, 2016.
[47] M. A. Nielsen and I. L. Chuang, *Quantum Computation and Quantum Information*. Cambridge, U.K.: Cambridge Univ. Press, 2010.
[48] C. Zalka, "Grover's quantum searching algorithm is optimal," *Phys. Rev. A*, vol. 60, no. 4, p. 2746, Oct. 1999.
[49] K. Deb, A. Pratap, S. Agarwal, and T. Meyarivan, "A fast and elitist multiobjective genetic algorithm: NSGA-II," *IEEE Trans. Evol. Comput.*, vol. 6, no. 2, pp. 182–197, Apr. 2002.
[50] W. W. Zachary, "An information flow model for conflict and fission in small groups," *J. Anthropol. Res.*, vol. 33, no. 4, pp. 452–473, 1977.
[51] L. Freeman, "A set of measures of centrality based on betweenness," *Sociometry*, vol. 40, no. 1, pp. 35–41, 1977.
[52] J. Hu, L.-L. Yang, and L. Hanzo, "Cross-layer design for wireless mesh networking aided content sharing in online social networks," *IEEE Trans. Veh. Technol.*, 2016. Under Review.
[53] X. Li, R. Zhang, and L. Hanzo, "Cooperative load balancing in hybrid visible light communications and WiFi," *IEEE Trans. Commun.*, vol. 63, no. 4, pp. 1319–1329, Apr. 2015.
[54] C. E. Shannon, "A mathematical theory of communication," *Bell Syst. Tech. J.*, vol. 27, no. 3, pp. 379–423, Jul. 1948.
[55] S. Kullback and R. A. Leibler, "On information and sufficiency," *Ann. Math. Statist.*, vol. 22, no. 1, pp. 79–86, Mar. 1951.
[56] T. van Erven and P. Harremos, "Rényi divergence and Kullback–Leibler divergence," *IEEE Trans. Inf. Theory*, vol. 60, no. 7, pp. 3797–3820, Jul. 2014.
[57] A. Hobson, *Concepts in Statistical Mechanics*. Boca Raton, FL, USA: CRC Press, 1971.
[58] R. Steele and L. Hanzo, *Mobile Radio Communications: Second and Third Generation Cellular and WATM Systems*. Hoboken, NJ, USA: Wiley, 1999.
[59] L. Hanzo, S. X. Ng, W. Webb, and T. Keller, *Quadrature Amplitude Modulation: From Basics to Adaptive Trellis-Coded, Turbo-Equalised and Space-Time Coded OFDM, CDMA and MC-CDMA Systems*. Hoboken, NJ, USA: Wiley, 2004.
[60] S. Yang, X. Xu, D. Alanis, S. X. Ng, and L. Hanzo, "Is the low-complexity mobile-relay-aided FFR-DAS capable of outperforming the high-complexity CoMP?" *IEEE Trans. Veh. Technol.*, vol. 65, no. 4, pp. 2154–2169, Apr. 2015.
[61] M. Abramowitz and I. A. Stegun, *Handbook of Mathematical Functions: With Formulas, Graphs, and Mathematical Tables*, Courier Corporation, 1964.
[62] P. Botsinis, S. X. Ng, and L. Hanzo, "Quantum search algorithms, quantum wireless, and a low-complexity maximum likelihood iterative quantum multi-user detector design," *IEEE Access*, vol. 1, pp. 94–122, 2013.
[63] E. Aïmeur, G. Brassard, and S. Gambs, "Quantum speed-up for unsupervised learning," *Mach. Learn.*, vol. 90, no. 2, pp. 261–287, Feb. 2013.
[64] H. Ishibuchi, N. Akedo, and Y. Nojima, "Behavior of multiobjective evolutionary algorithms on many-objective knapsack problems," *IEEE Trans. Evol. Comput.*, vol. 19, no. 2, pp. 264–283, Apr. 2015.
[65] W. Zhang, M. F. Brejza, T. Wang, R. G. Maunder, and L. Hanzo, "Irregular trellis for the near-capacity unary error correction coding of symbol values from an infinite set," *IEEE Trans. Commun.*, vol. 63, no. 12, pp. 5073–5088, Dec. 2015.
[66] A. J. Viterbi, "Error bounds for convolutional codes and an asymptotically optimum decoding algorithm," *IEEE Trans. Inf. Theory*, vol. 13, no. 2, pp. 260–269, Apr. 1967.
[67] L. Hanzo, Y. Akhtman, J. Akhtman, L. Wang, and M. Jiang, *MIMO-OFDM for LTE, WiFi and WiMAX: Coherent Versus Non-Coherent and Cooperative Turbo Transceivers*, vol. 9. Hoboken, NJ, USA: Wiley, 2010.

DIMITRIOS ALANIS (S'13) received the M.Eng. degree in electrical and computer engineering from the Aristotle University of Thessaloniki in 2011 and the M.Sc. degree in wireless communications from the University of Southampton in 2012, where he is currently pursuing the Ph.D. degree with the Southampton Wireless Group, School of Electronics and Computer Science.

His research interests include quantum computation and quantum information theory, quantum search algorithms, cooperative communications, resource allocation for self-organizing networks, bioinspired optimization algorithms, and classical and quantum game theory.

JIE HU (S'11–M'16) received the B.Eng. and M.Sc. degrees from the Beijing University of Posts and Telecommunications, China, in 2008 and 2011, respectively, and the Ph.D. degree from the Faculty of Physical Sciences and Engineering, University of Southampton, U.K., in 2015. Since 2016, he has been with the School of Communication and Information Engineering, University of Electronic Science and Technology of China, China, as a Lecturer. His research is funded by the Chinese Government and the National Natural Science Foundation of China. He is also in great partnership with industry, such as Huawei and ZTE. He has a broad range of interests in wireless communication and networking, such as cognitive radio and cognitive networks, mobile social networks, data and energy integrated networks, and communication and computation convergence.

PANAGIOTIS BOTSINIS (S'12–M'16) received the M.Eng. degree from the School of Electrical and Computer Engineering, National Technical University of Athens, Greece, in 2010, and the M.Sc. degree (Hons.) and the Ph.D. degree in wireless communications from the University of Southampton, U.K., in 2011 and 2015, respectively. He is currently a Research Fellow with the Southampton Wireless Group, School of Electronics and Computer Science, University of Southampton, U.K. Since 2010, he has been a member of the Technical Chamber of Greece.

His research interests include quantum-assisted communications, quantum computation, iterative detection, OFDM, MIMO, multiple access systems, coded modulation, channel coding, cooperative communications, and combinatorial optimization.

ZUNAIRA BABAR received the B.Eng. degree in electrical engineering from the National University of Science and Technology, Islamabad, Pakistan, in 2008, and the M.Sc. degree (Hons.) and the Ph.D. degree in wireless communications from the University of Southampton, U.K., in 2011 and 2015, respectively.

Her research interests include quantum error correction codes, channel coding, coded modulation, iterative detection, and cooperative communications.

SOON XIN NG (S'99–M'03–SM'08) received the B.Eng. degree (Hons.) in electronic engineering and the Ph.D. degree in telecommunications from the University of Southampton, Southampton, U.K., in 1999 and 2002, respectively. From 2003 to 2006, he was a Post-Doctoral Research Fellow, where he was involved in collaborative European research projects known as SCOUT, NEWCOM, and PHOENIX. Since 2006, he has been a member of academic staff with the School of Electronics and Computer Science, University of Southampton. He is involved in the OPTIMIX and CONCERTO European projects and the IU-ATC and UC4G projects. He is currently an Associate Professor in telecommunications with the University of Southampton.

He has authored over 200 papers and co-authored two John Wiley/IEEE Press books in this field. His research interests include adaptive coded modulation, coded modulation, channel coding, space-time coding, joint source and channel coding, iterative detection, OFDM, MIMO, cooperative communications, distributed coding, quantum error correction codes, and joint wireless-and-optical-fiber communications. He is a Chartered Engineer and a fellow of the Higher Education Academy, U.K.

LAJOS HANZO (M'91–SM'92–F'04) received the degree in electronics in 1976 and the Ph.D. degree in 1983. In 2009, he received the honorary doctorate Doctor Honoris Causa by the Technical University of Budapest. During his 38-year career in telecommunications, he has held various research and academic positions in Hungary, Germany, and the U.K. Since 1986, he has been with the School of Electronics and Computer Science, University of Southampton, U.K., where he holds the chair position in telecommunications. He has successfully supervised about 100 Ph.D. students, co-authored 20 John Wiley/IEEE Press books on mobile radio communications totalling in excess of 10 000 pages, and published over 1400 research entries at the IEEE Xplore. He served as a TPC and the General Chair of the IEEE conferences and presented keynote lectures. He has been received a number of distinctions. He is currently directing a 100-strong academic research team, involving in the range of research projects in the field of wireless multimedia communications sponsored by industry, the Engineering and Physical Sciences Research Council U.K., the European Research Councils Advanced Fellow Grant and the Royal Society's Wolfson Research Merit Award. He is also an enthusiastic supporter of industrial and academic liaison and he offers a range of industrial courses.

Dr. Hanzo is a fellow of the Royal Academy of Engineering, the Institution of Engineering and Technology, and the European Association for Signal Processing. He is also a Governor of the IEEE VTS. From 2008 to 2012, he was the Editor-in-Chief of the IEEE Press and a Chaired Professor at Tsinghua University, Beijing. He has over 24 000 citations.